STUDIES IN THE DECAY OF ^{235}U, ^{231}Th and ^{231}PA -----

THE FIRST THREE MEMBERS OF THE ACTINIUM SERIES

A Thesis

Submitted to

the

Faculty of Graduate Studies

University of Manitoba

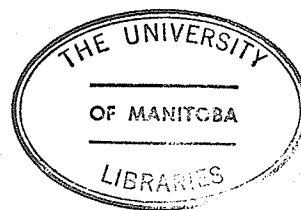In Partial Fulfilment

of the Requirement for the Degree

DOCTOR OF PHILOSOPHY

---

by

WILLIAM TEOH

JANUARY 1973

To

My   Aunt

ABSTRACT

An experimental determination of the decays of ^{231}Pa, ^{231}Th and ^{235}U has been carried out, using high resolution semi-conductor gamma ray detectors.

Due to the complexity of the gamma spectra observed, a computer programme was developed to analyse them numerically. The programme, code named CUTIPIE, utilizes a numerical second difference method for automatic peak searching, and a non-linear, multiparameter, iterative least squares fitting procedure for peak fitting. Two choices of peak and background shapes are available, and the programme can resolve overlapping peaks containing no more than six components.

A total of 73 gamma rays were observed in the ^{231}Pa decay. All but three had been reported recently. The three new transitions (161.0, 228.0 and 427.0 keV) were observed in the present work only in coincidence experiments. Conversion electrons were examined using a trochoidal spectrometer. The K conversion coefficients of 11 transitions were determined. Of these, two (the α_K of the 243.15 and 255.10 keV transitions) had not been reported previously. The coefficients for the two transitions were determined to be 0.54 ± 0.14 and

0.21 ± 0.05 respectively. All but one of the 73 gamma rays observed were placed in the decay scheme. Three new levels at 429.6, 457.7 and 641.0 keV are suggested based on the present investigation.

No new gamma rays were observed in the singles gamma ray spectra following the beta decay of ^{231}Th. Seven new transitions were observed however, in the gamma-gamma coincidence measurements. Their energies were determined to be 44.2, 45.8, 47.2, 71.8, 73.23, 104.1 and 115.9 keV. A total of 48 gamma rays were observed, and all but two (45.8 and 114.8 keV) were placed in the decay scheme. Only one new level is suggested, viz that at 294.5 keV.

The energies of the gamma rays emitted as a result of the decay of ^{235}U have been very carefully measured: some of the more intense lines have been calibrated to within 10 eV. A total of 28 gamma rays were observed, and only 17 of them had been previously reported. Eleven new transitions (31.50, 41.70, 41.96, 51.20, 96.09, 215.76, 275.35, 291.58, 345.84, 387.79 and 390.27 keV) are reported in this work for the first time, and all the 28 gamma rays observed were placed in the decay scheme. Three new levels (390.27, 317.42 and 240.82 keV) are suggested, based on the result of the present studies.

ACKNOWLEDGEMENT

TABLE OF CONTENTS

List of Figures

The investigation of the actinium series has been a project persued in this laboratory for the last ten years, and the present work endeavours to investigate the decay of the first three members of this series (namely, ^{235}U, ^{231}Th and ^{231}Pa).

The first member of the actinium series[1] is ^{235}U which is an alpha emitter with a half-life of 7.13×10^{8} years. The immediate decay product of ^{235}U is the 25.52 hour ^{231}Th. It is a beta emitter whose decay scheme has been known to be complex since the early fifties. This isotope decays to ^{231}Pa which has a half-life of 3.25×10^{4} years. The alpha spectrum of ^{231}Pa is known to be very complex, as is its gamma ray spectrum.

Investigations of the radiations from the decay of these isotopes[2] began as soon as they were decovered. The early investigations demonstrated that their decay schemes were complex, although the information obtained was far from being complete, due largely to the poor resolution of the spectrometers available then. With the introduction of high resolution semi-conductor detectors, large memory multi-channel analysers and

high speed computers, much more accurate information can be obtained nowadays. It is in the light of obtaining definitive decay schemes of these isotopes that the present work is being carried out.

Like most heavy nuclei which decay by alpha emission, the gamma radiations from the decay of ^{235}U and ^{231}Pa are expected to be low in energy[3] ($\leq$ 0.5 MeV) . For the case of ^{231}Th, it decays to ^{231}Pa by beta emission, the beta end point energy being 380 keV. Thus for all the three isotopes under investigation, all the gamma rays are low in energy.

All the three nuclei are deformed and exhibit rotational bands. The deformation in a nucleus is brought about by the additional nucleons partially filling a shell outside the closed shell. As a result, the nucleus assumes an ellipsoidal shape, as shown
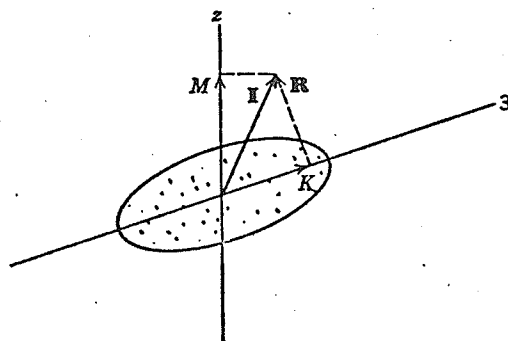
Usually, 1, 2 and 3 are the three axes of a reference frame fixed to the nucleus, and for convenience, the 3-axis is chosen to lie on the long axis of the ellipsoid as shown. (x,y,z) defines the laboratory fixed reference frame. Only the 3 and z-axes are shown. The detailed calculation has appeared in the literature[4], and will not be repeated here. In essence, the energy spectrum E_I due to the rotation of the nucleus is given by

$$E_I = E_o + \frac{\hbar^2}{2\vartheta}(I(I+1) - 2K^2)$$

where I is the total angular momentum of the nucleus, K is the projection of I on the 3-axis, and ϑ is the moment of inertia about the 1 or 2 axis. For the special case where K is zero,

$$E_I = E_o + \frac{\hbar^2}{2\vartheta}(I(I+1)).$$

In practice, there is a systematic deviation from this relation due to the coupling between the rotational motion and other modes of motion (vibrational, for example). Such a deviation could be corrected for by the addition of a term proportional to $[I(I+1)]^2$. Thus the energy levels of a rotational band can be approximated by the relation:

$$E_I = E_o + A(I(I+1)) + B(I(I+1))^2$$

here E_0, A and B are left as parameters to be adjusted. For the case where I=1/2, the rotational band can be described by the equation[5]:

$$E = E_0 + A(I(I+1)) + \delta_{\kappa,1/2} a (-1)^{I+1/2}(I+1/2)$$

where a is the decoupling parameter. $\delta_{\kappa,1/2}$ is the Kronecker delta.

In the present work, no attempt was made to measure the spins of the various levels, since the sources available were too weak to permit any gamma-gamma angular correlation experiments to be carried out. However, from the fairly reliably measured gamma energies and coincidence data, it is possible to determine the energies of the various levels, and a brief discussion is given at the end of each Chapters III, IV and V on the rotational structure of the nucleus under investigation.

CHAPTER I

I.1 INTRODUCTION

In this chapter, a discussion of the equipment
used throughout this work is presented. High
resolution semi-conductor detectors will be described,
but emphasis will not be placed on the physical
response or manufacturing details of such detectors.
Rather, the parameters of these detectors relevant to
the experimental work, will be presented. These
include resolution, detection efficiencies and
calibration. Where the equipment and its configuration
is conventional, the description given will be brief. A
gamma-gamma coincidence circuit is also presented and
discussed.

I.2 SEMI-CONDUCTOR DETECTORS

Ever since their invention, semi-conductor
detectors[1] have become very powerful tools to nuclear
spectroscopists. The advantage of these detectors over
the conventional ones (such as NaI(Tl) scintillators
and proportional counters) lies in their high
resolution[2,3]. This means that spectra taken with such
detectors yield much better detail: photopeaks that are
close together are more readily observable as they are

5

Table 1-1

Semi-conductor detectors

DETECTOR	SIZE	RESOLUTION	WINDOW	OPERATING VOLTAGE
Nuclear Diode	50 cc.	2.0 KeV at 1.33 MeV	0.5 mm Al	+2800 Volts
Ortec Ge(Li)	35 cc.	3.0 KeV at 1.33 MeV	0.5 mm Al	+1700 Volts
Ortec Ge(Li) X-ray	80 mm^2	250 eV at 5.9 KeV 523 eV at 122 KeV	0.13 mm Be	-1000 Volts
Ortec Ge(Li) X-ray	80 mm^2	290 eV at 5.9 KeV 560 eV at 122 KeV	0.25 mm Be	-1000 Volts
Kevex Si(Li) X-ray	80 mm^2	240 eV at 6.5 KeV	0.05 mm Be	- 900 Volts

not masked or overlapped by the neighbouring stronger ones. Also, a photopeak occupies only a small region of the spectrum taken with high resolution detectors, and relatively simple methods can be devised so that spectral analysis (namely, the determination of the energies and intensities of the photopeaks) can be performed by a computer. This will be elaborated in detail in Chapter II.

In the present work, two common types of semi-conductor detectors are used. They are lithium drifted silicon detectors Si(Li) and lithium drifted germanium detectors Ge(Li). Si(Li) detectors are excellent for examining gamma rays whose energies lie below 40 keV. Above 40 keV, their detection efficiency drops off very rapidly. However, they do have excellent resolution as well as a large peak to background ratio. Above 40 keV, Ge(Li) detectors become indespensible. Both Si(Li) and Ge(Li) detectors are superior to the NaI(Tl) scintillator detectors in that they have much better resolution, but are inferior in terms of efficiency. Even the large volume Ge(Li) detectors are seldom more than 10% as efficient as a 3"x3" NaI(Tl) detector, and in the case of Si(Li) detectors, the efficiency is even lower. Table I-1 shows the various detectors used, together with their

7

Figure I-1

A Ge(Li) gamma ray detector system
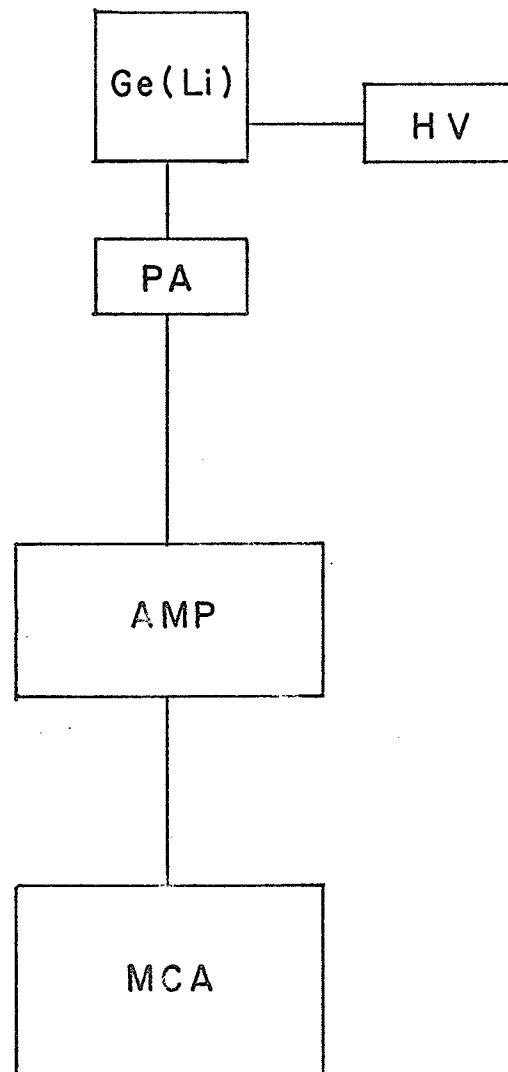
relevant parameters.

I.3 ASSOCIATED ELECTRONICS

To use semi-conductor detectors as spectrometers meaningfully, suitable pieces of electronic equipment are required. A typical arrangement is shown in Figure I-1. The output of the detector is fed into a pre-amplifier (PA) attached to the cryostat, and the signal is further magnified by the main amplifier (AMP). The amplifier output pulses, typically under 10 volts, are fed into a multi-channel analyser (MCA). In this work, the pre-amplifiers are normally supplied with the detectors for the following reason. The inherent problem in any electronic system is noise; maintaining the noise level at a minimum in the pre-amplifier stage is especially important, since the noise is amplified along with the real signals by the main amplifier, and hence degrades the resolution. In most detectors manufactured nowadays, a field effect transitor (FET) is used in the first stage of the pre-amplifier, and in order to minimize noise, the FET is cooled to liquid nitrogen temperature. Further, in order to attain the best resolution, the capacitance at the pre-amplifier should be kept minimal by keeping the cable connection between the detector and the pre-amplifier as short as possible. For these reasons,

the pre-amplifier is mounted on the cryostat casing and is supplied with the detector.

Two makes of amplifiers are used throughout this work. They are

(i) Tennelec TC200

(ii) Canberra 1417b.

The latter has the advantage that there is a built in pole-zero adjustment arrangement so that one can minimize pulse overshoot with ease.

The two multi-channel analysers used are:

(i) a Nuclear Data 160 dual ADC analyser with 1024 channels. Two parameter analysis is possible with this analyser.

(ii) a Nuclear Data 2200 analyser with three 4096 channel ADC's interfaced to a 4096 channel memory. This unit can be used as one, two or three analysers.

I.4 CALIBRATION

In order to use semi-conductor detectors as spectrometers, they must be calibrated so that the energies and intensities of the photopeaks can be determined.

(a) Energy calibration:

Energy calibration is carried out by collecting the spectrum of the isotope under study together with

10

Table I-2

IEAE gamma ray energy standards

ISOTOPE	HALF-LIFE	E_γ (KeV)
^{241}Am	458 years	59.536 ± 0.001
^{57}Co	268 days	122.061 ± 0.010
		136.471 ± 0.010
^{139}Ce	140 days	165.853 ± 0.007
^{203}Hg	47 days	279.190 ± 0.006
^{22}Na	2.6 years	511.006 ± 0.002
		1274.55 ± 0.04
^{137}Cs	30 years	661.635 ± 0.076
^{54}Mn	314 days	834.81 ± 0.03
^{88}Y	108 days	898.04 ± 0.04
		1836.13 ± 0.04
^{60}Co	5.26 years	1173.23 ± 0.04
		1332.49 ± 0.04

Table I-3

Secondary gamma ray energy standards

ISOTOPE	HALF-LIFE	E_γ (KeV)
^{182}Ta	115 days	67.750 ± 0.001
		84.680 ± 0.002
		100.105 ± 0.001
		113.673 ± 0.002
		116.418 ± 0.002
		152.434 ± 0.002
		156.387 ± 0.002
		179.393 ± 0.003
		198.356 ± 0.004
		221.110 ± 0.003
		229.322 ± 0.006
		264.072 ± 0.006
^{75}Se	120 days	96.732 ± 0.007
		121.113 ± 0.010
		135.998 ± 0.010
		198.600 ± 0.020
		264.651 ± 0.015
		279.525 ± 0.012
		303.895 ± 0.020
		400.640 ± 0.015
^{133}Ba	7.2 years	80.998 ± 0.008
		276.397 ± 0.012
		302.851 ± 0.015
		356.005 ± 0.017
		383.851 ± 0.020

the spectrum of the energy calibration standard sources. These standards are members of a set of radioactive nuclides whose gamma ray energies are accurately known[5-9]. The energies of the unknown photopeaks can then be inferred by interpolating between the calibration lines. Table I-2 lists the set of standards used. This set is obtained from ILAE, Vienna.

It was soon found that for accurate energy calibration, such a set of standards was far from being adequate. A second set of secondary standards was therefore adopted. They consist of the gamma rays of ^{75}Se, ^{133}Ba and ^{182}Ta. The energies of their gamma rays had been carefully measured[8-10] and are listed in Table I-3.

In addition, the well known" characteristic X-rays of various elements were used to calibrate the low energy portion of the spectrum. The X-rays may be produced in a radioactive decay, or as a result of electron capture, or by fluorescence. The characteristic X-rays may be produced by fluorescence by creating a vacancy in one of its electron shells using charged particles, other X-rays or gamma rays. In the present work, gamma rays were exclusively used. In all cases, the spectra of the X-rays are fairly well

13

L X-ray spectrum of Np

Figure 1-2

COUNTS PER CHANNEL

CHANNEL NUMBER

$L_{III} M_I$ 11·890

$L_{III} M_{IV}$ 13·7597
$L_{III} M_V$ 13·9441

$L_{II} M_I$ 15·876
$L_{III} N_I$ 16·13

$L_{III} N_V$ 16·840
$L_I M_{II}$ 17·989

$L_{II} M_{IV}$ 17·7502
$L_I M_{III}$ 17·989

$L_I M_{IV}$ 18·57
$L_I M_V$ 18·756

$L_{II} N_I$ 20·12

$L_{II} N_{IV}$ 20·7848

$L_I N_{II}$ 21·11
$L_I N_{III}$ 21·34

$L_I O_{II,III}$ 22·20
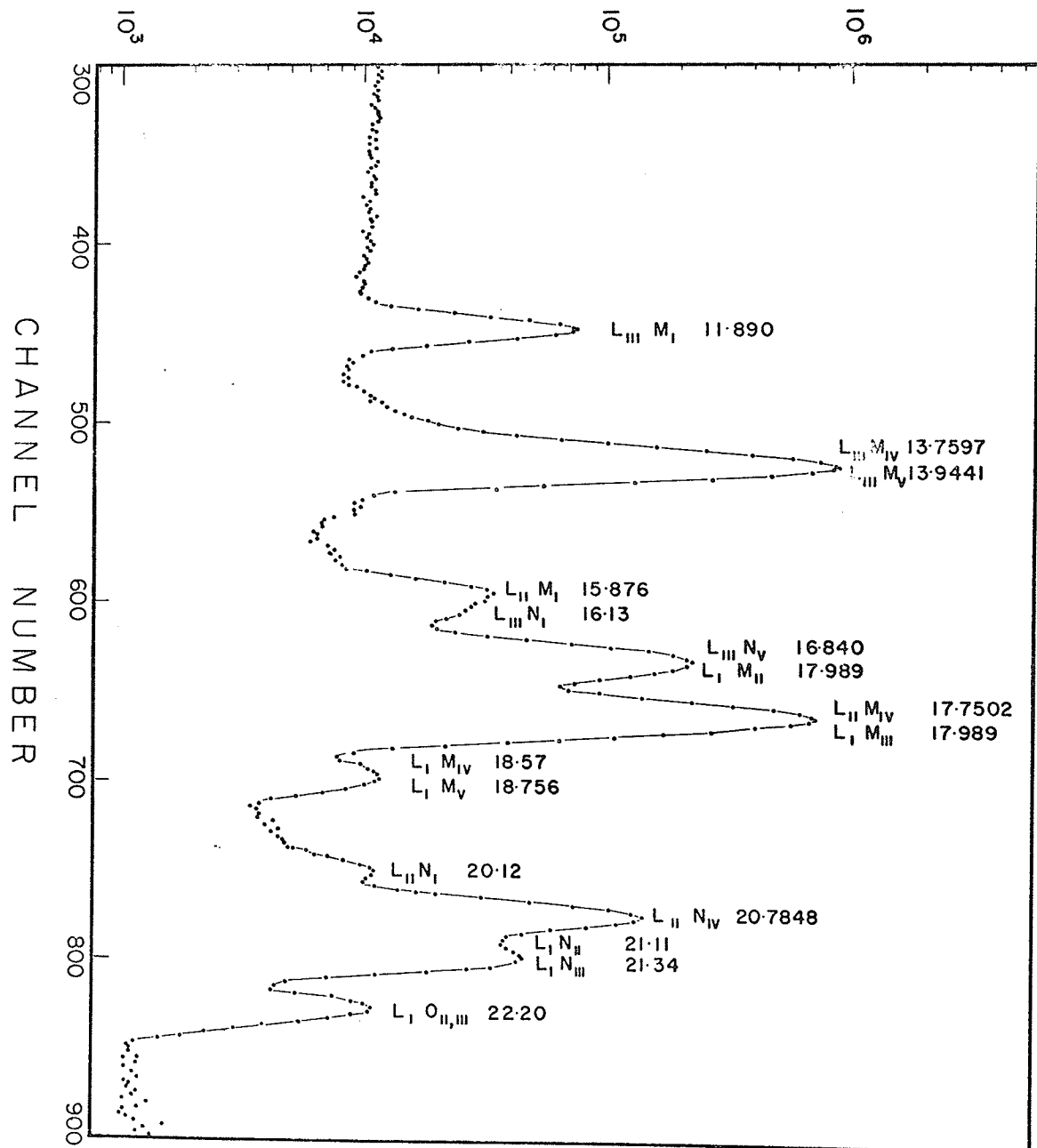
Figure I-3

K Xray spectrum of Ag
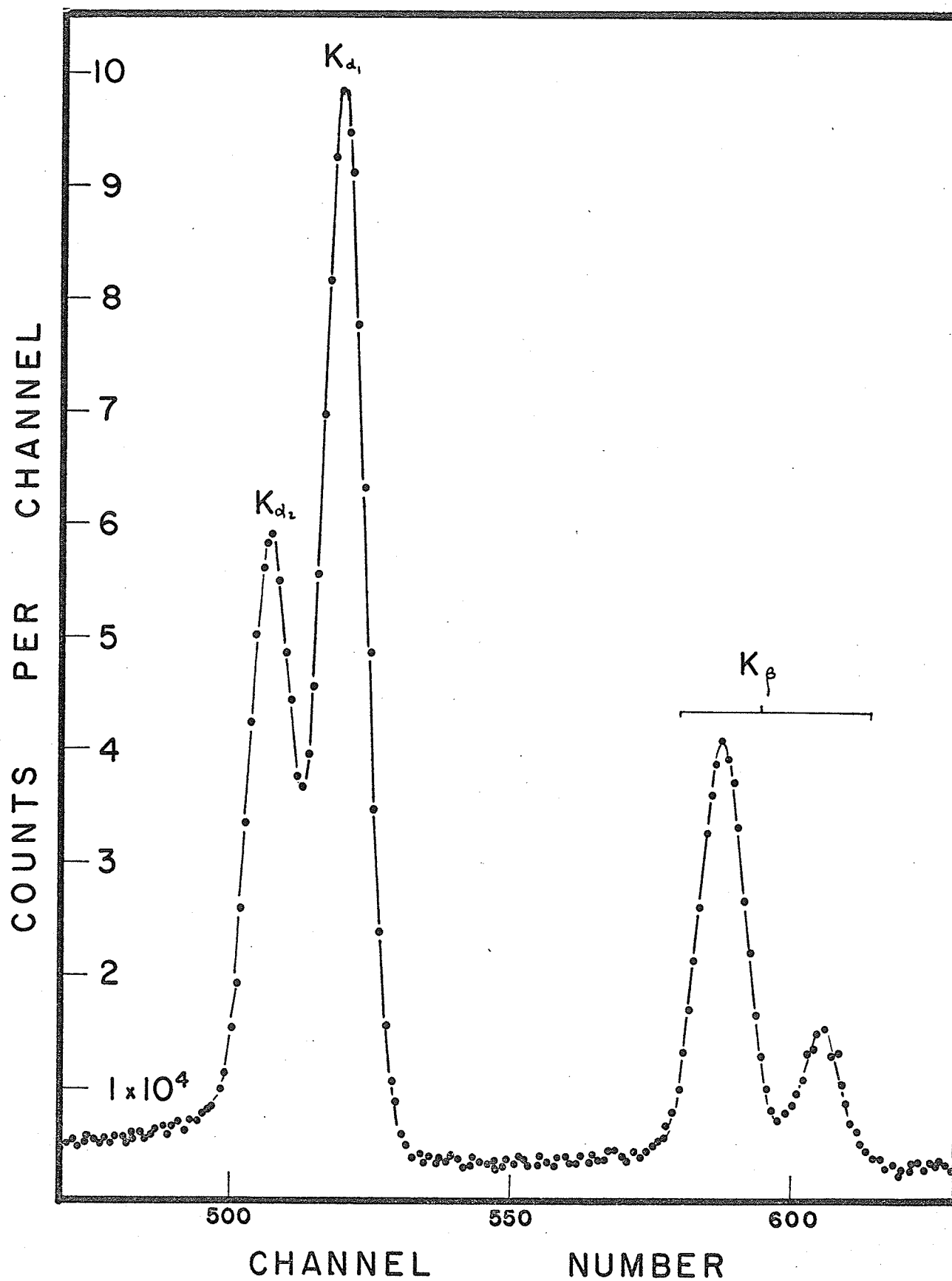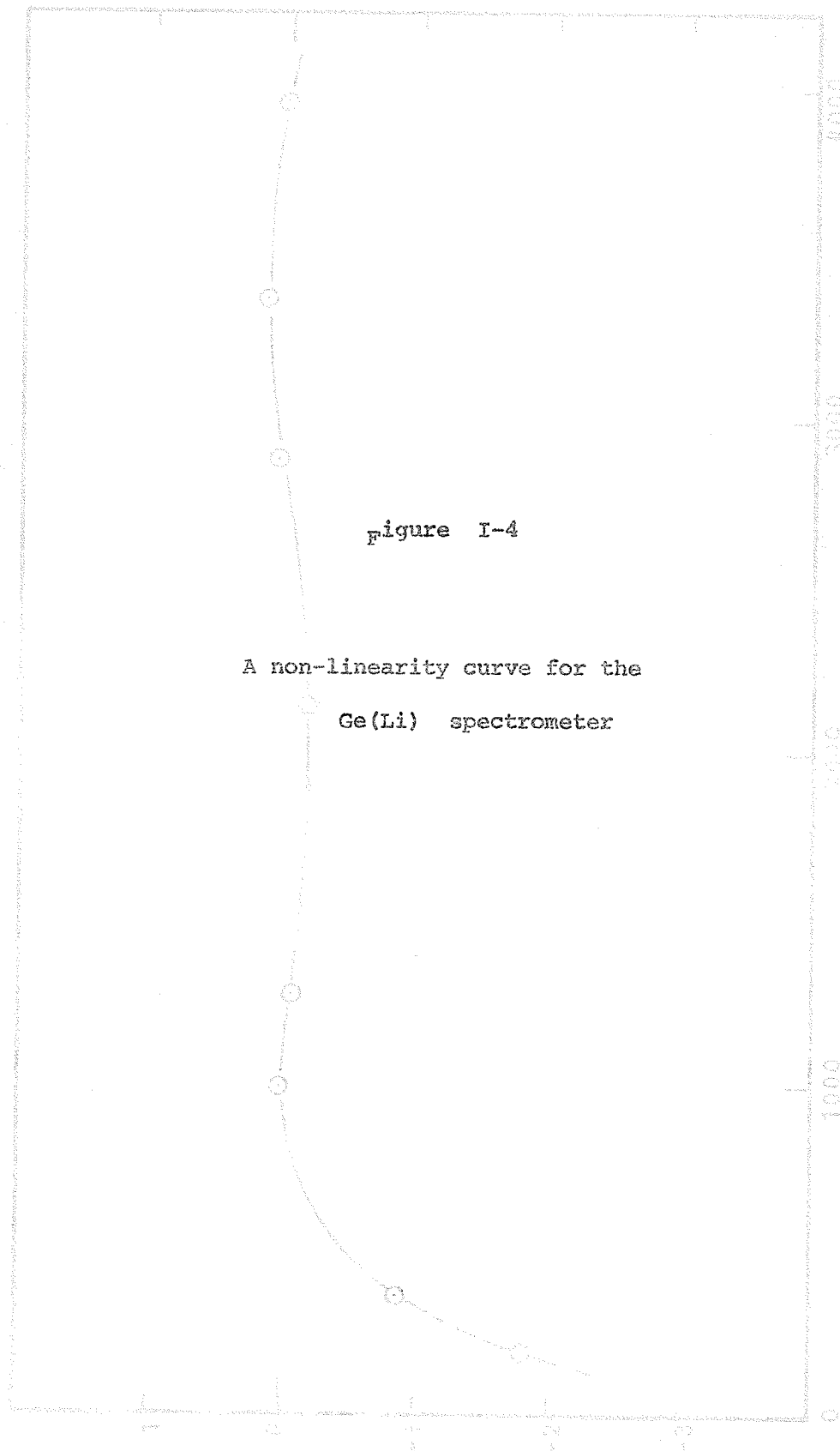
Figure I-4

A non-linearity curve for the

Ge(Li) spectrometer

Table I-4

Components of X-rays

used as energy standards

DESIGNATION	ORIGIN	ENERGY (KeV)
L_ℓ	$L_{III} - M_I$	2.6337
L_{α_2}	$L_{III} - M_{IV}$	2.97821
L_{α_1}	$L_{III} - M_V$	2.98431
K_{α_2}	$K - L_{II}$	21.9903
K_{α_1}	$K - L_{III}$	22.16292

known. Figure I-2 shows an L X-ray spectrum of Np, produced by internal conversion as a result of the alpha decay of ^{241}Am into ^{237}Np, taken with a Kevex Si(Li) X-ray detector having a resolution of 240 eV at 6.5 keV. Figure I-3 shows a typical K X-ray spectrum of Ag produced by fluorescence, by irradiating a silver foil with the 60 keV gamma ray from ^{241}Am. From the apparent complexity of the X-ray spectra, it is evident that only some of the components are suitable as energy calibration lines. They are listed in Table I-4. The energies quoted are those of silver X-rays. It should be noted that only the L X-rays of the heavy elements are suitable as calibration standards since the L X-rays of the light elements are too low in energy to be of any practical use. The energies of the various components of the X-rays of different elements had been carefully measured using bent crystal spectrometers by Bearden[11], and his values are adopted throughout the course of this work.

(b) Non-linearity corrections:

Ideally, a pulse height analysis system as shown in Figure I-1 should have a linear response, namely the position of a photopeak in a spectrum should be directly proportional to its energy, and the energy-channel number graph should be a straight line.

17

In practice, the linearity of such a system is only fair, with deviations from linearity being most severe at low energies. Corrections therefore has to be made if very accurate energy calibration is desirable. This can be done by means of a non-linearity curve constructed in the following manner. A set of sources whose photopeak energies are well known is put in front of the detector, and a spectrum is collected. Two suitable peaks are chosen, and a linear function of energy versus channel number is defined from their energies and positions. The energies of the other lines are calculated from their positions, using this function, and the deviations δ from their actual energies are plotted versus their positions (channel numbers). Such a graph is refered to as the non-linearity curve. A typical non-linearity curve is shown in Figure I-4. It can be seen that the deviation is most severe below channel 200. In general, the non-linearity depends on the detector used, the pre-amplifier, the main amplifier and to a greater extend, on the multi-channel analyser, so that a non-linearity curve must be constructed for each detector-analyser combination.

An alternative (and simpler) method of accounting for the system non-linearity is to perform a polynomial

Table I-5

Energies of gamma rays from

^{233}Pa   decay

ECIDY	CLINE	Nonlinear curve	Polynomial Fit
75.28 ± 0.01		75.28 ± 0.01	75.26
86.59 ± 0.01		86.59 ± 0.01	86.58
103.86 ± 0.02	103.864 ±0.010	103.865± 0.005	103.87 ± 0.01
271.48 ± 0.08	271.58 ± 0.04	271.53 ± 0.03	
300.12 ± 0.03	300.24 ±0.010	300.10 ± 0.010	300.14
311.98 ± 0.03		311.88 ± 0.01	311.92
340.50 ± 0.04	340.47 ±0.020	340.45 ± 0.01	340.49
375.45 ± 0.04	375.40 ± 0.05	375.35 ± 0.02	375.39
398.62 ± 0.08	398.49 ± 0.02	398.57 ± 0.05	398.36
415.76 ± 0.04	415.78 ± 0.02	415.76 ± 0.06	415.65

Table I-6

IEAE efficiency calibration

standards

Isotope	Activity (μC)	E (KeV)	Photons per 100 Disint.
^{241}Am	10.35 ± 0.6%	11.9	0.8 ± 0.1
		13.9	13.5 ± 0.3
		17.8	18.4 ± 0.4
		20.8	5.0 ± 0.1
		26.3	2.5 ± 0.2
		59.5	35.9 ± 0.6
^{57}Co	11.3 ± 0.9%	14.4	9.5 ± 0.03
		122.	85.0 ± 1.7
		136.4	11.4 ± 1.3
^{203}Hg	21.02 ± 1.0%	72.8	9.7 ± 0.5
		82.5	2.8 ± 0.2
		279.2	81.55± 0.15
^{22}Na	9.98 ± 0.9%	511.0	179.7 ± 0.8
		1274.6	99.95± 0.02
^{137}Cs	11.04 ± 1.3%	661.6	85.1 ± 0.4
^{54}Mn	11.09 ± 0.7%	834.8	100.
^{60}Co	11.13 ± 0.6%	1173.2	99.74±0.05
		1333.5	99.85± 0.03
^{88}Y	10.75 ± 0.9%	511.0	0.4 ± 0.02
		898.0	91.4 ± 0.7
		1836.1	99.4 ± 0.1
		2734.2	0.62±0.04

Figure I-5

Efficiency curve of Ge(Li)

detector

Absolute efficiency
Nuclear Diode 50 cc
Source to Window
    distance = 6.0 cm.
April, 1970
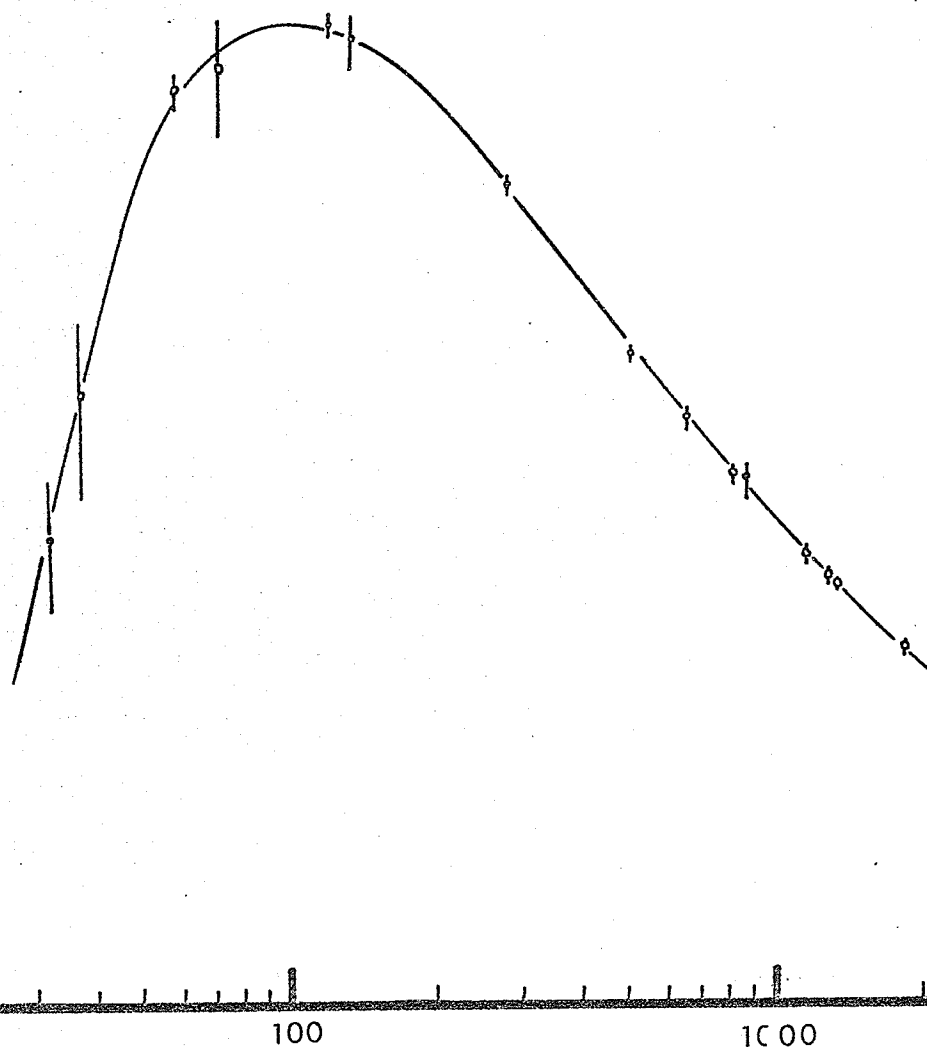
window at the source). Hence a set of calibration sources is required, and each detector has to be calibrated separately since the active volumes of two detectors are seldom, if ever, identical. The set of efficiency calibration standards issued by IEAE is shown in Table I-6. These standards are radioactive nuclides whose source strength had been carefully measured so that at any given moment, the absolute number of photons emitted can be calculated.

In an efficiency calibration process, a calibration source is put in front of the detector to be calibrated at a prescribed distance from the detector window. The number of counts in the photopeak is determined and is divided by the collection time to yield the rate N. This is then compared to the known number of photons emitted per second (N_0) by the source material, thereby yielding the efficiency e(E) at the energy (E) of the incident photon. This process is repeated for photons of various energies. A plot of the efficiency versus energy gives an efficiency curve for that geometry. One such curve is shown in Figure I-5. Subsequently, the intensity of a photopeak in an unknown spectrum may be obtained by taking the spectrum under the same geometrical conditions and dividing the number of counts under the photopeak by

Figure I-6

Efficiency curve of the

Ortec Ge(Li) X-ray detector

Absolute efficiency
Ortec Ge(Li)
X-ray detector
Source to window
distance = 1.0 cm
January, 1972

ENERGY (keV)
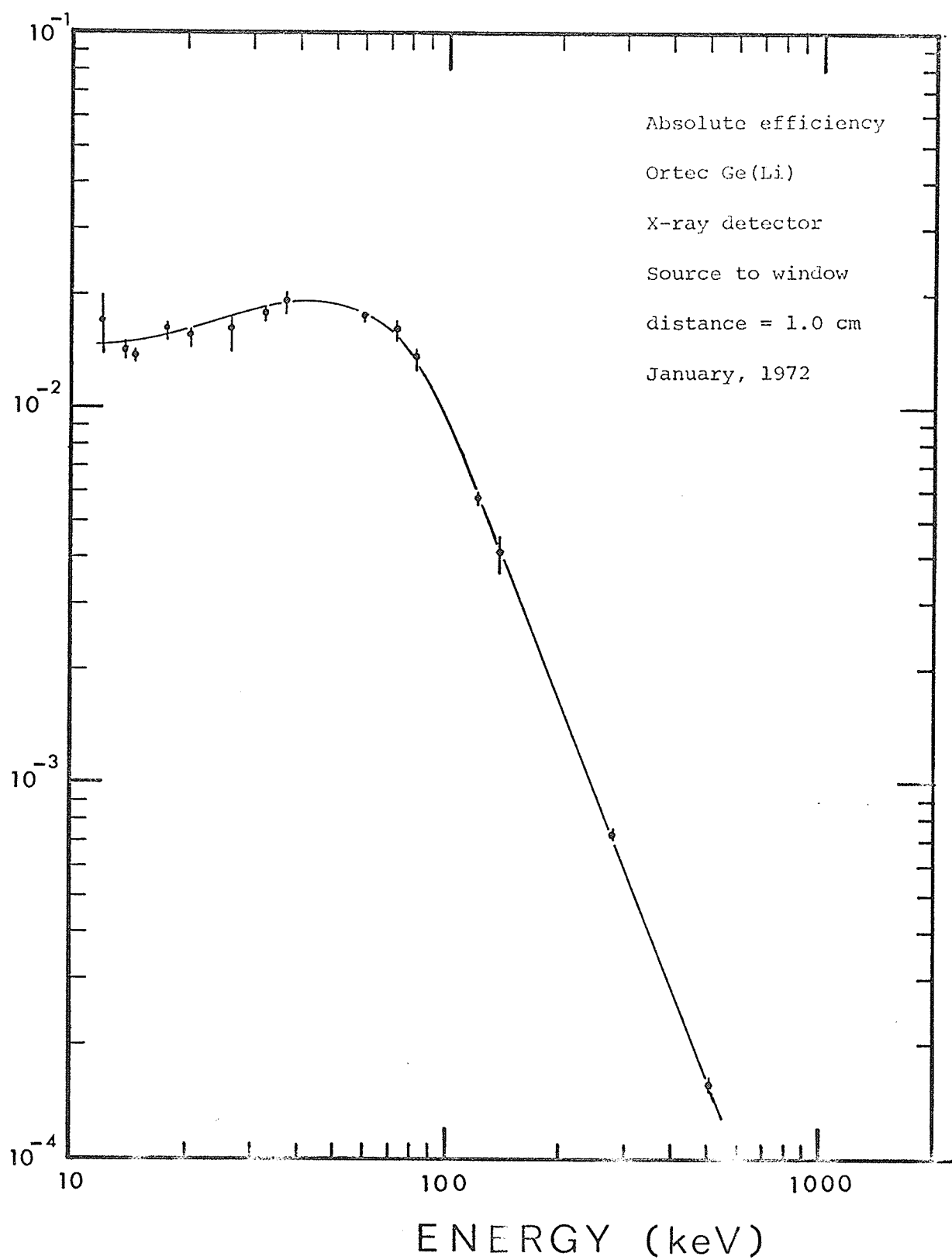
the efficiency (obtained by interpolation from the efficiency curve) at the same energy. For the sake of completeness, the efficiency curve of the Ortec Ge(Li) X-ray detector is shown in Figure I-6.

It should be noted that in both energy and efficiency calibration, the positions and areas of the photopeaks are required. A numerical method to obtain these quantities from a spectrum will be given in Chapter II.

I.5 A COINCIDENCE SYSTEM USING SEMI-CONDUCTOR DETECTORS

Semi-conductor detectors used in pairs can be made to yield information beyond the gamma ray energies and intensities.[5] A pair of semi-conductor detectors, together with the necessary electronics, can be used to determine the gamma rays that are in coincidence with each other. Such a mode of operation is generally refered to as gamma-gamma coincidence, and provides a very powerful technique in studying the decay scheme of a radioactive nuclide. In essence, one uses a detector to gate on a particular gamma ray of interest, and uses the other detector to look for coincident radiations. For simplicity, the electronics associated with the gating detector will be refered to as channel 1, while those associated with the other detector will be designated as channel 2.

Figure I-7

A simple coincidence circuit

using

two semi-conductor detectors

S

| PA | — | DET2 |

DET1 | — | PA |

AMP

AMP

DA

SCA

LG → MCA
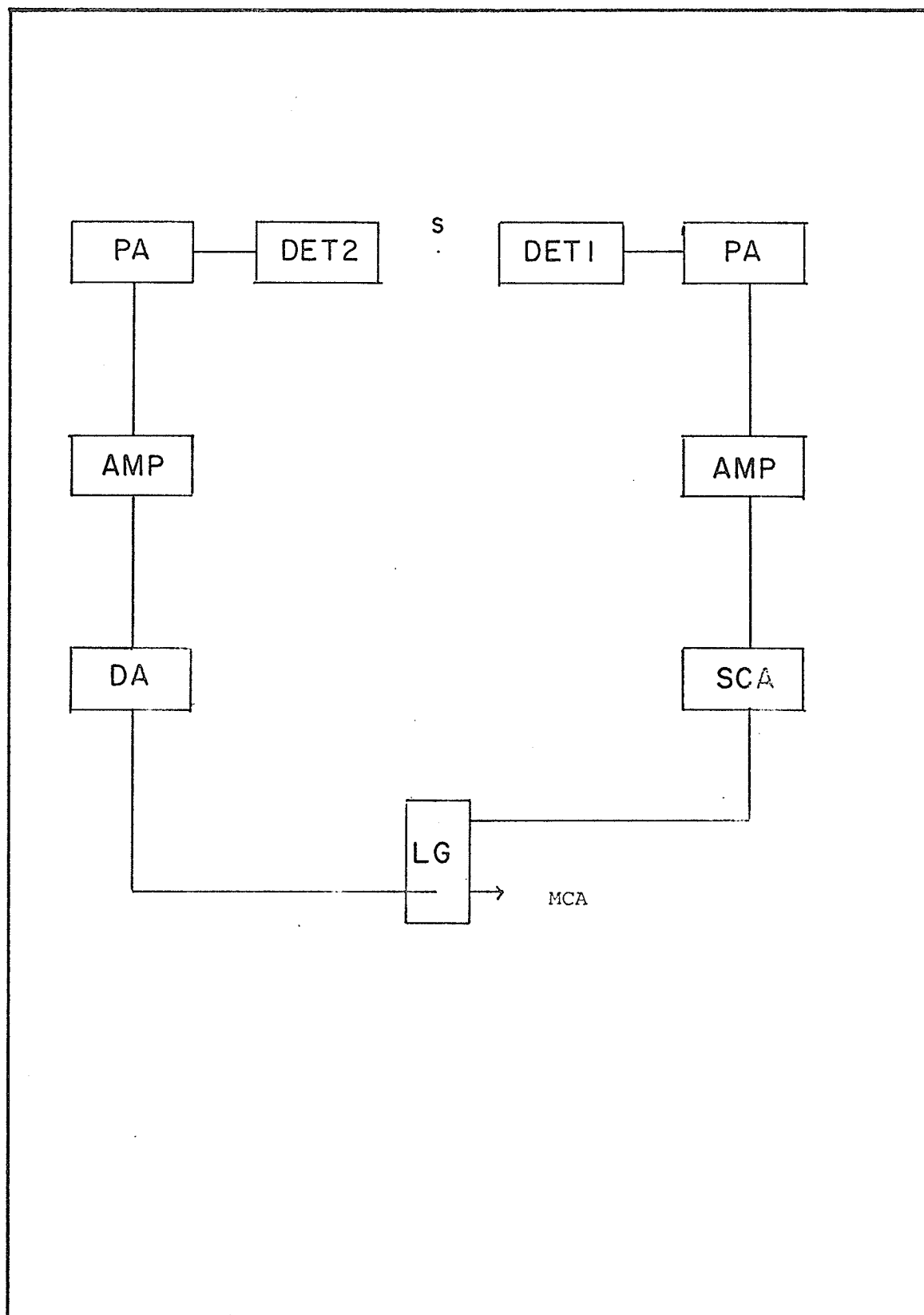
Figure I-7 shows a coincidence circuit that is rudimentary but workable. Here, detector 1 is the gating detector. The single channel analyser (SCA) is inserted after the main amplifier (AMP) in channel 1. If the amplifier output pulses satisfy the energy requirements (that is, they correspond to the gamma ray one is gating on, using the SCA), a logic pulse is generated by the SCA to open the linear gate (LG), thereby permitting the amplifier pulses from channel 2 to pass through. A delay amplifier (DA) is inserted in channel 2 to allow for the delay in the SCA. Only the pulses corresponding to the gamma rays in cascade with the gate will be allowed to pass through the gate, consitituting the true coincident events. But because of the finite resolving time of the system, pulses which do not satisfy the energy requirements may also pass through the gate by chance, constituting the random events. The ratio of true to random events is a measure of the performance of the coincidence system. It should be noted that the relative intensities of the gamma rays collected due to random events are in the same ratio as that in the singles spectrum, although they are much reduced in intensity. When pulses are collected in the multi-channel analyser, one obtains a pulse height spectrum consisting of random events

Figure   I-8

A conventional

fast-slow coincidence circuit
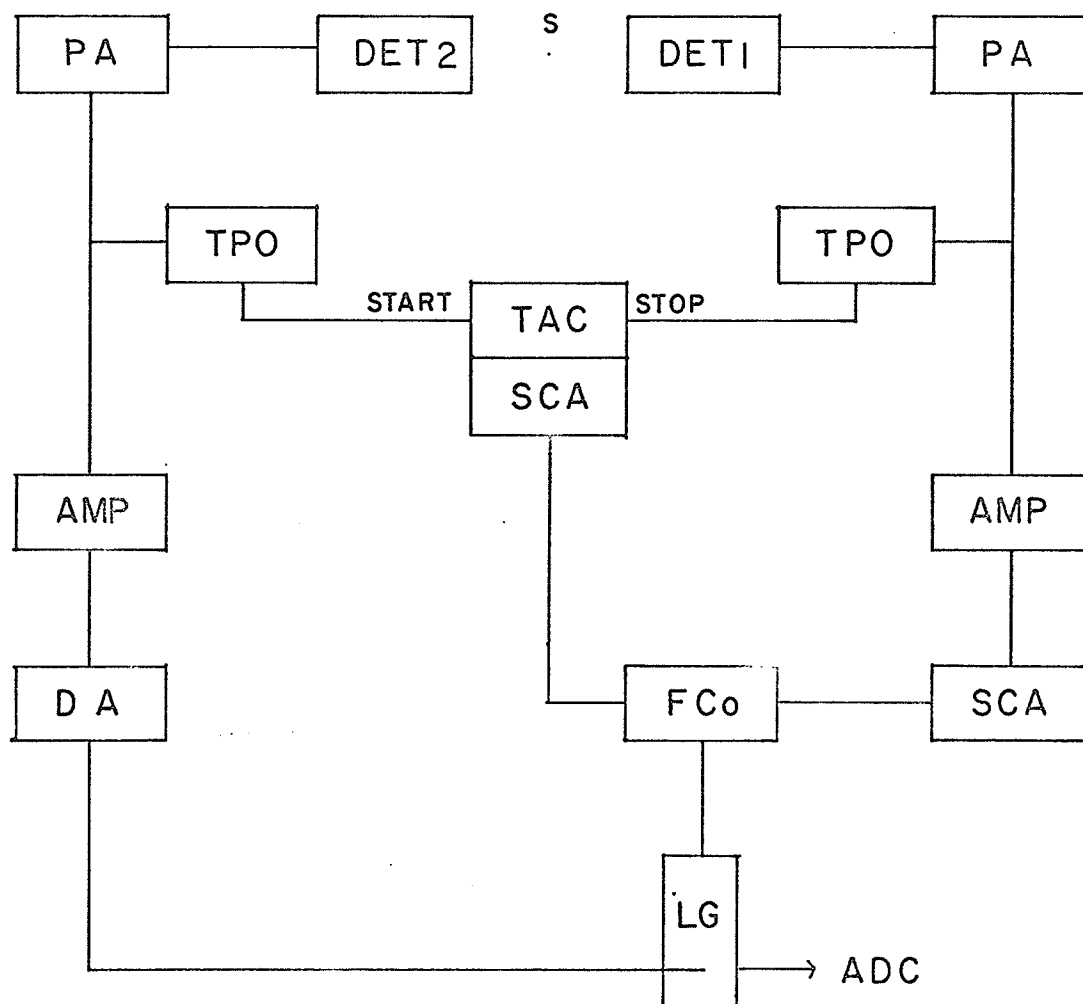
superimposed on the strongly enhanced true coincident counts. A spectrum collected in the multi-channel analyser this way is generally refered to as the coincidence spectrum.

As mentioned above, this circuit is workable, but is not very satisfactory, because of the following reason: Two gamma rays appear in coincidence if one of them is emitted within a short time of each other. If a coincidence circuit is to function properly, the true coincident events must take place within the time resolution of the system. In short, in addition to an energy requirement mentioned above, a time requirement is also needed. To impose such a requirement, a 'fast circuit' is inserted[16] as shown in Figure I-8. Timing can be effectuated by using a pair of time-pick-off units (TPO) on each channel. Each time a fast rising pre-amplifier pulse enters the TPO, a fast logic pulse is generated and appears at the output of the TPO. These pulses are fed into the start and stop inputs of a time-analogue-converter (TAC). The TAC output consists of pulses whose height is proportional to the time difference between the start and stop pulses. A pulse height spectrum yields a time spectrum. In the present work, the TAC has a built-in SCA so that one can reject any timing events that take place outside

Figure I-9

circuit used for

measuring time resolution
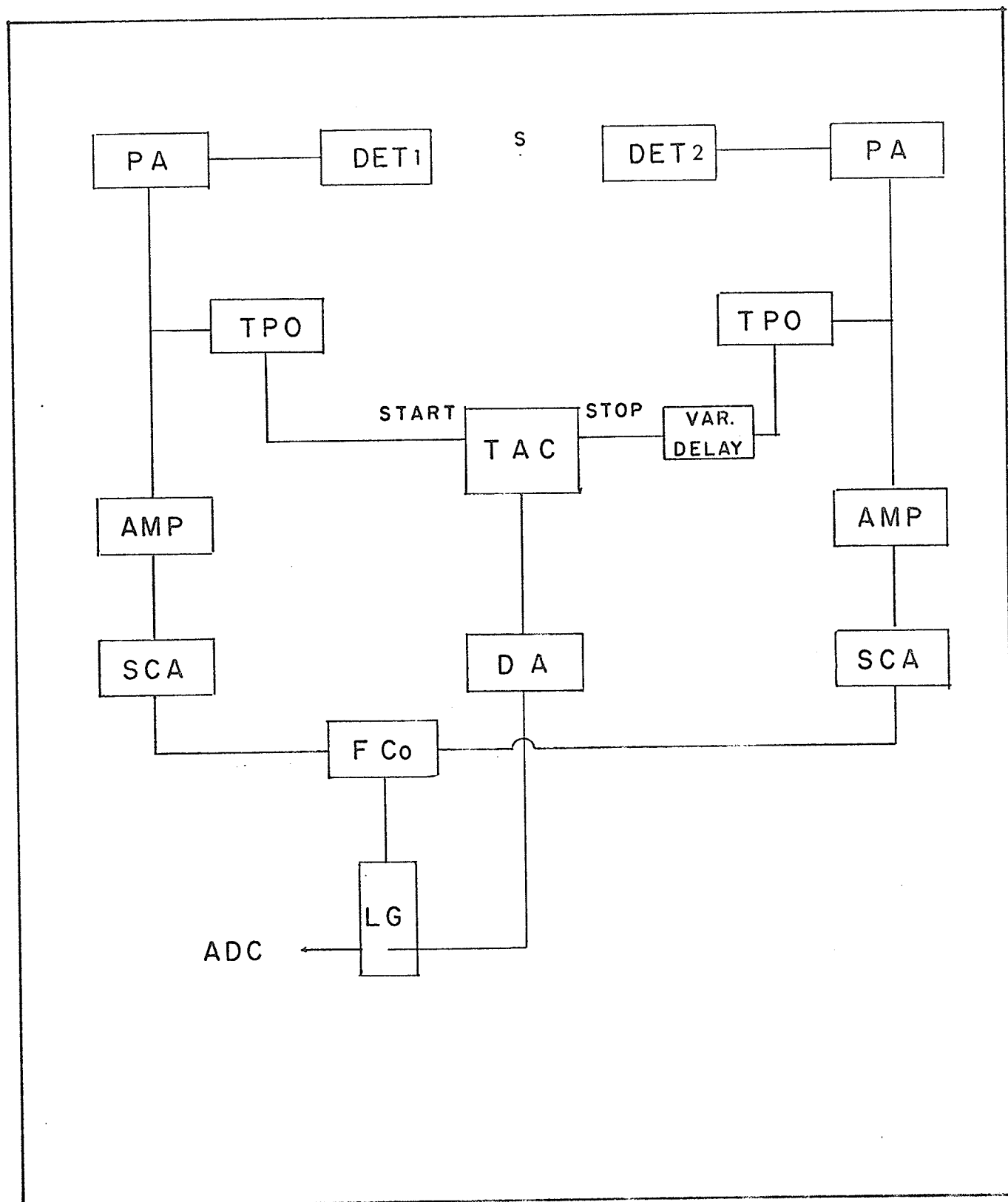
the resolving time of the system. A further disussion
on the time resolution will be given later in this
chapter.

The TAC and SCA output will generate a logic pulse
if they arrive at the fast coincidence (FCo) at the
same time, and the FCo output is used to open the
linear gate. Only those amplifier pulses from channel 2
which satisfy both the time and energy requirement can
pass through the linear gate. Such a conventional
fast-slow type coincidence circuit is adopted through
the course of the present work. The time resolution of
such a system is of the order of 50 nanoseconds, and a
true to random ratio of 40 to 1 can be achieved, as in
the present case.

To measure the time resolution of the system, the
circuit used is as shown in Figure I-9. A radioactive
isotope known to have a very short lived state and well
isolated gamma rays populating and de-exciting this
state is used. The SCA in channel 1 is used to gate on
the gamma ray populating this state while the output of
the TPO in the same channel is used to start the TAC.
The SCA in channel 2 is used to gate on the other gamma
ray de-populating the same state, while the TPO output
in this channel is used to stop the TAC. The SCA
pulses in both channels, when reaching the FCo at the

Figure I-10

Time spectrum with different delays
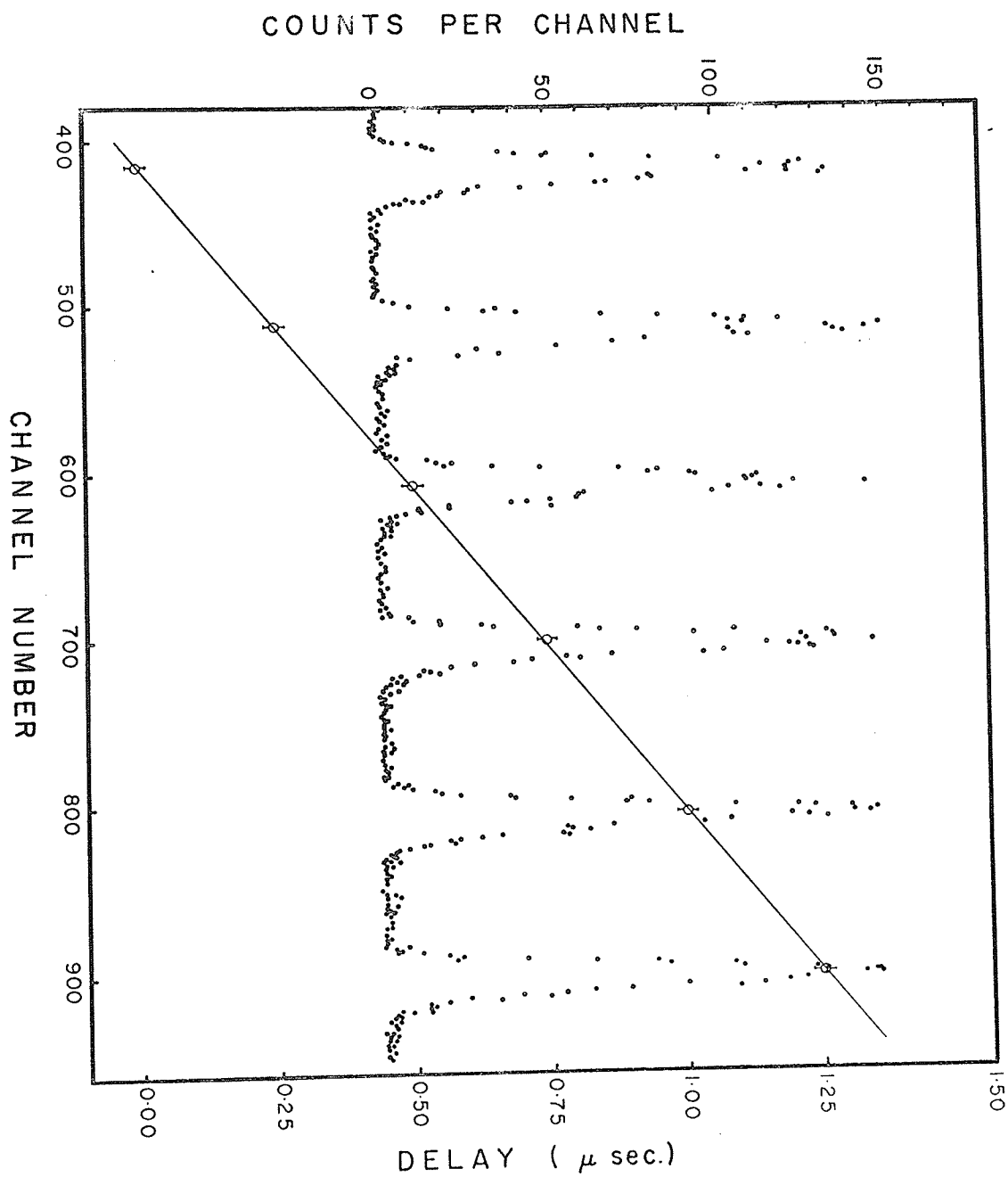
Figure I-11

Decay scheme for the

^{75}Se decay
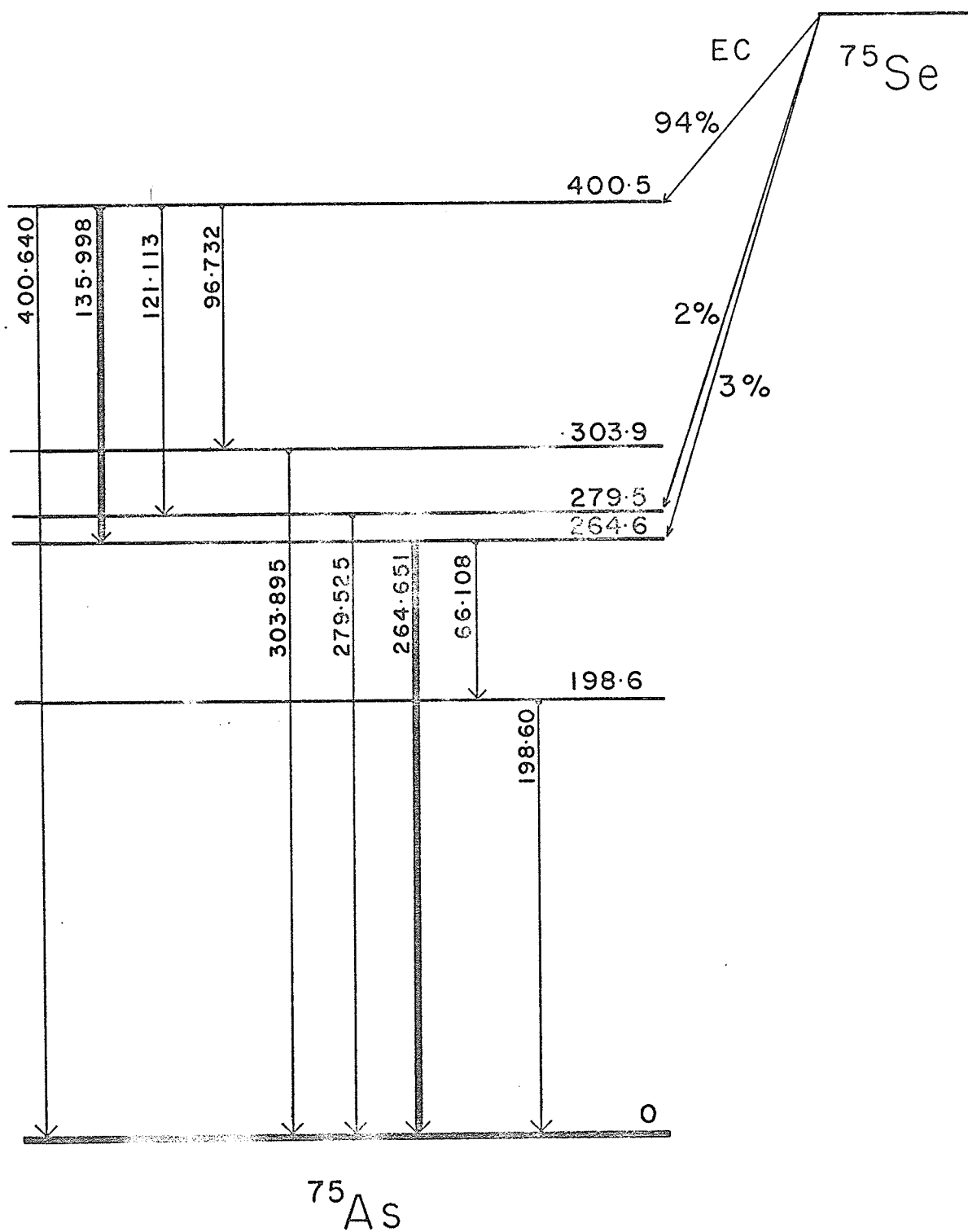
same time, opens the LG to let the TAC pulses pass through. A time spectrum can be collected in the MCA, and the position and the FWHM (in channels) of the time peak is noted. A known delay is introduced in the stop signal into the TAC, thereby shifting the position of the time peak. The process can be repeated , and a plot of the delay introduced versus the position of the time peak (in channels) gives a straight line (see Figure I-10) and from the slope, one obtains the conversion factor in delay per channel. The time resolution is simply the full width at half maximum (FWHM) of the time peak expressed in units of time, obtained by multiplying the FWHM (in channels) by the conversion factor.

It is known that irregular charge collection time in the detector crystal can affect the time resolution of the system.[17] This effect is strongly geometry dependent. To illustrate this, a coincidence system was set up using two Ge(Li) detectors. The source chosen was ^{75}Se, and the relevant part of the decay scheme is shown in Figure I-11. The gates were set on the 135.998 and 264.651 keV gamma rays. The lifetime of the level populated by the 135.998 keV gamma ray is known to be 10.9 picoseconds,[18] and as far as the present system is concerned, it may be considered as prompt.

Figure I-12

Detector arrangement to demonstrate

the effect of geometry

on the time resolution

GEOMETRY A

135°

×
SOURCE

50 cc Ge(Li)

35 cc
Ge(Li)

GEOMETRY B

SOURCE

50cc Ge(Li)

×

35cc
Ge(Li)

LEAD   COLLIMATOR
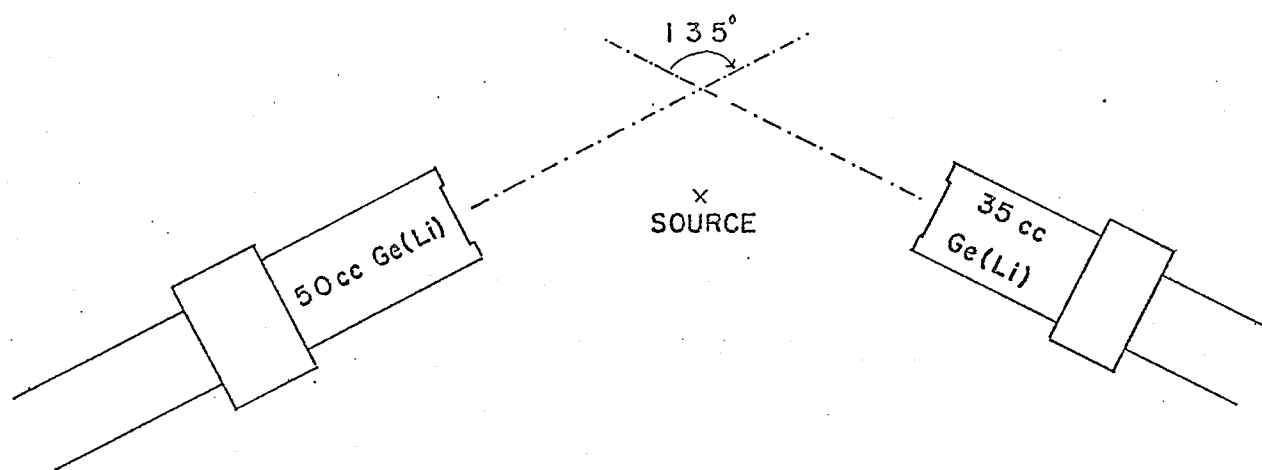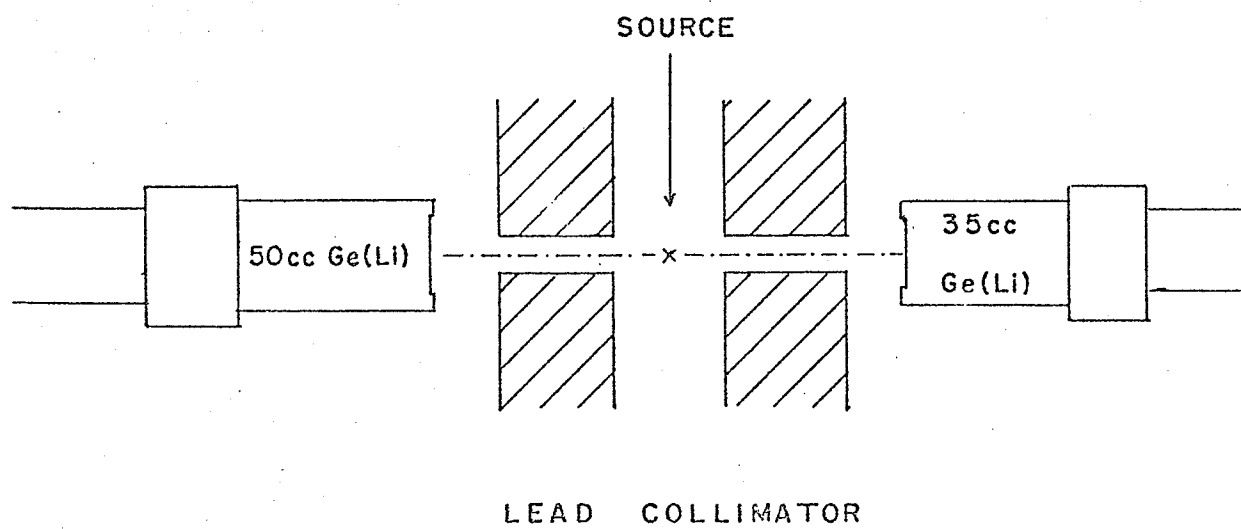
Figure I-13

Time   spectra   obtained

for the two geometries in Fig. I-12
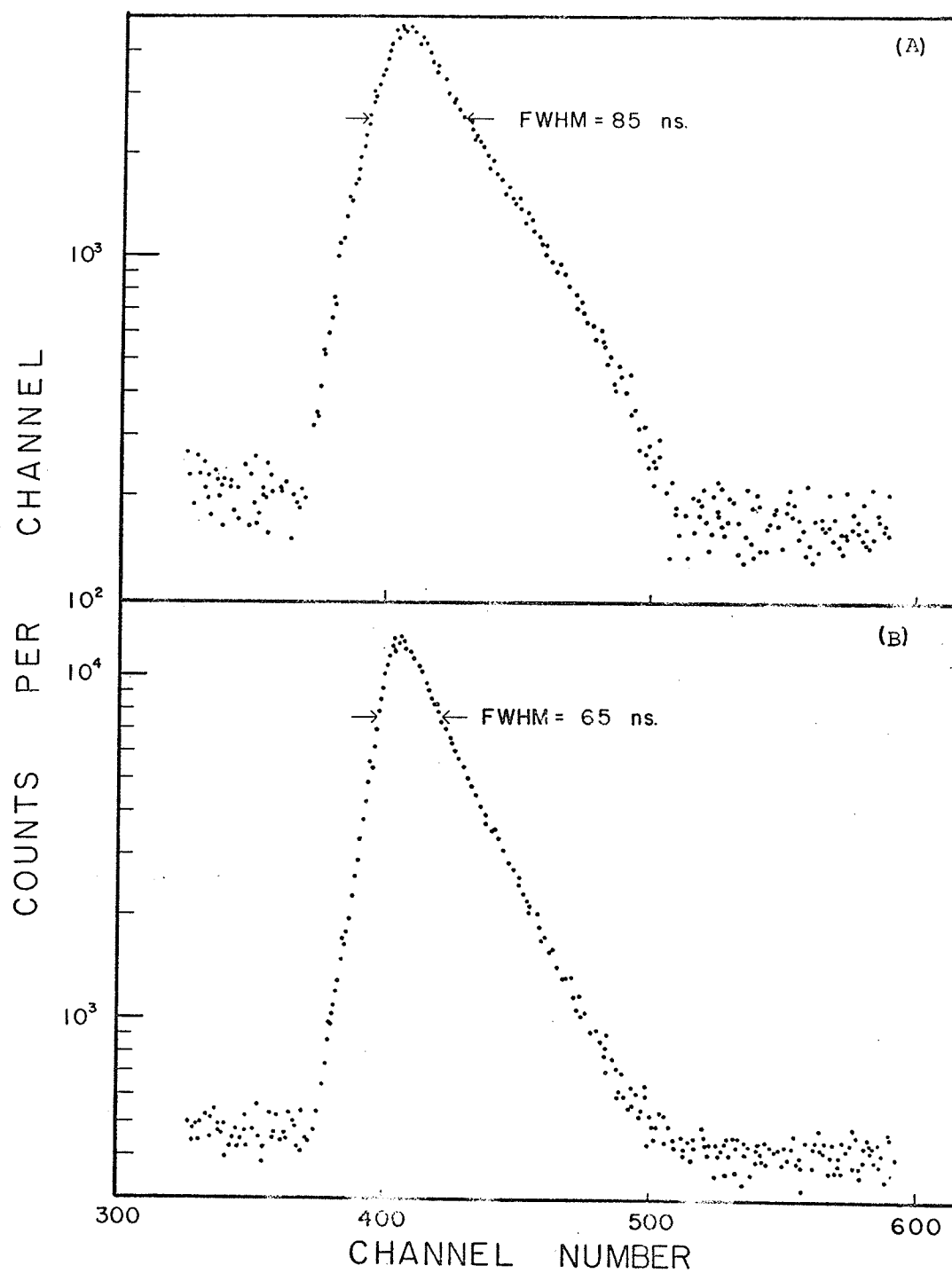
Figure I-14

(a) Self gated singles of ^{75}Se

(b) Coincidence spectrum with the 264.651 keV
     gamma ray

(c) Coincidence spectrum with the 135.998 keV
     gamma ray
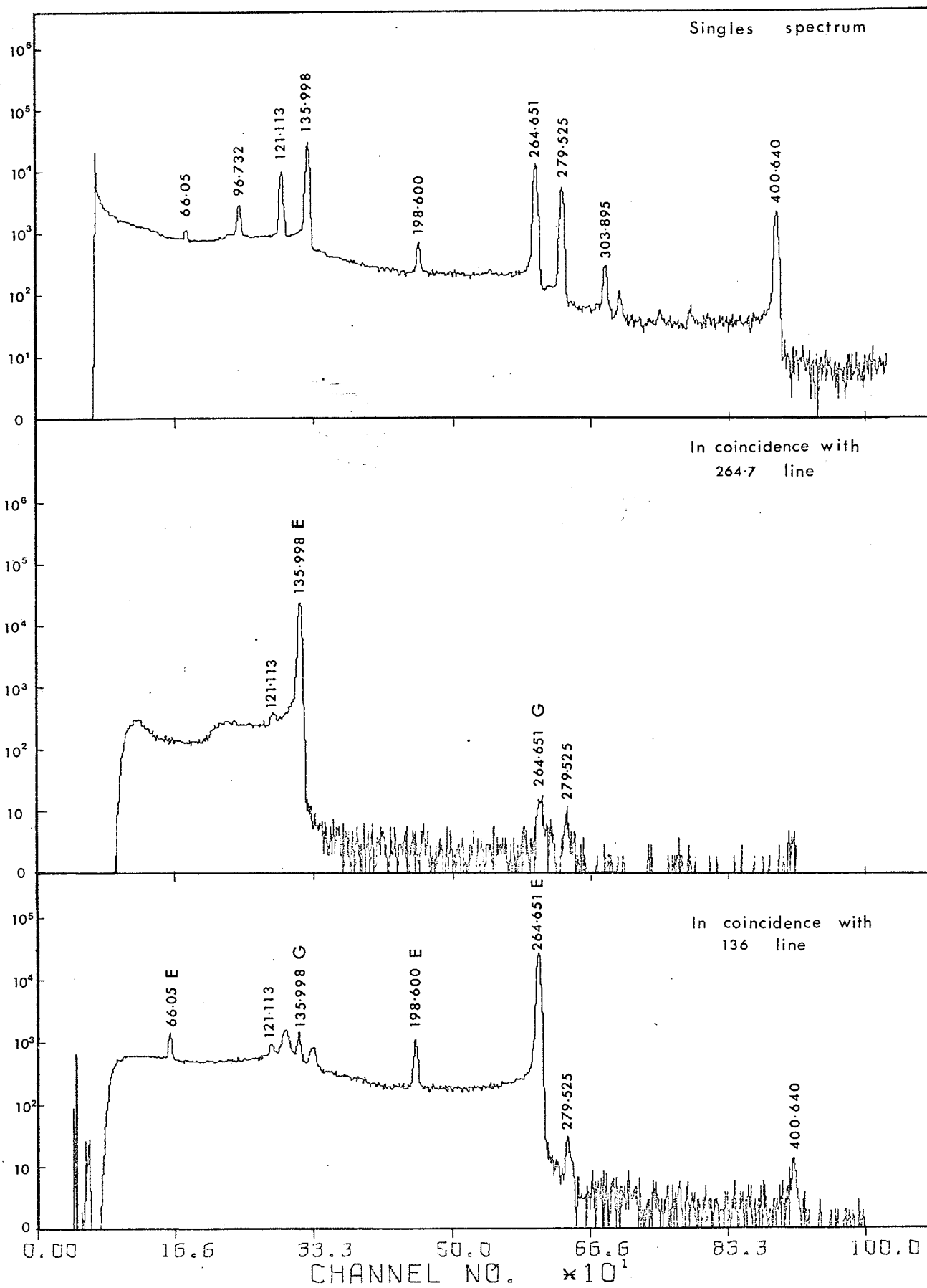
The geometry was deliberately made unsatifactory by having the long axis of the detectors inclined at an angle of 135 degrees to each other, and the source was put in a position as shown in Figure I-12A. The resultant time resolution was determined to be 85 nanoseconds, and the shape of the time peak was far from being satisfactory (See Figure I-13A). The geometry was then re-arranged so that the long axis of the two detectors as well as the geometric centre of the source , all lie in the same straight line. Further, collimators were used so that only the centre parts of the detectors were used. Here, the time resolution was found to be 65 nanoseconds, and a much better shaped time peak was obtained, as shown in Figure I-13B. Thus, in all the coincidence works attempted in the present investigation, emphasis was placed, whenever possible, on maintaining good geometry to optimize the time resolution.

To ensure that the system works properly, the coincidence system was tested using ^{75}Se, since its decay scheme is very well known. Gates were selected at 264.651 and 135.998 keV gamma rays, and the respective coincidence spectra, together with the self gated singles spectrum, is shown in Figure I-14. It was immediately obvious that only those gamma rays in

cascade with the gate (G) were enhanced (E), indicating that the system used is in good working order.

The coincidence spectra obtained in the present work (See Chapters III, IV and V) are all analysed in the conventional manner. The method consists of comparing a coincidence spectrum with a self gated singles spectrum obtained with the same amplifier gain. As mentioned earlier, the gamma rays that appear due to random events are in the same intensity ratio as they would appear in the singles spectrum. Thus, by normalizing the areas of the gamma rays in the self gated singles to a gamma ray known to occur due entirely to random events in the coincidence spectrum, the random events can be subtracted.

In all the coincidence shown in the subsequent Chapters, the randoms have not been subtracted. Also, self gated singles spectra will not be provided.

CHAPTER II

DATA HANDLING AND ANALYSIS

II.1 INTRODUCTION

It is unquestionable that the use of computers in data acquisition and analysis has become a necessity nowadays, because of their high speed and accuracy. In the present work, an IBM 360/65 computer was used to perform the data analysis, and a slower IBM 1620 computer was used to produce cards from paper tapes. A PDP-15 computer, located in the University of Manitoba Cyclotron control room, was occasionally used for data manipulation. A teletypewriter terminal was installed in the laboratory to provide access to the IBM 360/65 computer. To do this, it is necessary to use a computer programme called MUM[1] (Manitoba University Monitor) developed at this University.

II.2 DATA HANDLING

Throughout the course of this work, experimental data is accumulated in multi-channel analysers as described in Chapter I. The analyser outputs are of two forms:

(a) Graphical: the channel contents of the analyser

can be displayed on a CRT or plotted on paper, using a Moseley X-Y plotter.

(b) Numerical: the channel contents can be either typed out on an IBM Selectric typewriter or punched out on a paper tape using a Tally punch.

Of all these outputs, only the data punched on paper tapes provide a convenient form for numerical analysis. To convey the data to the computer, the following methods are adopted:

(1) If the amount of data is small, say the contents of a few hundred channels, the teletypewriter is used to read the data on the paper tape, and sends it to the computer over a phone line (see later section). But this method is inefficient because the speed of the tape reader on the teletypewriter is quite low.

(2) If the amount of data is large, the paper tapes containing the data are read into the PDP-15 computer, and the data is then transmitted to the IBM 360 computer via a data link between the computer centre and the PDP-15.

(3) More often, the paper tapes are carried to the computer centre, fed into IBM 1620 computer, and the data is punched on cards, which are then fed into the IBM 360 computer.

In all the above mentioned methods, data is first

40

Figure II - 1

Schematic diagram of teletype terminal

with acoustic coupler
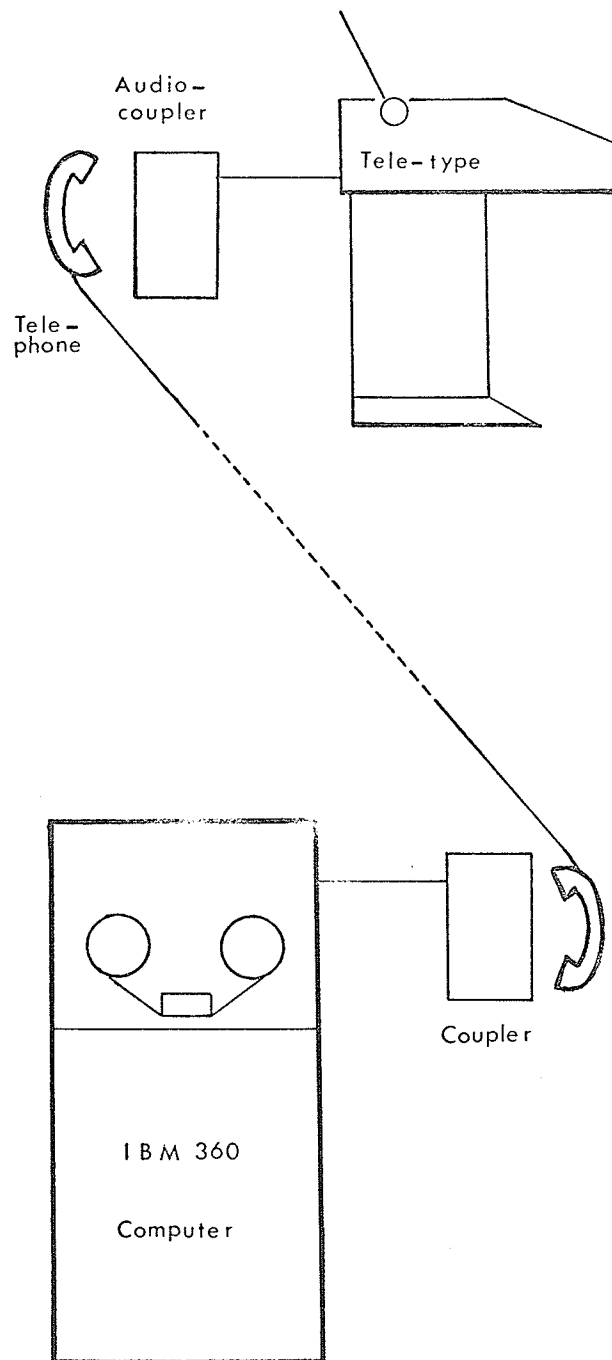
stored on a magnetic disk prior to actual analysis. Each set of data is also written onto a magnetic tape for back up storage.[2]

II.3 MANITOBA UNIVERSITY MONITOR (MUM)

The teletypewriter terminal is acoustically coupled to the University IBM 360/65 computer using an Anderson Jacobson ADC260 audio-coupler. A schematic diagramme is shown in Figure II-1. The coupler receives information from the teletypewriter, translates it into signals at audio frequencies, and sends them over the telephone to the computer. At the computer room, similar units decode the audio signals into information again. Information can be transmitted either way in this manner, and the teletypewriter is, in effect, a computer "terminal".

It must be mentioned that such an acoustic coupling does not constitute a direct access to the computer. In fact, the terminal is indirectly linked to the computer through a remote terminal programme called MUM (short for Manitoba University Monitor), which acts as an interface between the terminal and the computer. A detailed description of MUM has already appeared in the literature.[1] In the present work, the frequently used programmes are stored on magnetic disks, as is the data. Thus through MUM data analysis can be initiated

42

in the laboratory using the teletypewriter.[3]

II.4 CUTIPIE

A number of programmes have been developed to assist in data analysis. They are mostly "standard" programmes, like polynomial fitting. A very frequently used programme developed by the writer in this laboratory is called CUTIPIE, and the rest of the chapter will be devoted to describing it.

CUTIPIE is designed to determine the positions and areas (energies and intensities) of photopeaks in a gamma ray spectrum. It is developed with the following considerations in mind:

(a) That it should have a peak search routine to detect peaks with sufficient reliability. To do this, this routine must employ some sort of smoothing procedure, so that it will not "detect" spurious peaks when statistics are poor.

(b) That it should have a fitting procedure from which the desired parameters may be obtained.

(c) That the automatic analysis can be overridden so that one can direct CUTIPIE to analyse portions of the spectrum as desired.

(d) That the input information must be a minimum and yet the programme must be sufficiently reliable.

Before going into the detailed discussion of the

43

programme, it should be pointed out that data obtained
with semi-conductor detectors are relatively easier to
analyse than those obtained with NaI(Tl) scintillation
detectors. Semi-conductor detectors have much better
resolution, so that photopeaks exhibit themselves as
sharp peaks sitting on a relatively flat background,
and they are well isolated from each other. Usually,
the features of interest in a gamma-ray spectrum are
photopeaks themselves, hence, one needs to analyse only
a small region of the spectrum, namely the vicinity of
the individual photopeaks. Simple analytical functions
can be chosen to describe the shapes of the peaks,
without having to know a priori, the detailed response
of the detection system. In fact, the function chosen
to describe the peak shape does not even have to be
physically meaningful (see Ref. 17). As an example,
Robinson[4] has described the shape of a photopeak as
consisting of two gaussian distributions on a
background consisting of an arctangent function plus a
quadratic function. Thus, there is some arbitrariness
in the choice of a function describing the peak shape,
and a further arbitrariness in the choice of background
shape. However, provided a reasonable choice is made,
and applied consistently, satisfactory results may be
obtained. Consistency here means using the same

analysis throughout ---- even for calibrating the system.

The advantage of this analysis is in its simplicity --- one does away with the cumbersome successive stripping method so characteristic of scintillation spectrum analysis. A number of programmes which perform spectral analysis has been reported[5-10]. In most cases, the least squares fitting technique is used. Gaussian functions fitted to photopeaks by the method of maximum likelihood have been reported by Cliampi and Daddi[11]. A number of smoothing procedures have also been reported[12-15].

Logically, CUTIPIE has three main parts. They are:

(a) Input-output routine.

(b) Peak searching routine.

(c) Peak fitting routine.

(a) INPUT/OUTPUT ROUTINE

This routine manipulates information into and out of the computer. Being a trivial and standard procedure, this routine will not be described in detail here.

(b) PEAK SEARCHING ROUTINE

This procedure searches for photopeaks in a spectrum automatically, and the basic principle is quite simple. Consider a small portion of a spectrum. It can crudely be described by the function $f(x)$, thus

$$f(x) = ax + b + \begin{cases} g(x) & \text{if there is a peak} \\ 0 & \text{if there is no peak} \end{cases} \qquad \text{II-1}$$

where

x is channel number

ax+b is a straight line describing the background

g(x) is a gaussian distribution describing a photopeak, and is given by

$$g(x) = C \exp\{ -(x - d)^2/2\sigma^2 \} \qquad \text{II-2}$$

where C is the height of the gaussian distribution about d with standard deviation σ. Thus

$$f''(x) = \begin{cases} g''(x) & \text{if there is a peak} \\ 0 & \text{if there is no peak} \end{cases} \qquad \text{II-3}$$

where g''(x) can be verified to be

$$g''(x) = g(x) \{ \sigma^2 - (x - d)^2 \}/(\sigma^4) \qquad \text{II-4}$$

The behaviour of g''(x) is immediately obvious: if $(x-d) \gg d$, g''(x) tends to zero for the exponential term predominates. As x approaches d, g''(x) is first negative, then positive, and as x passes d, g''(x) becomes negative again. Further, g''(x) is zero at $(x - d) = \pm \sigma$ and is maximum at x = d. Hence, the deviation of g''(x) from zero indicates the presence of a photopeak. Also, the positive portion of g''(x) can be used to estimate the peak position. In this work, the position d is given by the equation:

46

(B)   Plot of $g''(x)$ versus x

(A)   Plot of $g(x)$ versus x

Figure   II-2
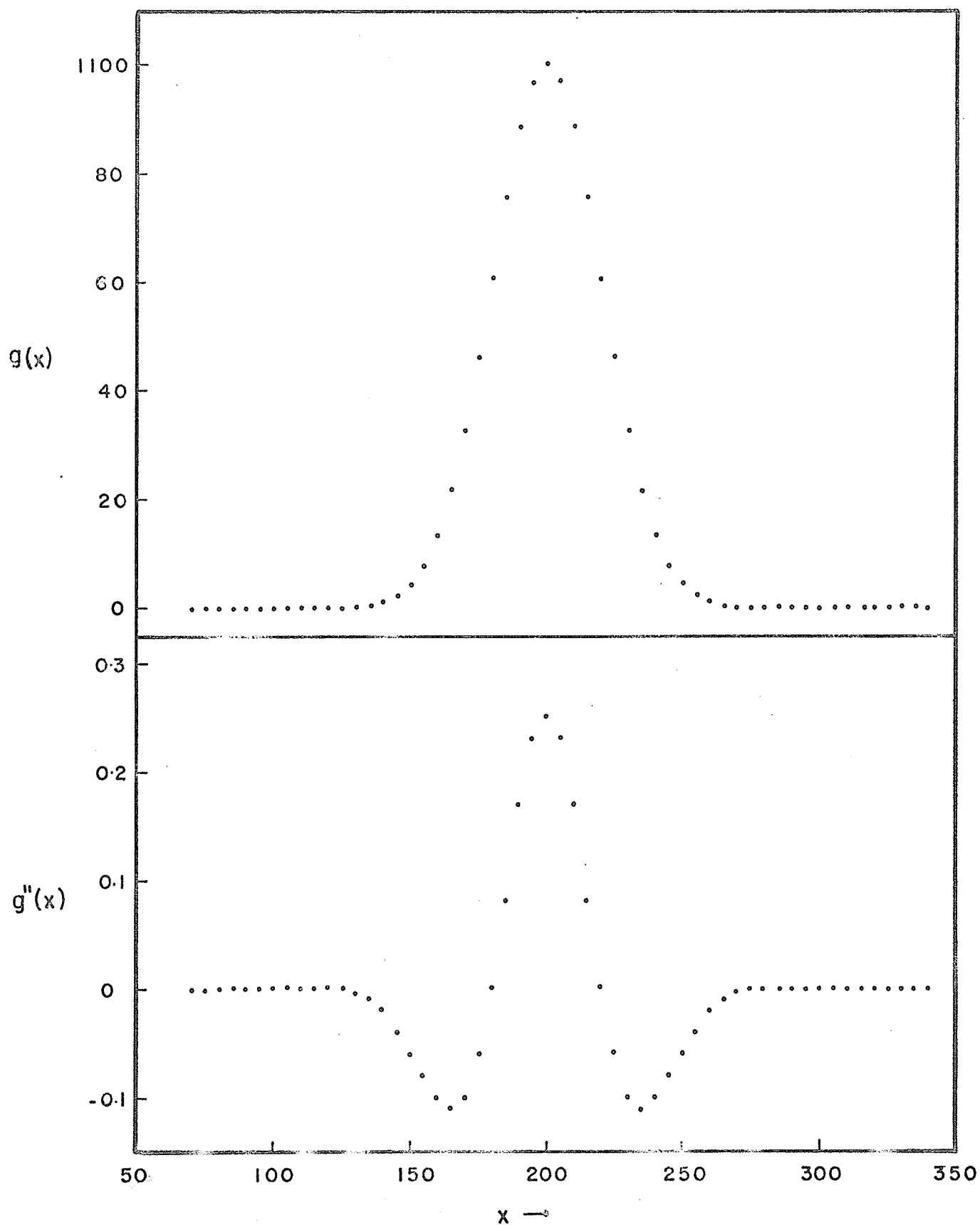
$$d = \{ \int_{-\sigma}^{\sigma} g''(x)x\,dx \} / \{ \int_{-\sigma}^{\sigma} g''(x)\,dx \} \qquad\qquad \text{II-5}$$

Hence, a peak searching routine reduces to calculating the second derivative $g''(x)$ at each channel, and looking for non-zero values of $g''(x)$ (see Figure II-2).

This method can be applied to spectral data, except that the second derivative must be replaced by the second differences, since the data is discrete rather than continuous. Moreover, the peak is not symmetric[21] (i.e., is not a simple gaussian) and so in practice the position of the centroid would only be approximate.

A numerical second difference dd_i at channel i can be expressed as:

$$dd_i = -n_{i-1} + 2n_i - n_{i+1} = \sum_{j=-1}^{1} c_j n_{i+j} \qquad\qquad \text{II-6}$$

where

$$c_{-1} = c_1 = -1 \qquad\qquad c_0 = 2$$

To improve on this, and to incorporate some smoothing to minimize statistical fluctuation, a generalized second difference method due to Mariscotti[16] is adopted. In essence, Equation II-6 is generalized by defining $(2k+1)$ multipliers c_j, such that

$$dd_i = \sum_{j=-k}^{k} c_j n_{i+j} \qquad\qquad \text{II-7}$$

and the standard deviation sd_i at channel i is

Figure II-3

(A) Plot of experimental data

(B) Generalized second differences ss_i

49
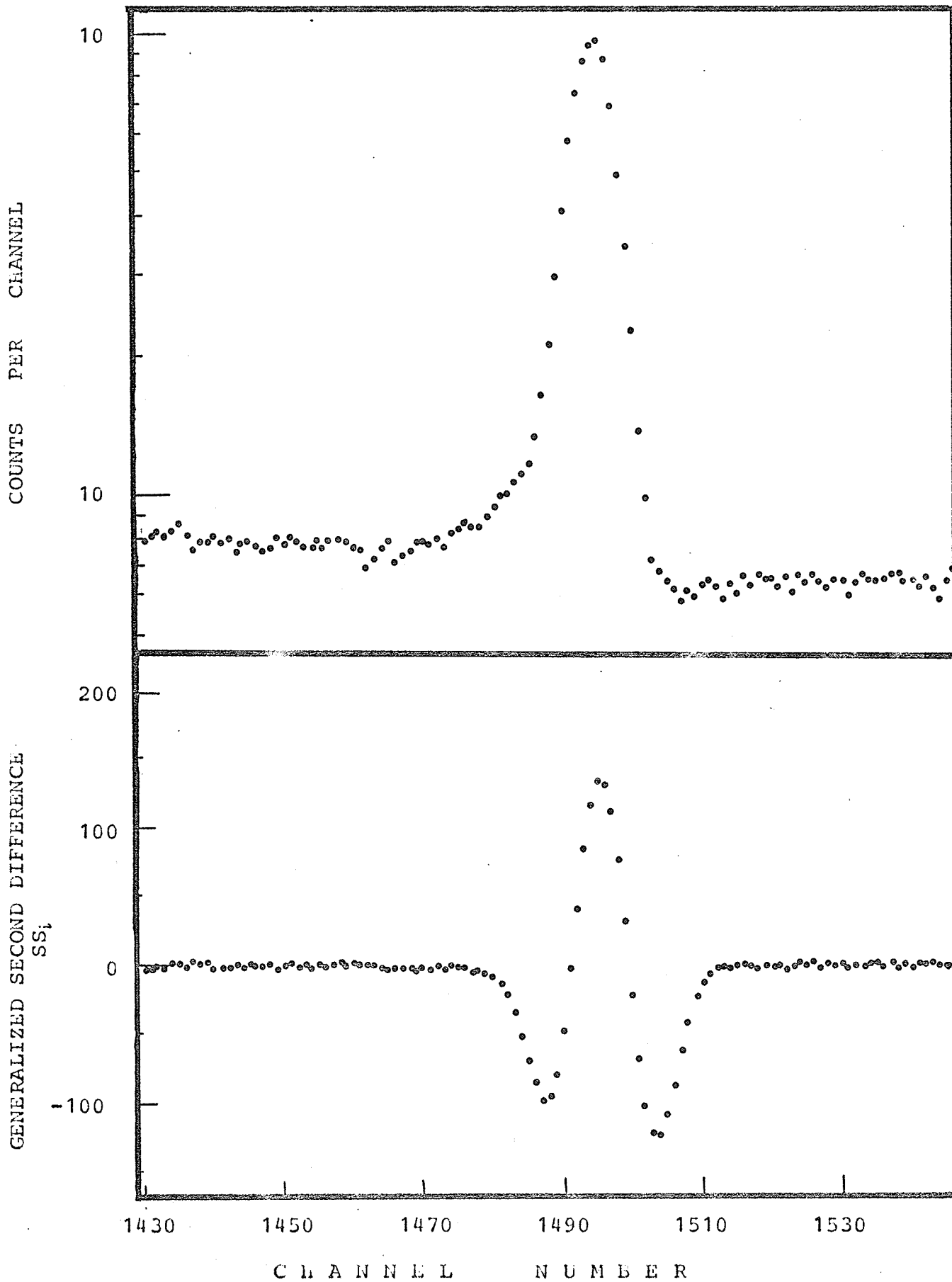
$$sd_i = \left[\sum_{j=-k}^{k} c_j^2 \, n_{i+j} \right]^{1/2} \qquad\qquad \text{II-8}$$

The coefficients c_j should be so chosen as to detect as small a peak as possible. In the present work, they are chosen to be the second derivative of a gaussian distribution, following Routti's[7] suggestion, namely,

$$c_j = G_j(\sigma^2 - j^2)/\sigma^4 \qquad\qquad \text{II-9}$$

where

$$G_j = \exp(-j^2/2\sigma^2)$$

k is chosen so that:

$$|c_{k+1}| < 0.01c_0$$

In this work, the generalized second difference ss_i at channel i (i.e., the second difference expressed in units of standard deviation) is defined to be:

$$ss_i = dd_i / sd_i \qquad\qquad \text{II-10}$$

the quantity ss_i as defined in Equation II-10 can be used to locate photopeaks in a spectrum. Figure II-3 shows a portion of a spectrum in which a photopeak is present. Directly below is plotted the generalized second differences ss_i In the region devoid of the photopeak, ss_i is zero or very close to zero. As one approaches the photopeak, ss_i behaves like $g''(x)$ in Equation II-3 as discussed above. The assymmetry of

ss_i about the centroid of the photopeak reflects the assymmetry of the photopeak. Further, the approximate position of the peak can be estimated by determining the centroid of the positive values of ss_i. Mathematically:

$$\text{peak position} = \left(\sum iss_i\right) \bigg/ \left(\sum ss_i\right) \quad \text{for all } ss_i > 0$$

In general, if no photopeak is present, the values of ss_i are quite small and are distributed randomly about zero. By trial and error, it is found that $ss_i > 3.0$ gives a fairly good indication of the presence of a photopeak. The performance of such a method will be presented at the end of this chapter. A more detailed discussion of the generalized second difference method for peak searching and data smoothing has already appeared in the literature[7,16].

(c) PEAK FITTING ROUTINE

Once the set of peaks are located by the peak search routine, the programme re-examines each peak, determines the region about the peak to be fitted, and the number of peaks that are to be fitted together, and the fitting routine is called for.

The method used for the fitting is the well known Gauss-Seidel method.[17] Essentially, it is a non-linear, multi-parameter iterative type of least

Figure II-4

Portion of a gamma ray spectrum

with one peak
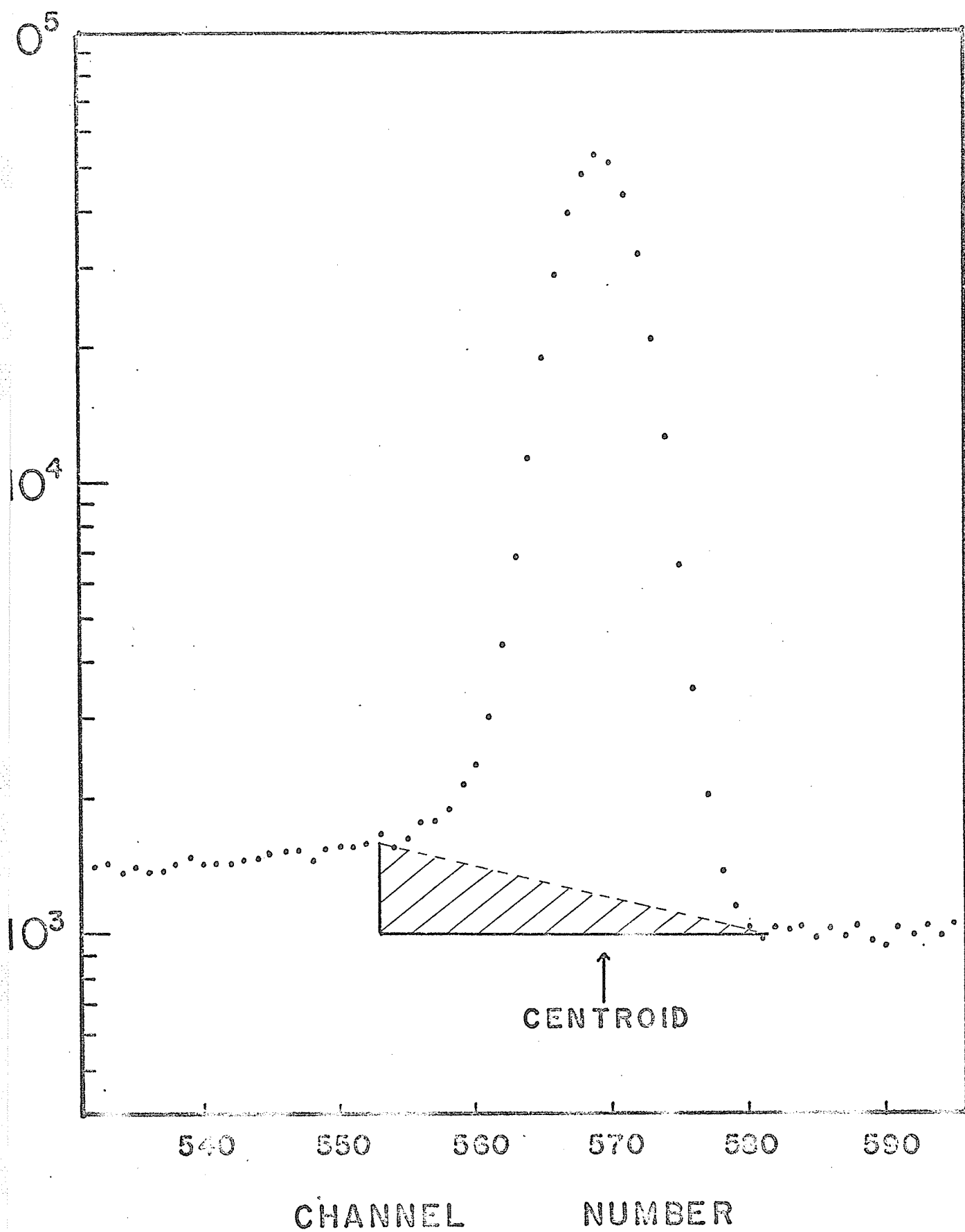
squares fitting procedure. The theory of this method is well known, and will not be elaborated here. Being of the iterative type, an initial estimate of the parameters is required to start the fitting process. The initial estimates, except the full width at half maximum (FWHM), are generated internally by the programme, and so need not be supplied but the approximate value of the FWHM must be supplied.

One assumption was made when coding CUTIPIE: All peaks overlapping in a given region of the spectrum are assumed to have the same width. For gamma ray spectra, this is not an unreasonable assumption, since the peak width is a slowly varying function of energy, and as the peaks overlap, they are close in energy. In view of this assumption, CUTIPIE is coded to unwrap up to a maximum of six overlapping peaks. The choice of six is quite arbitrary, but is adequate in most situations.

Before discussing the function which represents the shape used in fitting the peak, it is worthwhile to digress at this point to discuss the background shape. The dots in Figure II-4 show the experimental points of a portion of an isolated gamma ray spectrum. The most marked feature is the presence of a relatively flat plateau on the low energy side, which is higher than that on the high energy side. There is no question that

the presence of this high plateau is due to the presence of the gamma ray. The question remains as to whether or not one should include this plateau as part of the photopeak area, and if one does, how much of it should be included.

It has been suggested[18] that the following analysis be adopted as a reasonable one: The background is assumed horizontal and a portion of the plateau, say 2.5 FWHM wide, measured from the centroid to the low energy side, be included in the peak area, as indicated by the solid line in Figure II-4. This method has two main objections:

(a) The choice of the factor 2.5 is quite arbitrary, and is purely a matter of personal preference.

(b) When overlapping peaks are encountered, the analysis becomes very time consuming and inaccurate. Successive stripping becomes unavoidable, and this stripping method is likely to introduce errors larger than those produced by an alternative method described below.

Another approach is to select two convenient points on either side of the photopeak, and fit between them a straight line to approximate the background, as shown by the dash line in Figure II-4. Effectively, the higher plateau is ignored. This analysis has the same

Figure II-5

A typical fit by CUTIPIE
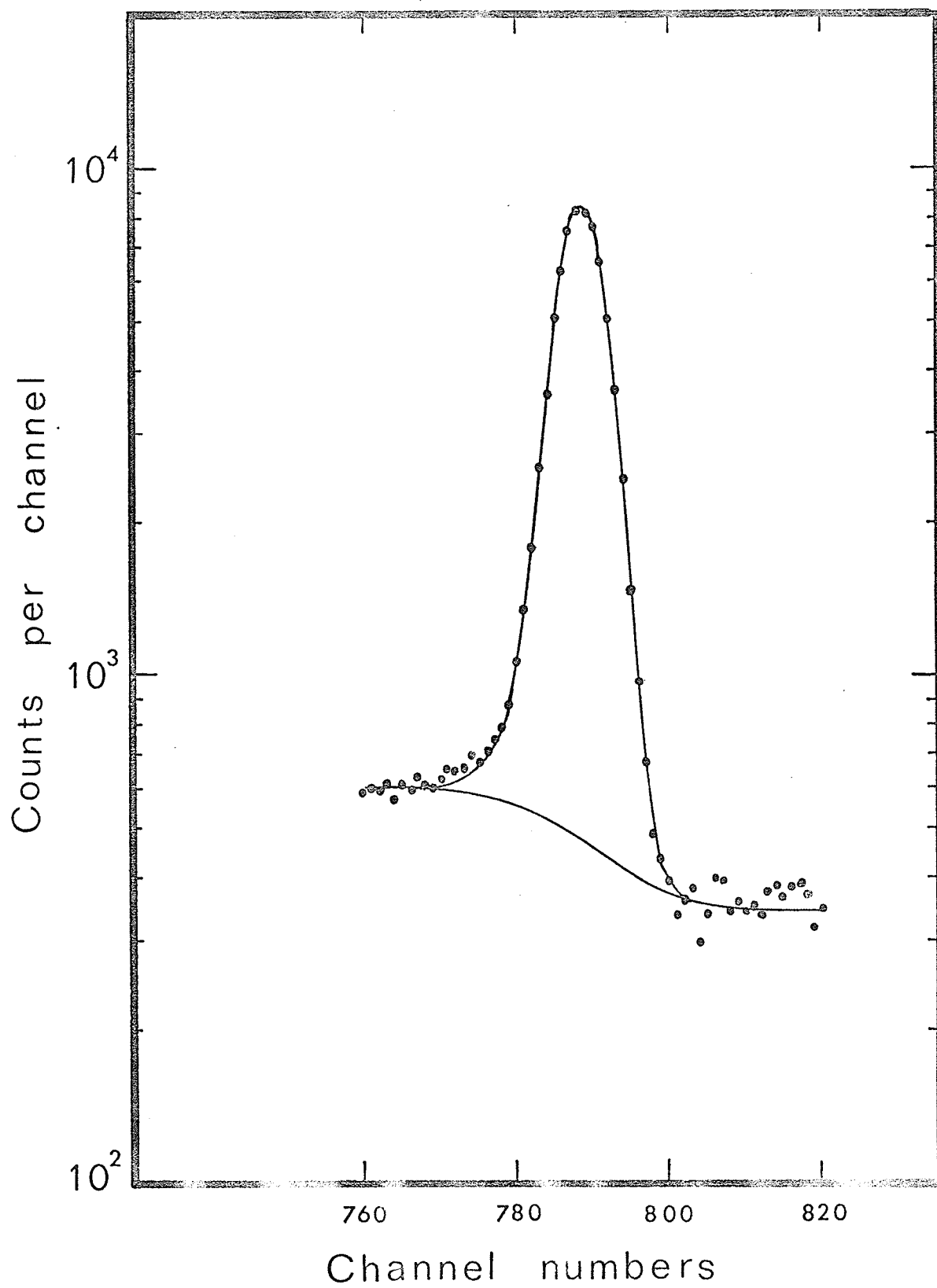
disadvantage as the previous one in that the choice of the two points is quite arbitrary, but has the advantage that when overlapping peaks are encountered, the successive stripping method can be avoided, since the one background serves for all the components.

It must be realised that neither of the analyses mentioned above is wrong. There is no way to justify the correctness of one over the other, since no one can tell with certainty what the background should look like, and hence its choice becomes a matter of personal preference. The only relevant point is that whatever method adopted, the analysis must be consistent throughout: When detectors are calibrated for efficiency, the same analysis must be used.

In CUTIPIE, the latter method of background treatment is adopted , but instead of a straight line, a function[19] $B(i)$ is chosen to pass through the plateaux on either side of the photopeak, as shown in Figure II-5. Such a background shape is more reasonable in that it is continuous and smoothly varying. The function $B(i)$ has the form:

$$B(i) = a_1 + a_2 /\{ 1.0 + \exp((i-p)/W) \}$$

where

a_1, a_2 are parameters to be determined by the fitting

56

procedure,

i   is the channel number,

p   is the centroid of the photopeak (and for the case
of overlapping peaks, the centroid of the whole complex
peaks is used instead),

W   is   chosen   to   be   0.75 FWHM,   a value which is
determined by experience as giving the best fit.   This
formula resembles   the   nuclear charge density formula
due   to Hofstadter et al.[20] The   choice of such a
background is quite artificial, and like all other
choices,   there is no physical significance to justify
it, but it does offer a shape that is reasonable.

The function used to represent the shape of the
photopeak is deduced in the following manner. Usually a
photopeak resembles a skewed gaussian,[21] so a photopeak
can be represented by a gaussian distribution, but at
some point at the low energy side, the gaussian
distribution is replaced by an exponential function to
simulate the   "tailing".   The two functions join
smoothly at this point, which is left as a parameter to
be determined by the fitting process. This is the shape
adopted in CUTIPIE. Mathematically, it is given by:

$$f(i) = B(i) + \sum_{j=1}^{N} P_j(i)$$

where

N   is the number of overlapping peaks to be fitted together, and is no greater than 6,

$B(i)$ is as defined earlier,

$P_j(i)$ is the jth   peak to be fitted, and is given by the expression:

$$P_j(i) = \begin{cases} a_{2j+3}\exp\{ -a_3 (i - a_{2j+4})^2 \} & \text{for } i > \delta \\[2em] a_{2j+3}\exp\{ a_3 a_4 (2i - a_{2j+4} + a_4)\} & \text{for } i < \delta \end{cases}$$

where

a_{2j+3} is the height of the jth peak,

a_{2j+4} is the centroid of the gaussian, taken to be   the position of the jth peak,

a_4 is the distance between the joining point and the jth peak position, and is related to δ by

$$\delta = a_{2j+4} - a_4$$

a_3 is related to the FWHM by the relation

$$a_3 = 2.7726/(\text{FWHM})^2$$

i is the channel number.

Figure II-5 shows a typical fit of an isolated photopeak. The exponential tail seems to account for the assymmetry, and the background looks reasonable as well. When the statistics of the data are poor, or when the number of channels under the peak is small, the peak shape is not well defined. In this case, a simpler function is used in CUTIPIE. It consists of a simple

Figure II-6

K X-ray spectrum of U and Th
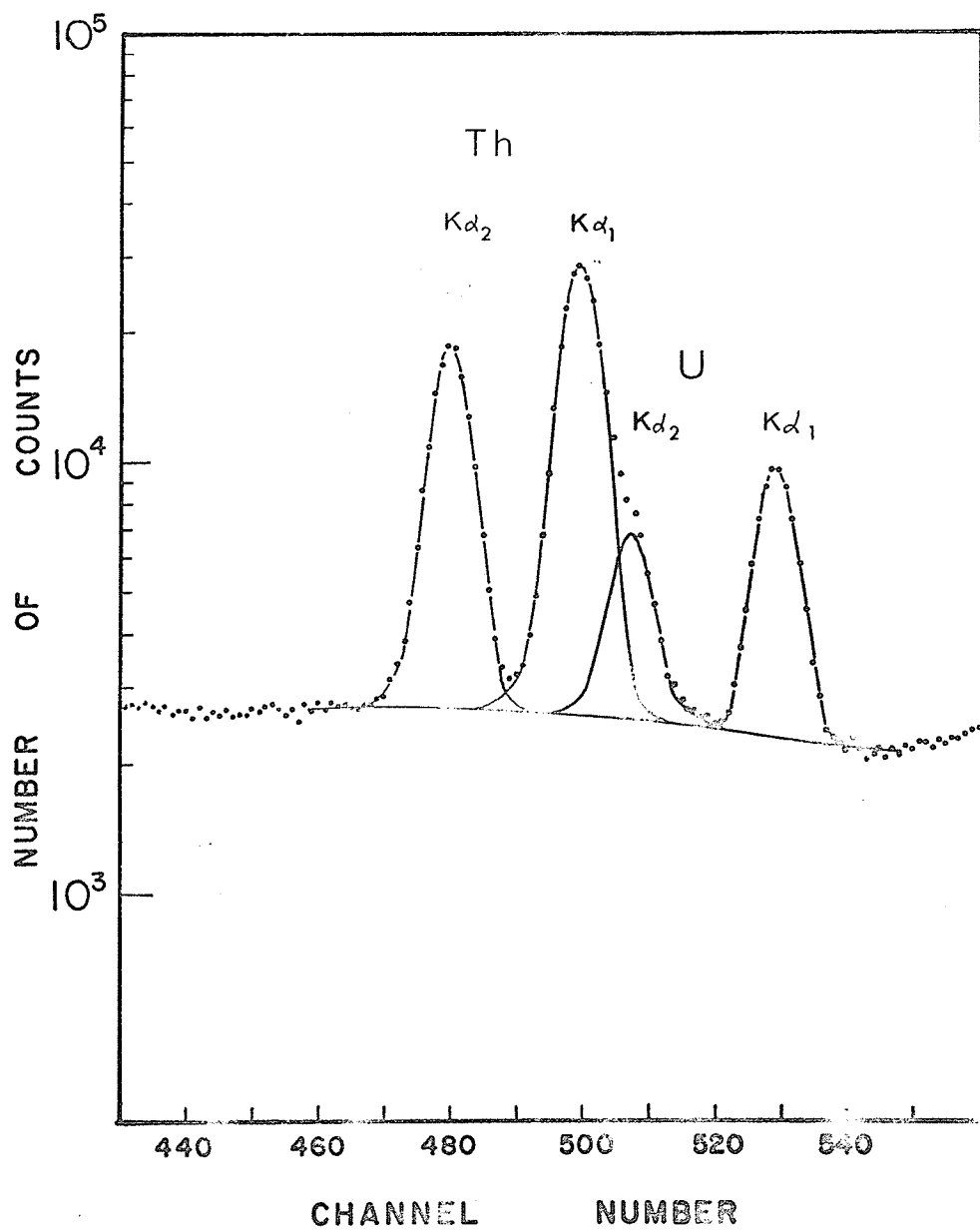
Table II-1

Comparison of CUTIPIE analysis

of U and Th X-rays

with the reported values

Peak	Position	Energy, (keV)	Reported value (ref 11)
Th K_{α_2}	480·245 ± ·017	89·953	89·953
Th K_{α_1}	499·952 ± ·013	93·349 ± ·015	93·350
U K_{α_2}	507·713 ± ·085	94·??? ± ·029	94·665
U K_{α_1}	529·475 ± ·037	98·439	98·439

Peak	Area (total counts)	$K_{\alpha_2}/K_{\alpha_1}$ ratio	Reported value		
			ref 10	ref 14	ref 13
Th K_{α_2}	120217 ± 1·3%				
Th K_{α_1}	195554 ± 1·2%	0·615 ± 1·8%	0·616	0·610	0·56
U K_{α_2}	33962 ± 2·9%				
U K_{α_1}	55104 ± 1·9%	0·616 ± 3·5%	0·625	0·610	0·56

gaussian distribution for the shape of the photopeak., while a straight line is used to approximate the background. Mathematically, the function f(i) has the form:

$$f(i) = a_1 i + a_2 + \sum_{j=1}^{N} a_{2j+3} \exp\{-a_3(i-a_{2j+4})^2\}$$

where i and N have the same interpretation as before. This shape is most useful in fitting photopeaks in coincidence spectra in which the peak shape is generally not very well defined. This simpler shape is included in the programme.

The performance of CUTIPIE was checked in the following ways:

(i) The programme was used to analyse the alpha components ($K-L_{II}$, $K-L_{III}$) of the K X-rays of various elements. A typical result is shown in Figure II-6. The thorium X-rays were produced following the alpha decay of ^{235}U into ^{231}Th, while the uranium X-rays were produced by fluorescence in the source material. The $K_{\alpha_2}/K_{\alpha_1}$ ratio obtained in this analysis are in excellent agreement with the previously reported values.[22,23] Also, using K_{α_1} of thorium X-ray and K_{α_2} of uranium X-ray, the energies of the K_{α_2} of thorium and K_{α_1} of uranium were determined. The result obtained was in good agreement with the measured values[24] as shown in Table II-1.

Figure II-7

Composite gamma ray spectrum of

^{182}Ta, ^{133}Ba, ^{75}Se and ^{57}Co

COUNTS PER CHANNEL

CHANNEL NUMBER
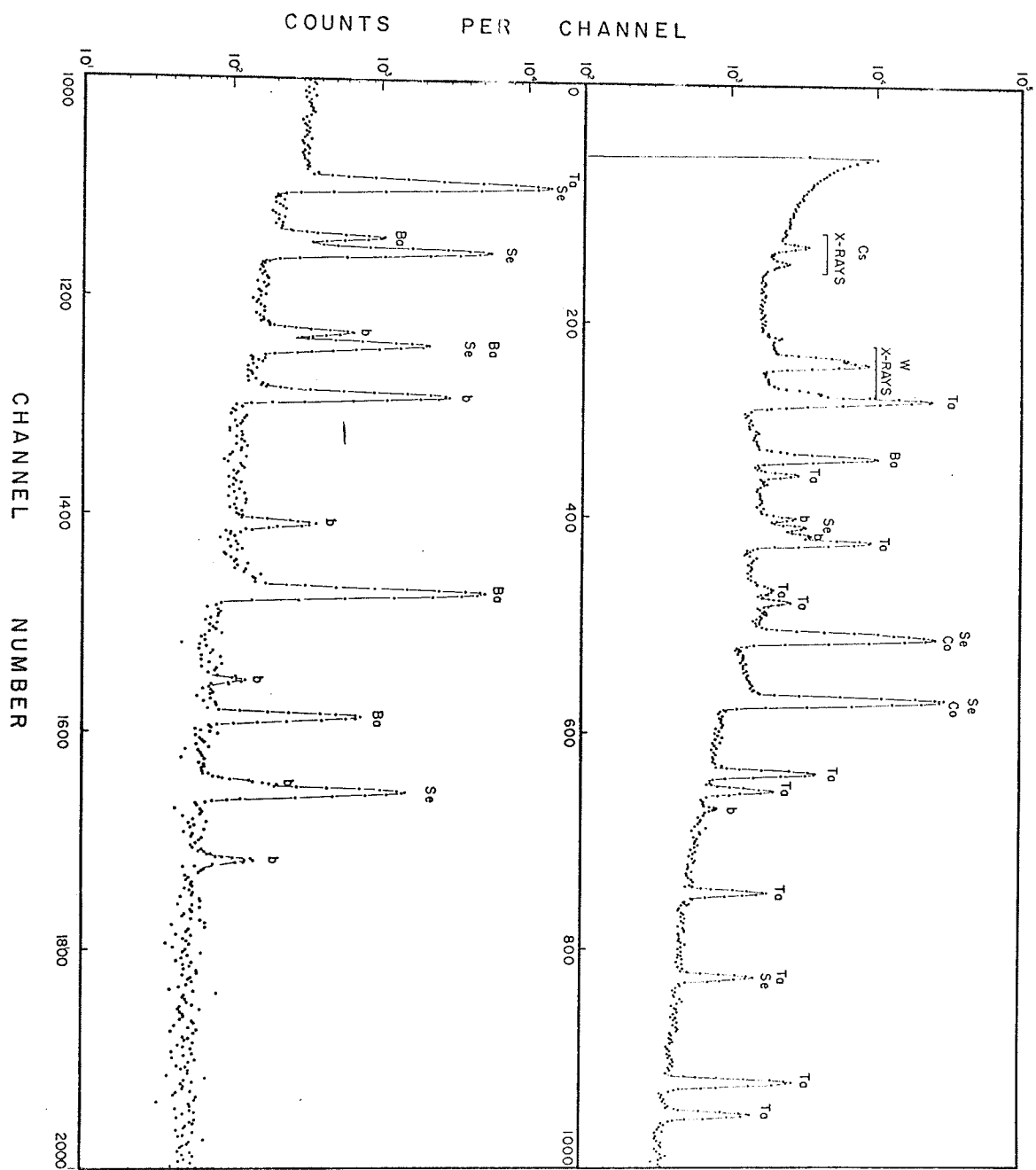
Table II-2

Energies and intensities

of

gamma rays of ^{75}Se

Present Work		Reported Value[25]	
E_γ	I_γ	E_γ	I_γ
66.108±0.010	2.0±0.5	66.108±0.010	1.63±0.06
99.732±0.005	5.0±0.5	96.732±0.007	5.3±0.5
121.109±0.010	25.8±2.5	121.113±0.010	28.0±2.8
136.008±0.010	94.6±8.2	135.998±0.010	95.0±9.0
198.577±0.020	2.2±0.2	198.600±0.020	2.4±0.3
264.681±0.025	100.0	264.651±0.015	100.0
279.489±0.030	40.0±2.2	279.525±0.012	43.0±4.3
400.630±0.050	19.6±1.7	400.640±0.015	22.0±2.2

Figure II-8

Portion of gamma ray spectrum of ^{231}Th

Pa K-M$_{IV}$ 108.99

Pa K-M$_{III}$ 108.77

Pa K-M$_{II}$ 107.60

105.7 · 106.7

102.32

99.33

Pa K-L$_{III}$ 95.868

92.91

Pa K-L$_{II}$ 92.287

89.95

Bi K$_\beta$ X rays

84.20

82.06

81.20

Bi K$_\alpha$ X rays

72.74

Numbers

Channel

Counts per Channel

10^4

10^3

10^2

900

1000

1100

1200

1300

1400
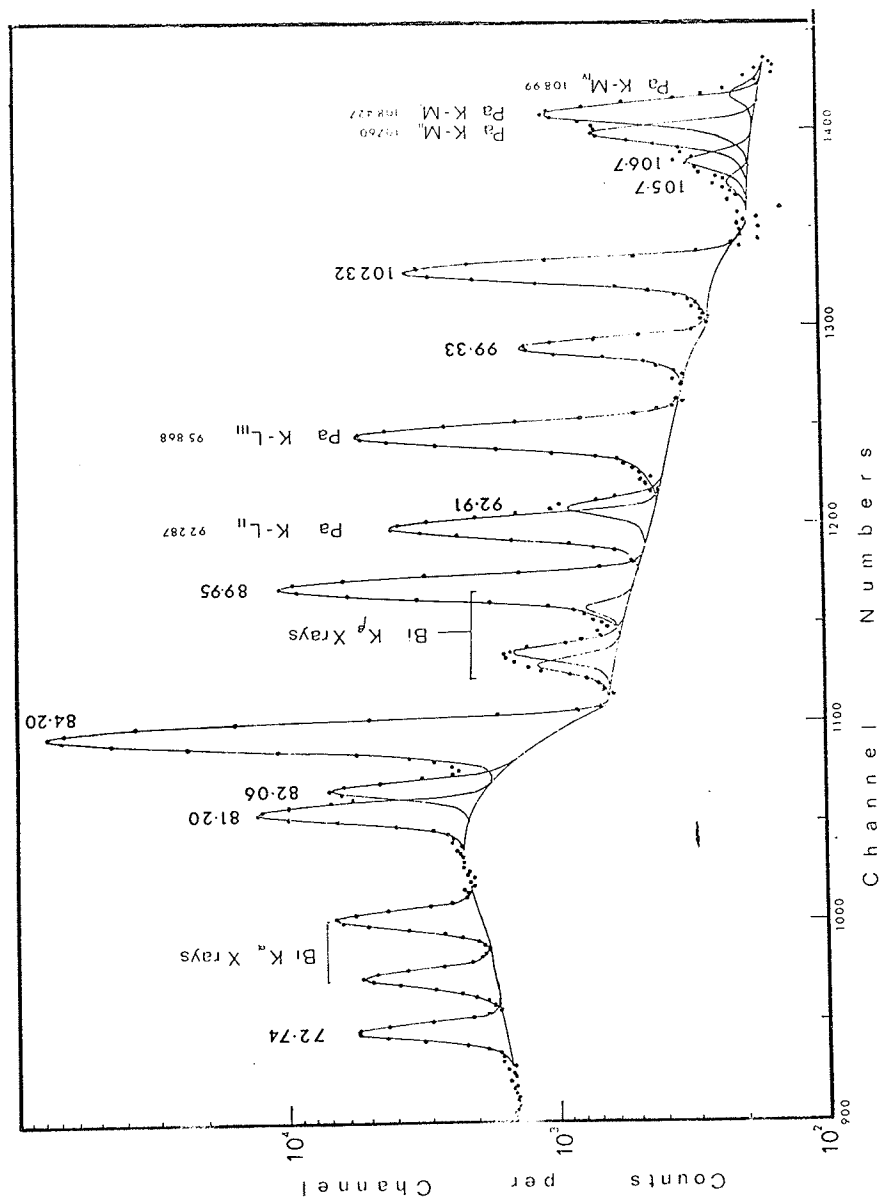
Table II-3

Energies and relative intensities

(relative to $I_\gamma(84.20) = 100.$)

of ^{231}Th

Brown		Present Work	
E_γ	I_γ	E_γ	I_γ
72·66 ±0·06	4·0	72·74 ±0·05	3·8 ±0·2
81·18 ±0·05	14·2	81·20 ±0·06	13·5 ±0·9
82·02 ±0·06	7·2	82·06 ±0·07	6·8 ±0·4
84·17	100·0	84·20	100·0
89·94 ±0·05	15·3	89·95 ±0·04	15·3 ±0·8
93·00 ±0·10	1·1	92·91 ±0·10	0·9 ±0·2
99·30 ±0·05	2·0	99·33 ±0·05	2·2 ±0·2
102·30 ±0·05	6·7	102·32 ±0·04	6·8 ±0·4
105·73 ±0·10	0·13	105·74 ±0·10	0·13 ±0·08
106·58 ±0·10	0·34	106·66 ±0·08	0·33 ±0·10

(ii) A more exhaustive test was carried out by artificially generating a complicated gamma ray spectrum using the photopeaks of ^{133}Ba, ^{75}Se, ^{182}Ta and ^{57}Co. These isotopes are calibration standards and their gamma-ray energies and intensities[25] are very well known. The energies of the gamma rays of ^{75}Se was determined using those of ^{133}Ba, ^{182}Ta and ^{57}Co as standards. A portion of this complex spectrum is shown in Figure II-7. From this spectrum, the energies and the relative intensities of the gamma rays of ^{75}Se were determined, as shown in Table II-2. The agreement with the reported values is very good[25].

The programme has been succesfully used to analyse a number of gamma ray spectra. Figure II-8 shows a portion of a gamma ray spectrum of ^{231}Th, taken with the Ge(Li) detector having a resolution of 290 eV at 5.9 keV. A small amount of stable bismuth is present in the source material and its X-rays are produced by fluorescence. The result of the analysis is shown in Table II-3, and is in good agreement with that reported by Brown[26]. The successful unfolding of a group of five lines at about channel 1400 should be noted.

It must be mentioned at this point that the numerical second difference method used in the peak searching routine is more sensitive in locating weak

Figure II-9

Portion of gamma ray spectrum of ^{231}Pa

    (A)   a poor fit with a weak peak
            missing

    (B)   re-fit with the proper
            number of peaks
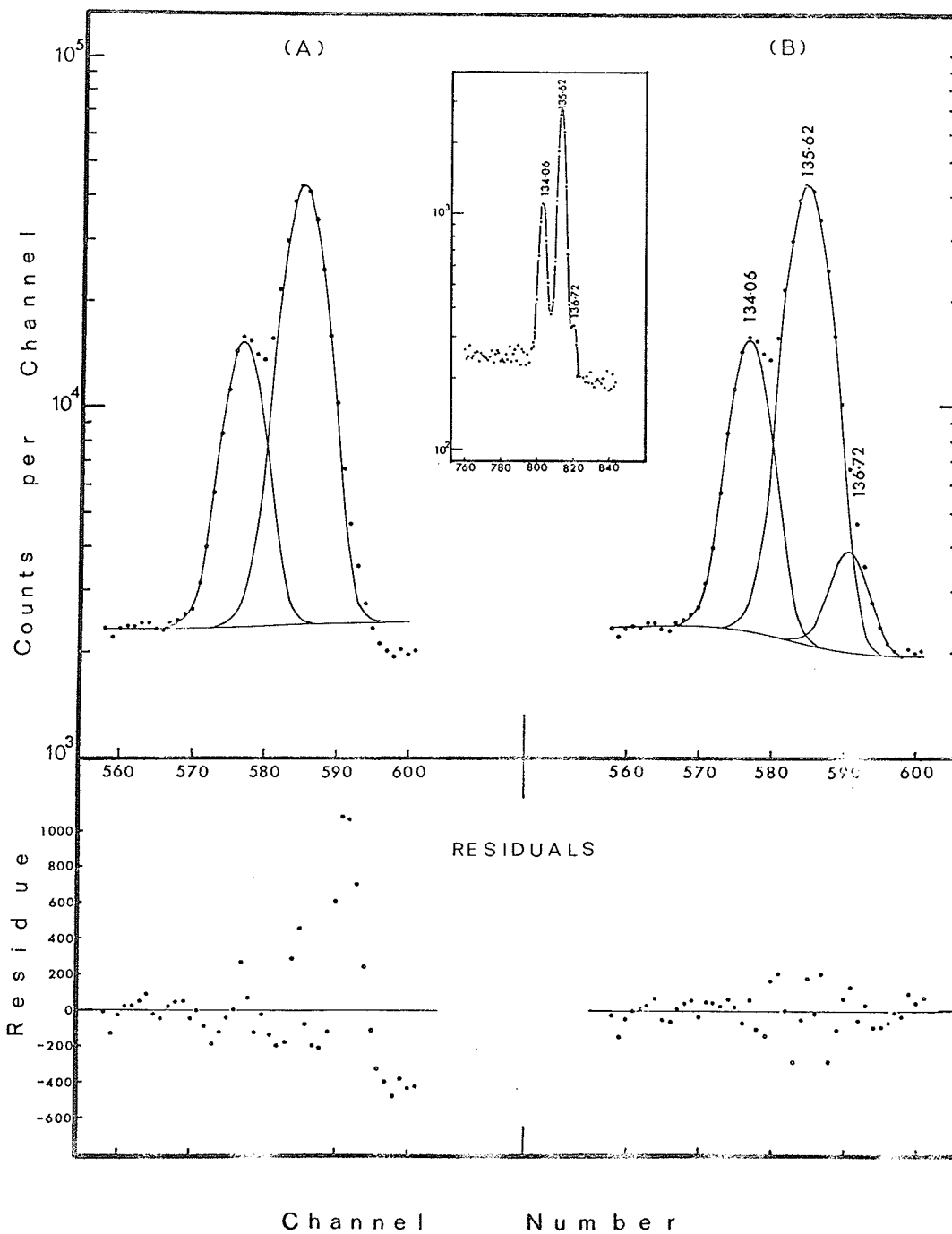
isolated photopeaks than locating all the components in a group of overlapping peaks. Generally, the peak search routine can not differentiate two peaks that are less than 0.5 FWHM apart if one of them is very weak. Figure II-9A shows a typical situation in which analysis was carried out, but a weak component had been 'overlooked'. This is a portion of a gamma ray spectrum of ^{231}Th taken with the 50 cc Ge(Li) detector whose resolution is 2.0 keV at 1.33 MeV. The fit, as shown by the solid line, is obviously poor, and the residual shows a definite non-random distribution. A refit with the proper number of components yields a much better fit (Figure II-9B) as indicated by the randomly distributed residuals. A subsequent re-examination of the same region with a high resolution Ge(Li) X-ray detector confirms the existence of the 136.72 keV gamma ray, as shown in the insert in Figure II-9. A subroutine has therefore been included in CUTIPIE to examine the residuals after each fit. Should the residuals indicate that a component has been missed, the approximate position of the missed peak is calculated, and a refit is automatically called for. This subroutine has been shown to work very well, thereby compensating for the slight inadequacy of the peak searching procedure.

Figure   II-10

A   CUTIPIE   fit to   the

K   conversion electron line

of

^{203}Hg

CHANNEL   NUMBER
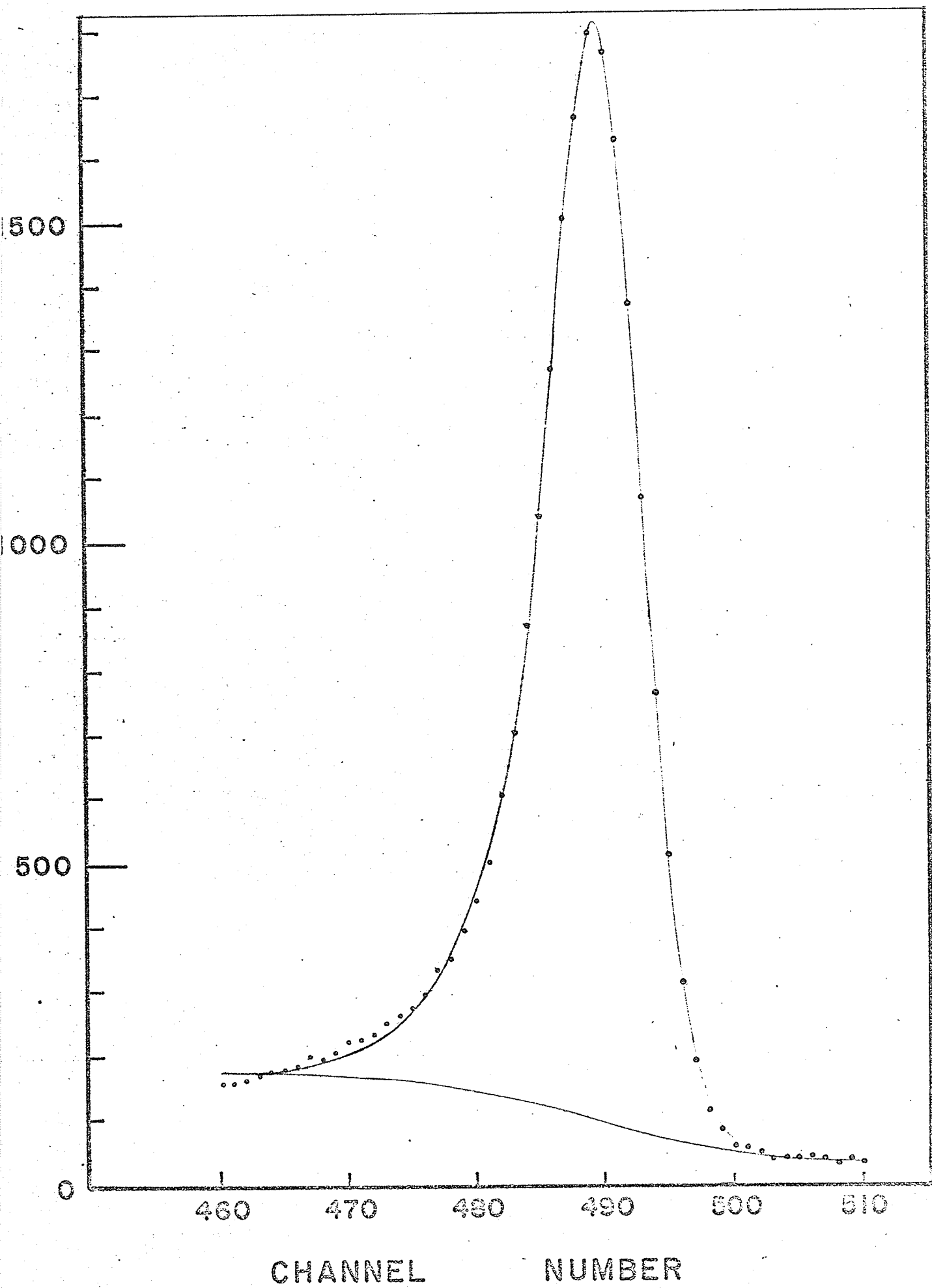
Figure II-11

Fit to a time spectrum

Source: ^{60}Co

Time/Channel = 14 psec

• data

— L.S.Fit

280×10^{-12} sec fwhm

counts per channel

10^3

10^2

10

940   960   980   1000   1020   1040   1060   1080

channel number
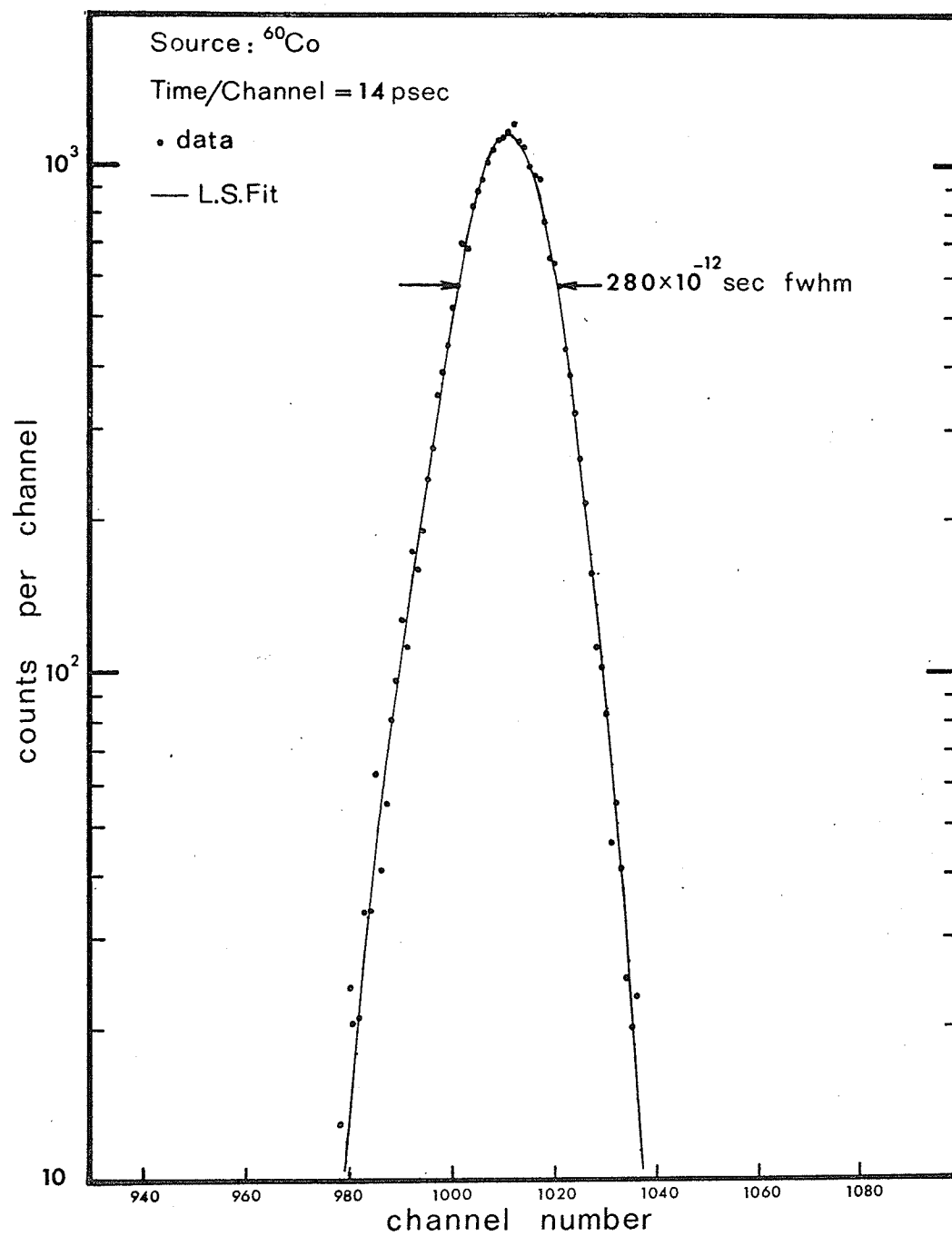
In conclusion, CUTIPIE has been used quite successfully in this laboratory. It has also been used by some members of the Cyclotron Group and by members of Trace Element Analysis Group of this University. The same programme was used to fit a conversion electron line, as shown in Figure II-10. The fit is reasonably acceptable, except at the extreme tail on the low energy side. Modified version of CUTIPIE has been used with success in fast timing spectroscopy.[27] Figure II-11 shows a prompt time peak obtained using fast plastic scintillators. The dots are the actual data points while the continuous line represents the result of the fit. The fit is excellent.

CHAPTER III

THE DECAY OF ^{231}Pa

III.1 INTRODUCTION

^{231}Pa is found in all minerals containing uranium. It is an alpha emitter with a half-life of 3.25 X 10^4 years[1]. The alpha groups emitted by ^{231}Pa had been studied as far back as 1949[2], and are known to be quite complex[3-5]. Meitner[6] first examined the conversion electron spectra, and her result was later confirmed by Haggstrom[7], Scharff-Goldhaber and Mckeown[8]. Since 1952, enormous advances in the understanding of this isotope have been reported[9-12], but even though much work had been done, the level scheme of ^{227}Ac is still not complete. More recent work on this isotope had been reported by Lange et al[13], Barnett et al[14], Hagee et al[15], Leang[16] and Pinho et al[17]. There are variations between their works, and it one of the purposes of the present work to clarify the discrepancies.

III.2 SOURCE PREPARATION

^{231}Pa was purchased from the Radiochemical centre, Amersham, England. The shipment, in chloride form, was

72

found by examination of the spectrum, to contain impurities, mainly ^{227}Th (and hence ^{227}Ac) which are daughter products, the decay chain being: ^{231}Pa $\xrightarrow[\alpha]{325 \times 10^4 \text{yr}}$ ^{227}Ac $\xrightarrow[\beta]{216 \text{ yr}}$ ^{227}Th $\xrightarrow[\alpha]{18.2 \text{ d}}$ ^{223}Ra $\xrightarrow[\alpha]{11.43 \text{ d}}$ short lived daughters. Other inert impurities were present as revealed by their fluorescent X-rays. Thus the source needed chemical purification before it could be used, and it is necessary to re-purify ^{231}Pa to remove the unwanted activities every two months.

Purification was performed in the following way. 9M HCl and 0.1M HF was added to the ^{231}Pa solution and extracted with two equal volumes of di-isopropyl ketone (DIPK) to remove Po, Fe and other impurities, with only Pa remaining in the aqueous phase[2.5]. Boric acid was added and two successive extractions with fresh DIPK was made, and Pa was transfered to the organic solvent (eg. DIPK). The solvent was then treated three times with small volumes of 9M HCl to remove any impurities that may be still present. Pa was recovered from the solvent by treating with equal volume of 2M HCl. At this acidity, Pa was dissolved in the hydrochloric acid, which was then evaporated to a small volume and was then ready for counting.

For the periodic removal of radioactive daughter products, the purification process consisted of cycling

Figure III-1

Low energy spectrum of ^{231}Pa decay,

taken with a Si(Li) detector

NUMBER OF COUNTS

CHANNEL NUMBER

10^5
10^4
10^3
10^2
10

0   100   200   300   400   500   600   700   800

8·6 keV

10·87 keV
($L_{III} - M_I$)

12·5008 keV
($L_{III} - M_{IV}$)
12·6520 keV
($L_{III} - M_V$)

13·3 keV
($L_I - M_I$)

14·08keV
($L_I - M_{III}$)

14·602
($L_{III} - N_I$)

15·232 keV
($L_{III} - N_V$)

15·791 keV
($L_{III} - O_I$)

15·931 keV
($L_I - M_{III}$)

16·621 keV
($L_I - M_V$)

17·814
($L_I - N_I$)

18·408 keV
($L_I - N_{II}$)

18·949 keV ($L_I - N_{IV}$)
19·003 keV ($L_{III} - O_{II}$)

19·625 keV
($L_I - O_{III}$)

2536

2738
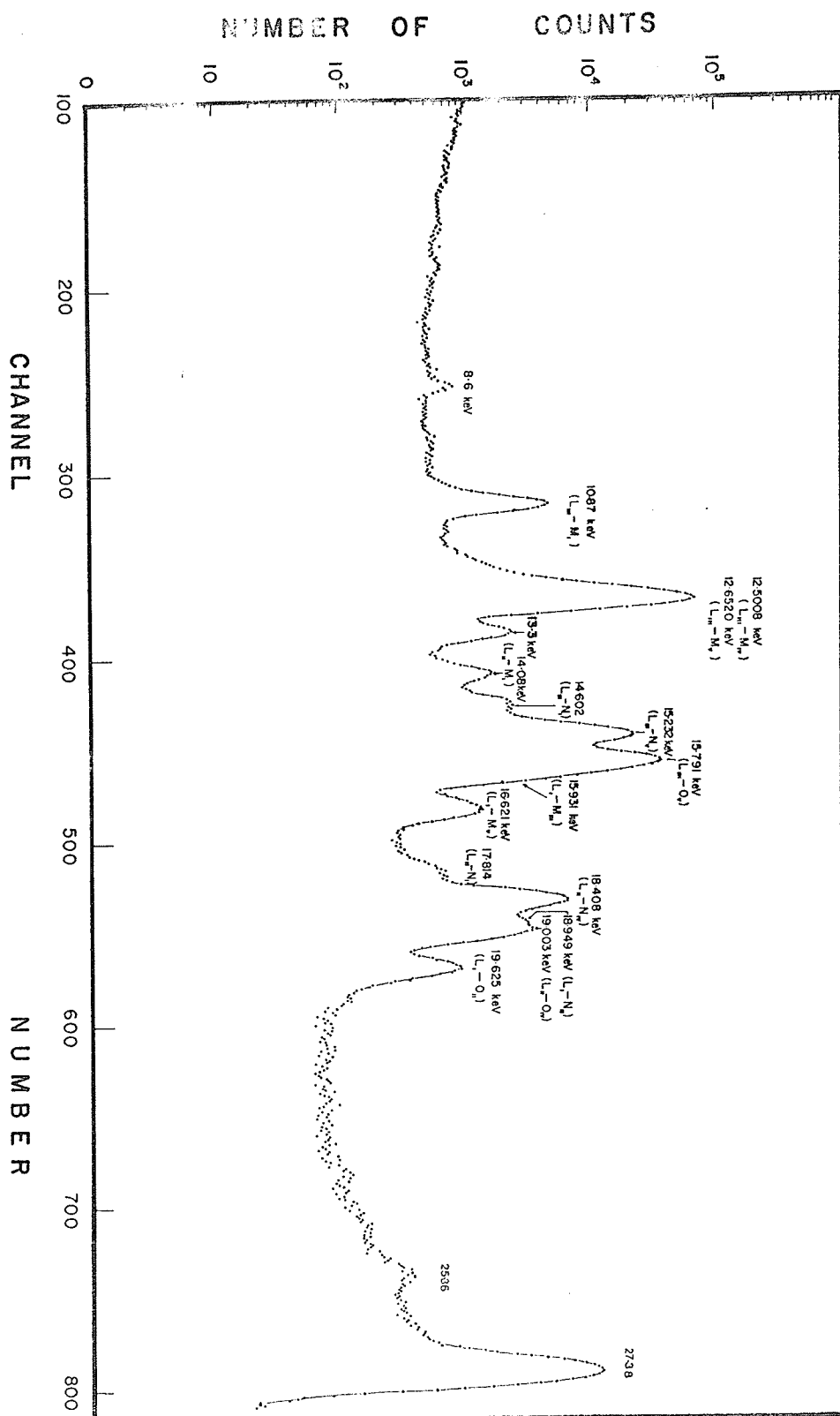
Pa between 9M HCl, DIPK and 2M HCl, and became a routine procedure.

III.3 SINGLES GAMMA RAY SPECTRA

A very interesting feature of the gamma ray spectrum of ^{231}Pa decay is that it is very rich in gamma rays. Further, the gamma rays seem to be present in two groups (20 to 100 keV and 240 to 600 keV), with a relatively empty region, extending from 100 to 240 keV, between them. A total of 73 gamma rays were observed in the present work, and this should give some indication of the complexity of the decay.

Figure III-1 shows a portion of the low energy gamma ray spectrum, from approximately 2 to 28 keV, taken with a Si(Li) X-ray detector whose resolution was 240 eV at 6.5 keV. The weak peak at 8.6 keV is the K X-ray of Zn, which is present in the source as an impurity. The lines at 24.5, 25.36 and 27.38 keV are the gamma rays coming from ^{231}Pa decay, the last one (27.38 keV) being the strongest transition in the entire decay. Transitions of energies 11.0, 14.1, 16.5, 18.2, 19.0, 19.6 and 22.7 keV had been reported[4,17,18] from conversion electron studies, but the photopeaks at these energies are not observed in the present work

75

Figure III-2

Low energy spectrum of ^{231}Pa decay,

taken wihh a Ge(Li) detector
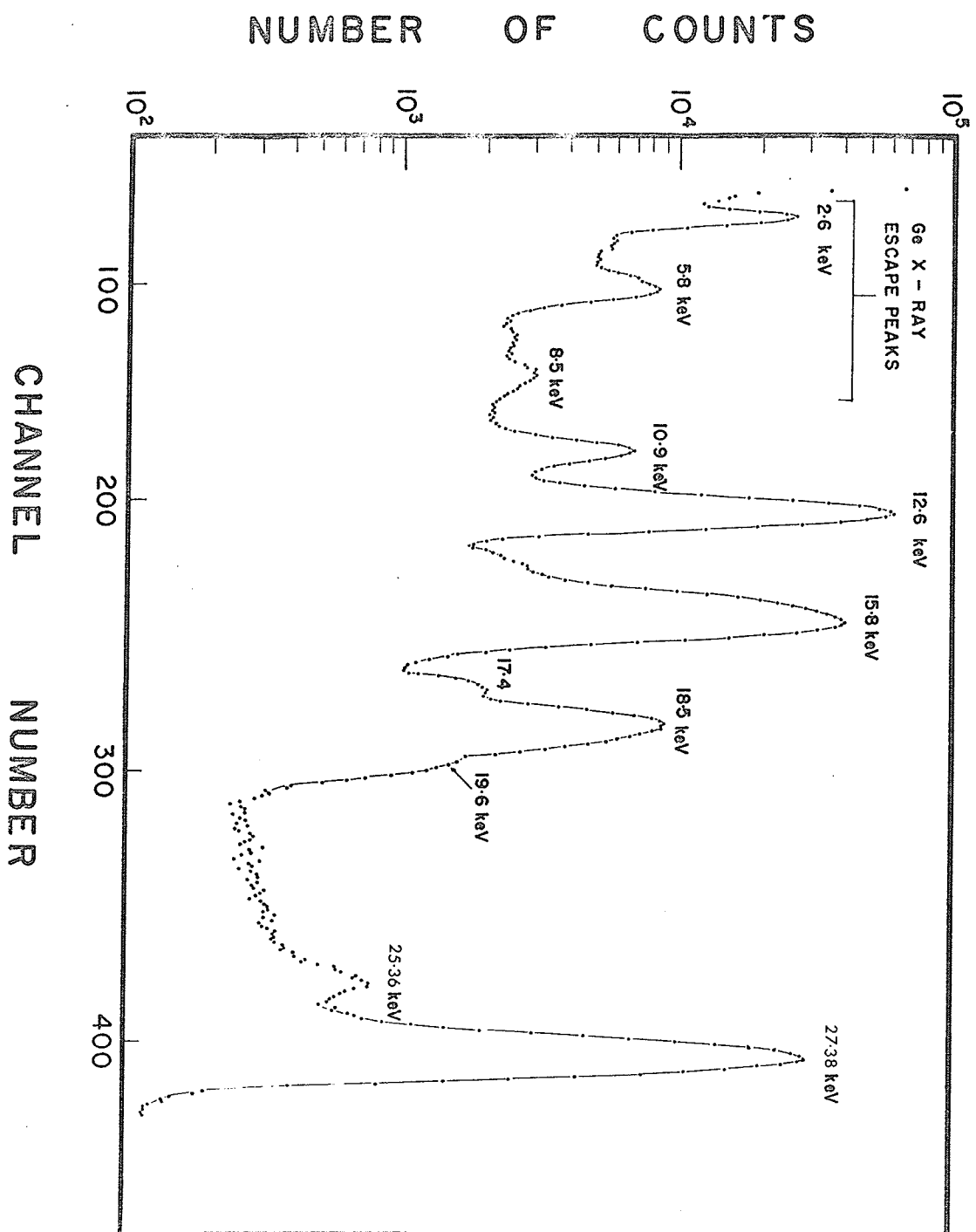
Figure III-3

Gamma ray spectrum of ^{231}Pa decay

(10 - 110 keV)
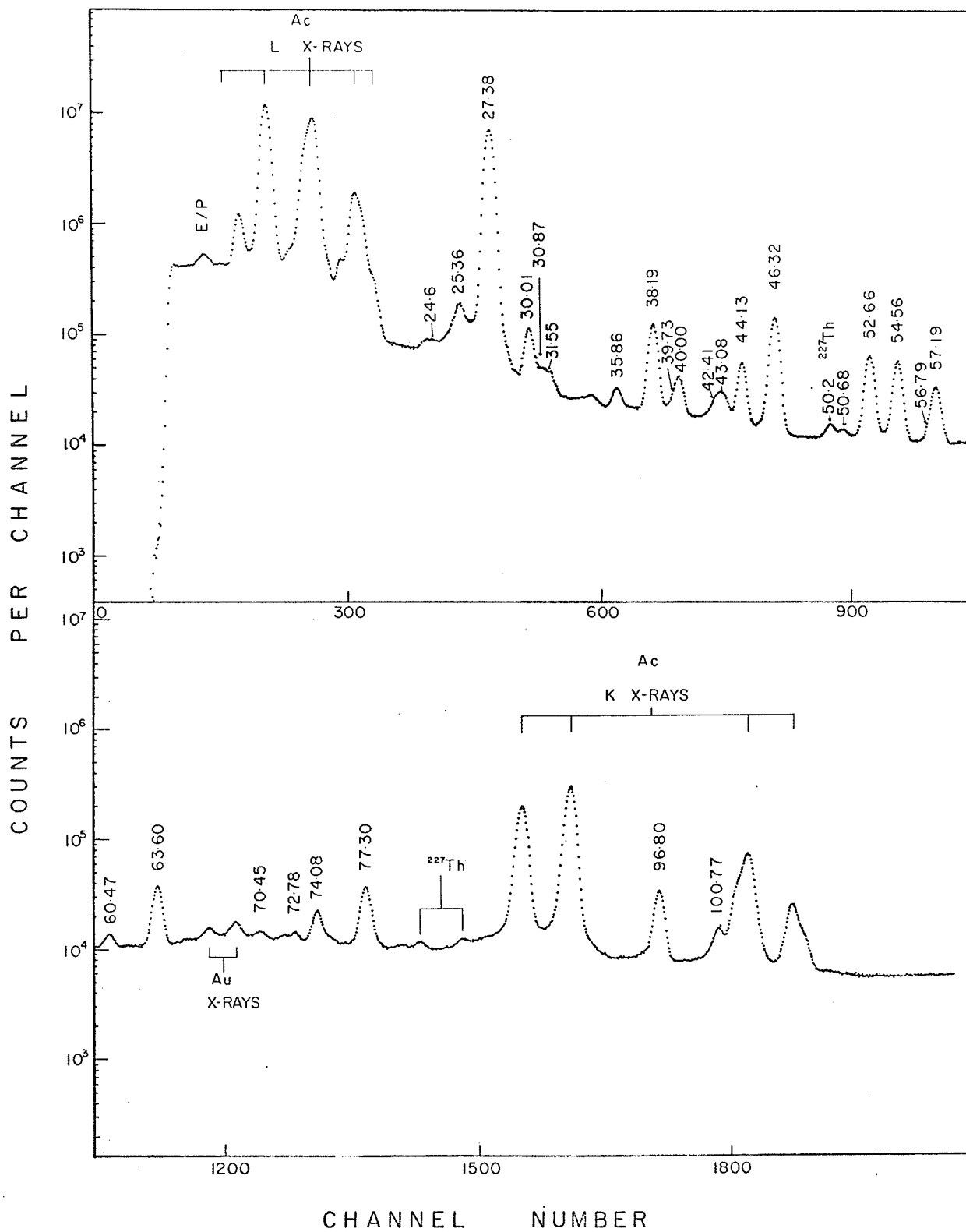
either because they are masked by the intense L X-rays or they are so strongly converted that they can be observed only from the low energy conversion electron studies.

Figure III-2 shows the spectrum in the same energy region, but taken with a Ge(Li) X-ray detector whose resolution is 290 eV at 5.9 keV. Note that apart from the fact that the detector has a poorer resolution, the Ge X-ray escape peaks are present in the spectrum, and these escape peaks tend to obscure portions of the spectrum. This demonstrates that for very low energy work, there is indeed a distinct advantage in using Si(Li) as opposed to Ge(Li) X-ray detectors, even though the detection efficiency may be lower.

Figure III-3 shows a portion of the spectrum from 10 to 110 keV, taken with the Ge(Li) X-ray detector. It is obvious that this region is very rich in gamma rays. The gold X-rays are produced by fluorescence, due to the presence of a layer of of gold about 50 $\overset{o}{A}$ thick, evaporated onto the front of the detector in manufacture. The only unusual aspect of this portion of the spectrum is that both Pinho[17] and Leang[16] reported having observed photopeaks at 100.5 and 102.6 keV. The intensities of these lines (relative to $I_\gamma(283.65) = 100.0$) are given in the table below. The

Figure III-4

(A) Simulation of Ac K X-rays

(B) Actual spectral data

COUNTS PER CHANNEL

(A)

CHANNEL NUMBER

K-M$_{II}$ 102·10

K-M$_{III}$ 102·85

K-M$_{IV}$ 103·39
K-M$_{V}$ 103·54

K-N$_{II}$ 105·68
K-N$_{III}$ 105·87
K-N$_{IV,V}$ 106·09

K-O$_{II,III}$ 106·56

(B)
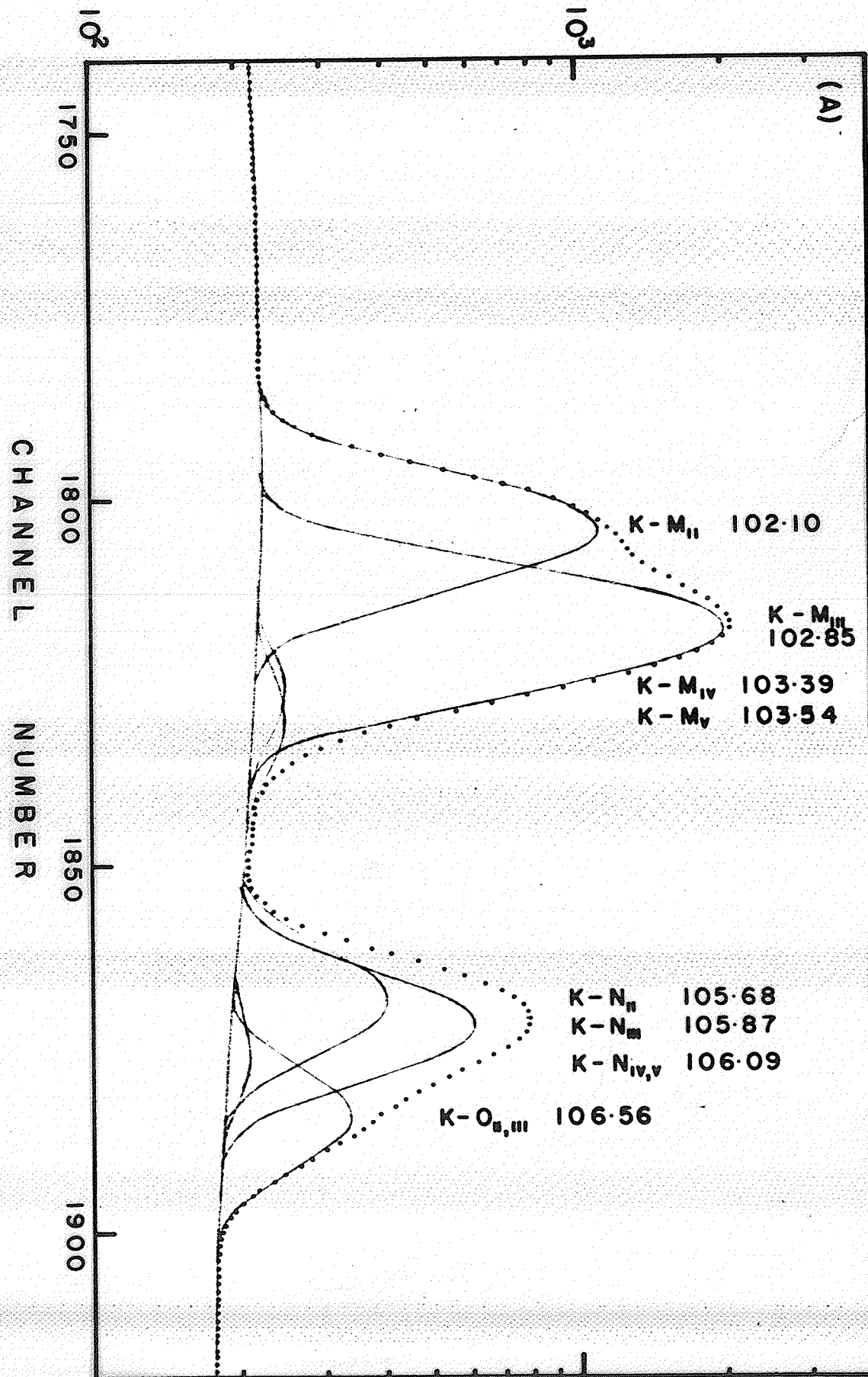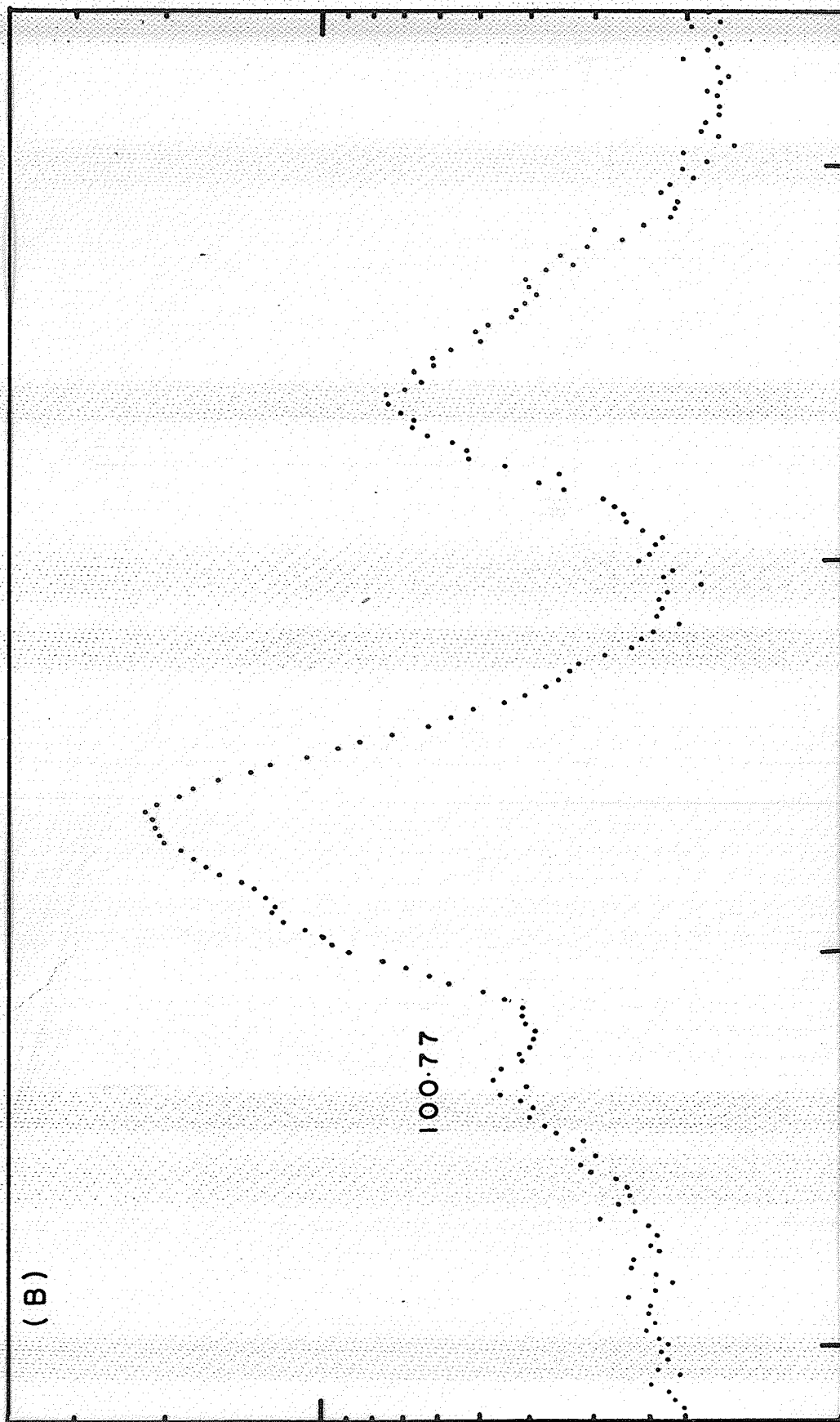
100.77

100.5 keV gamma ray is presumably that of energy 100.77 keV as shown in Figure III-3, (see below). It is not immediately obvious that a gamma ray at 102.6 keV exists, since it (if present) would be masked by the actinium X-rays. Only an upper limit of 0.8 can be given to this transition.

Energy	Pinho	Leang	Present Work
100.5	2.01	0.75	1.66
102.6	1.25	2.75	<0.8

On account of the complexity of the X-ray groups, it would be impractical to try numerical unwrapping, since the error associated with such a process would be tremendous. Instead, a set of the K X-rays of Ac is generated in the following manner. From the analysis of the gamma rays and the K_{α_2}, K_{α_1} X-rays, the widths of the other X-ray components are obtained by interpolation. The relative intensities of the various components (relative to the K_{α_1}) are obtained by interpolation from Scofield's data[20] The result of the simulation is shown in Figure III-4A. The The experimental data is plotted in Figure III-4B. When the simulation is superposed on the experimental data, it is clear that the 100.5 keV gamma ray reported by Pinho and Leang is the 100.77 keV transition in the present work (see Table III-1), but the 102.6 keV line reported by them is not present. This analysis does not exclude

Figure III-5

Gamma ray spectrum of ^{231}Pa decay

(190 - 700 keV)

COUNTS PER CHANNEL

CHANNEL NUMBER

435·03
438·1
438·8

B/G

486·8

501·0

510·9
511·

516·1

536·6

546·6

571·0

B/G

B/G

198·89

236·0   ²²⁷Th
B/G
242·16
245·77   243·15
246·05
255·76
258·54
260·23

B/G
273·15
277·10
283·65
286·60

300·02
302·65

310·0
312·94

327·26
330·06

B/G
340·77

351·6 B/G
354·57
357·21
359·75
363·93

375·01
379·41

384·7

391·67
395·49
398·10
B/G
407·80
410·1
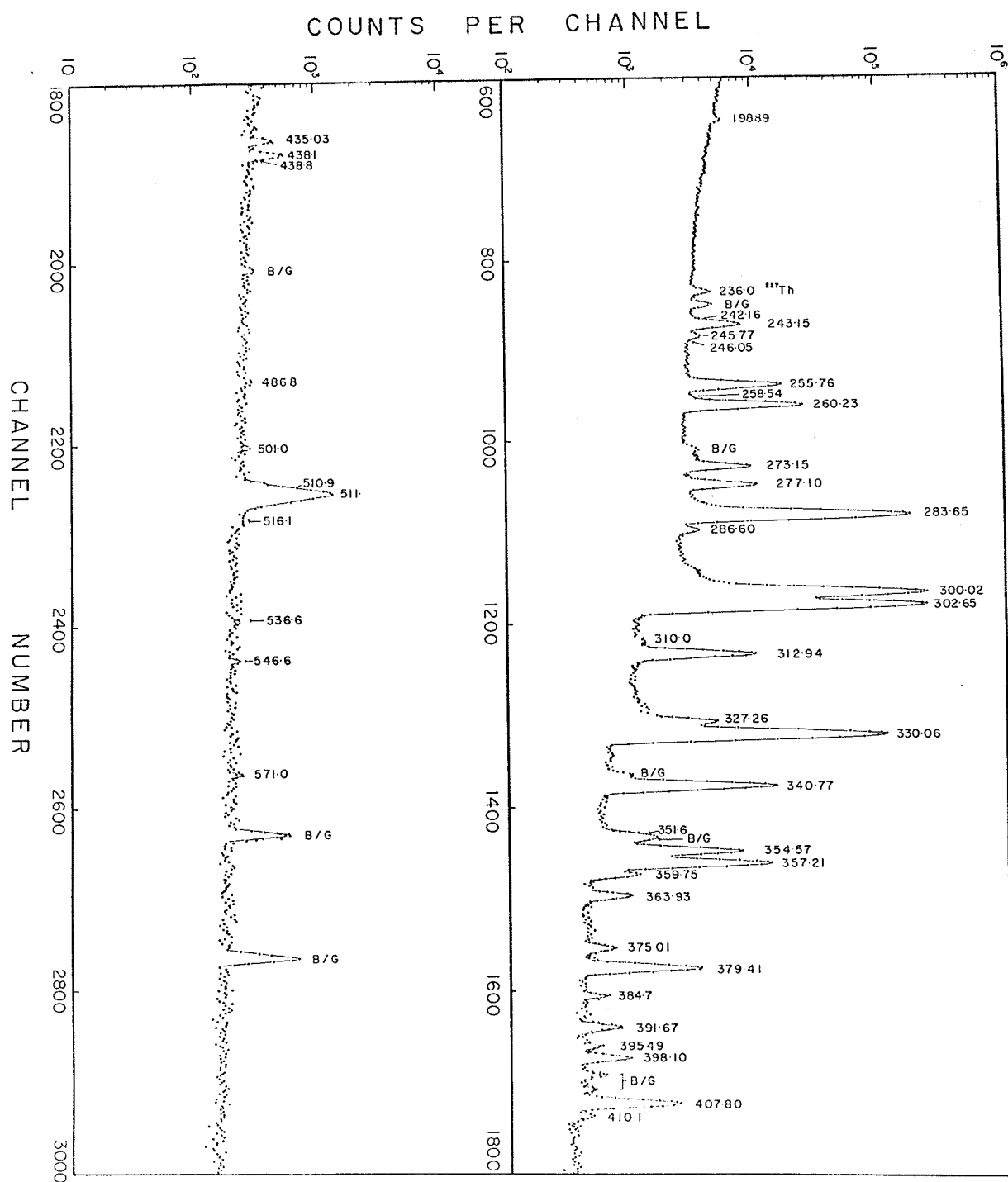
Table III-1

Energies of the gamma rays

following ^{231}Pa decay

(C) Observed in coincidence only

Present Work	Pinho	Leang	Hagee	Baranov
	14.1 ± 0.1			
	16.5 ± 0.1			16.5
	19			19.6
25.36 ± 0.08	25.54 ± 0.06	25.2 ± 0.2		25.4
27.38 ± 0.02	27.35 ± 0.02	27.3 ± 0.2	27.3	27.4
30.01 ± 0.03	29.95 ± 0.02	29.9 ± 0.2	30.7	29.4
30.87 ± 0.04	30.00 ± 0.05			
31.55 ± 0.05	31.54 ± 0.05			34.0
35.86 ± 0.04	35.82 ± 0.03	35.8 ± 0.3	35.5	
38.19 ± 0.02	38.20 ± 0.02	38.1 ± 0.2	38.0	38.2
39.73 ± 0.03	39.57 ± 0.04		39.6	
40.00 ± 0.03	39.97 ± 0.02			
42.41 ± 0.04	42.48 ± 0.05			
43.08 ± 0.04	43.05 ± 0.05			
44.13 ± 0.02	44.16 ± 0.02	44.1 ± 0.2	43.9	
46.32 ± 0.02	46.37 ± 0.02	46.2 ± 0.2	46.1	
50.68 ± 0.06	50.98 ± 0.05			
52.66 ± 0.03	52.74 ± 0.02	52.6 ± 0.2	52.4	
54.56 ± 0.03	54.61 ± 0.02	54.5 ± 0.2	54.8	
56.79 ± 0.04	56.76 ± 0.04	57.0 ± 0.2		57.0
57.19 ± 0.03	57.19 ± 0.03	57.0 ± 0.2		57.0
60.49 ± 0.08	60.50 ± 0.03	60.2 ± 0.3	59.4	
63.60 ± 0.04	63.67 ± 0.3	63.5 ± 0.2	63.3	63.3
70.45 ± 0.08	70.50 ± 0.05			
	71.9 ± 0.1			
72.78 ± 0.08	72.5 ± 0.1			
74.08 ± 0.06	74.18	74.1 ± 0.3		

Present Work	Pinho	Leang	Hagee	Baranov
77.30 ± 0.04	77.36 ± 0.03	77.2 ± 0.2	77.1	
96.80 ± 0.03	96.88 ± 0.03	96.7		96.0 / 97.0
100.77 ± 0.04	100.92 ± 0.4	100.5 ± 0.5		
	102.6	102.5 ± 0.4	102.5	102.5
124.56 ± 0.08	124.6 ± 0.1	124.4 ± 0.5		126.8
144.33 ± 0.8	144.5 ± 0.1	144.4 ± 0.5		
161.0 ± 1.0				
198.89 ± 0.10	199 ± 1	198.7 ± 0.6		
228.0 ± 1.0				
242.16 ± 0.08	242.2 ± 0.1	242.9 ± 0.4		
243.15 ± 0.09	243.0 ± 0.1		243.0	
245.77 ± 0.09	245.4 ± 0.5	245.3 ± 0.5		
246.05 ± 0.09	246.0 ± 0.2			
255.76 ± 0.08	255.78 ± 0.07	255.9 ± 0.3	256.1	
258.54 ± 0.15	258.4 ± 0.1			
260.23 ± 0.08	260.14 ± 0.08	260.2 ± 0.3	260.2	260.5
273.15 ± 0.09	273.08 ± 0.09	273.2 ± 0.3	273.5	
277.10 ± 0.09	276.00 ± 0.09	277.2 ± 0.3	277.7	
283.65 ± 0.05	283.56 ± 0.06	283.7 ± 0.3	283.9	285
286.60 ± 0.10	286.55 ± 0.10			
300.02 ± 0.05	299.94 ± 0.6	300.10 ± 0.02	300.5	300.
302.65 ± 0.15	302.52 ± 0.6	302.7 ± 0.2	303.2	303.
310.0	310.0 ± 0.1			
312.94 ± 0.05	312.88 ± 0.08	312.9 ± 0.3	313.0	
		318.1		
327.26 ± 0.10	327.02 ± 0.10	327.2 ± 0.4		
330.06 ± 0.05	329.89 ± 0.06	330.0 ± 0.2	330.2	330.
340.77 ± 0.06	340.61 ± 0.07	340.8 ± 0.2	341.0	

Present Work	Pinho	Leang	Hagee	Baranov
351.6 ± 0.1	351.4 ± 0.1			
354.57 ± 0.08	354.38 ± 0.08	354.6		354.5
357.21 ± 0.06	356.96	357.2	356.6	
359.75 ± 0.10	359.25 ± 0.10	358.6 ± 0.4		
363.93 ± 0.10	363.74 ± 0.10	363.9 ± 0.4	364.2	
375.01 ± 0.10	374.9 ± 0.1	374.9 ± 0.4		
379.41 ± 0.06	379.09	379.2 ± 0.3	379.5	380.
384.7 ± 0.10	384.7 ± 0.1	384.8 ± 0.3		
	387.0 ± 0.1			
391.67 ± 0.09	391.5 ± 0.1	391.7 ± 0.3	392.5	
395.49 ± 0.10	395.5 ± 0.1	395.7		
398.19 ± 0.09	398.10 ± 0.08	398.1 ± 0.3	398.4	
407.80 ± 0.05	407.71 ± 0.06	407.7 ± 0.3	408.1	
410.1 ± 0.10	410.5 ± 0.1	410.3 ± 0.1	410.5	
427.0				
435.0 ± 0.10	435.1 ± 0.1	434.9 ± 0.8		
438.1 ± 0.09	437.9 ± 0.1	437.9 ± 0.8	437.9	
438.8 ± 0.2	438.7 ± 0.1			
	491.0 ± 0.6	491. ± 2.		
501.0 ± 1.0	501.6 ± 0.5	501. ± 1.		
510.0 ± 1.0	509. ± 1.	510. ± 1.	512.2	
516.1 ± 1.0	516.2 ± 0.6	516. ± 1.	516.2	
536.6 ± 1.0	635.3 ± 0.7			
546.6 ± 1.0	546.6 ± 0.7			
571.0 ± 1.0	572.1 ± 0.8			
583.		583. ± 2.		
609		609 ± 2		

the existence of a weak photopeak at this energy, since the conversion lines of this transition have been observed before[18] However, it does show that the intensity of the 102.6 keV line is quite small, and in the present work, a value of 0.8 (relative to $I_\gamma(283.65)=100.0$) is estimated to be the upper limit of the intensity of this gamma ray. This seems to agree better with the value of 1.25 reported by Pinho than that reported by Leang.

The region between 120 to 200 keV (not shown) is rather uninteresting in that it contains only three very weak lines whose energies are 124.56 ± 0.08, 144.33 ± 0.08 and 198.89 ± 0.10 keV. The rest of the gamma ray spectrum from the decay of ^{231}Pa is shown in Figure III-5. The line at 236.0 keV is the strongest gamma ray[26] coming from the decay of ^{227}Th, which is the immediate decay product of ^{227}Ac. In the present work, the presence of this gamma ray is the signal that the source (^{231}Pa) requires purification, the gamma rays emitted in the decay of ^{227}Ac being of low energies and intensities. The highest energy gamma ray occurs at 571.0 keV, and gamma rays of higher energies were searched for but none could be attributed to ^{231}Pa decay. A list of gamma ray energies is shown in Table III-1. Also listed for comparison are those

Table   III-2

Relative intensities of the

gamma   rays

of

^{231}Pa decay

(relative to I_γ(283.65)=100.)

(C)   Observed in coincidence only

E_γ (KeV)	I_γ	
	Present Work	Pinho
24.6	0.7 ± 0.3	0.6
25.36	6.9 ± 1.0	5.9
27.38	640. ±50	592. ±28.
30.01	6.5 ± 0.5	5.9 ± 0.8
30.87	0.5 ± 0.1	0.59± 0.15
31.55	0.47 ± 0.04	0.41± 0.14
35.86	0.94 ± 0.05	1.06± 0.17
38.19	9.4 ± 0.5	9.46± 1.39
39.73	0.14 ± 0.01	0.09± 0.05
40.00	1.22 ± 0.06	0.77± 0.15
42.41	0.3 ± 0.1	0.35± 0.07
43.08	0.41 ± 0.11	0.41± 0.02
44.13	3.77 ± 0.40	3.85± 0.60
46.32	12.97 ± 0.64	13.25± 0.63
50.68	0.08 ± 0.04	0.09± 0.04
52.66	4.85 ± 0.34	5.38± 0.78
54.56	4.33 ± 0.35	5.14± 0.71
56.79	0.27 ± 0.04	0.36± 0.08
57.19	2.54 ± 0.26	2.49± 0.35
60.47	0.3 ± 0.1	0.41± 0.08
63.60	2.7 ± 0.3	3.2 ± 0.4
70.45	0.6 ± 0.2	0.41± 0.08
72.78	0.2 ± 0.1	0.24± 0.13
74.08	1.24 ± 0.20	1.6 ± 0.3
77.30	4.31 ± 0.20	4.32± 0.20
96.80	5.62 ± 0.28	5.62± 0.86

E_γ (KeV)	I_γ	
	Present Work	Pinho
100.77	1.66 ± 0.25	2.01± 0.40
102.6	<0.8	1.18
124.56	0.29 ± 0.09	0.29± 0.13
144.33	0.64 ± 0.30	0.77± 0.27
161.0	(C)	
198.89	0.23 ± 0.10	0.36± 0.14
228.	(C)	
242.16	0.5 ± 0.2	0.53± 0.08
243.15	2.97 ± 0.24	2.19± 0.28
245.77	0.58 ± 0.15	0.47± 0.08
246.05	0.01 ± 0.005	0.6
255.76	6.34 ± 0.41	6.45± 0.66
258.54	0.15 ± 0.05	0.15± 0.04
260.23	11.39 ± 0.57	11.01± 1.17
273.15	3.48 ± 0.24	3.67± 0.35
277.10	3.88 ± 0.25	4.26± 0.44
283.65	100.0	100.
286.60	0.8 ± 0.3	0.59± 0.09
300.02	149.6 ± 7.5	144.4± 15.0
302.65	150.4 ± 8.0	149.1± 15.3
310.0	0.07 ± 0.03	0.09± 0.03
312.94	7.05 ± 0.56	6.03± 0.64
327.26	2.27 ± 0.28	1.89± 1.27
330.06	81.9 ± 6.5	82.8 ± 8.0
340.77	10.9 ± 1.3	10.53± 1.03
351.6	0.15 ± 0.06	0.22± 0.03

E_γ (KeV)	I_γ	
	Present Work	Pinho
354.57	5.07 ± 0.56	6.03± 0.64
357.21	9.67 ± 0.82	11.07± 1.17
359.75	0.41 ± 0.18	0.57± 0.07
363.93	0.42 ± 0.15	0.47± 0.06
375.61	0.24 ± 0.10	0.29± 0.04
379.41	2.89 ± 0.23	3.14± 0.38
384.7	0.18 ± 0.04	0.26± 0.04
387.0	not seen	0.03± 0.01
391.67	0.52 ± 0.08	0.43± 0.06
395.49	0.11 ± 0.02	0.17± 0.03
398.19	0.49 ± 0.09	0.59± 0.13
407.80	2.13 ± 0.18	2.31± 0.29
410.1	0.19 ± 0.04	0.12± 0.02
427.0	(C)	
435.0	0.12 ± 0.03	0.21± 0.03
438.1	0.20 ± 0.06	0.26± 0.04
438.8	0.07 ± 0.02	0.09± 0.03
486.8	0.15 ± 0.05	0.11± 0.03
491	not seen	0.03
501.0	0.05 ± 0.02	0.04± 0.02
510.0	0.05 ± 0.02	0.04± 0.02
516.1	0.06 ± 0.02	0.01± 0.003
536.6	0.05 ± 0.02	0.03± 0.01
546.6	0.04	0.04± 0.02
571.0	0.04	0.03± 0.01

Figure III-6

A trochoidal spectrometer

VACUUM GAUGE

10 cm

DETECTOR

POLE TIP

COLD TRAP

SOURCE HOLDER

DETECTOR

TO PUMP
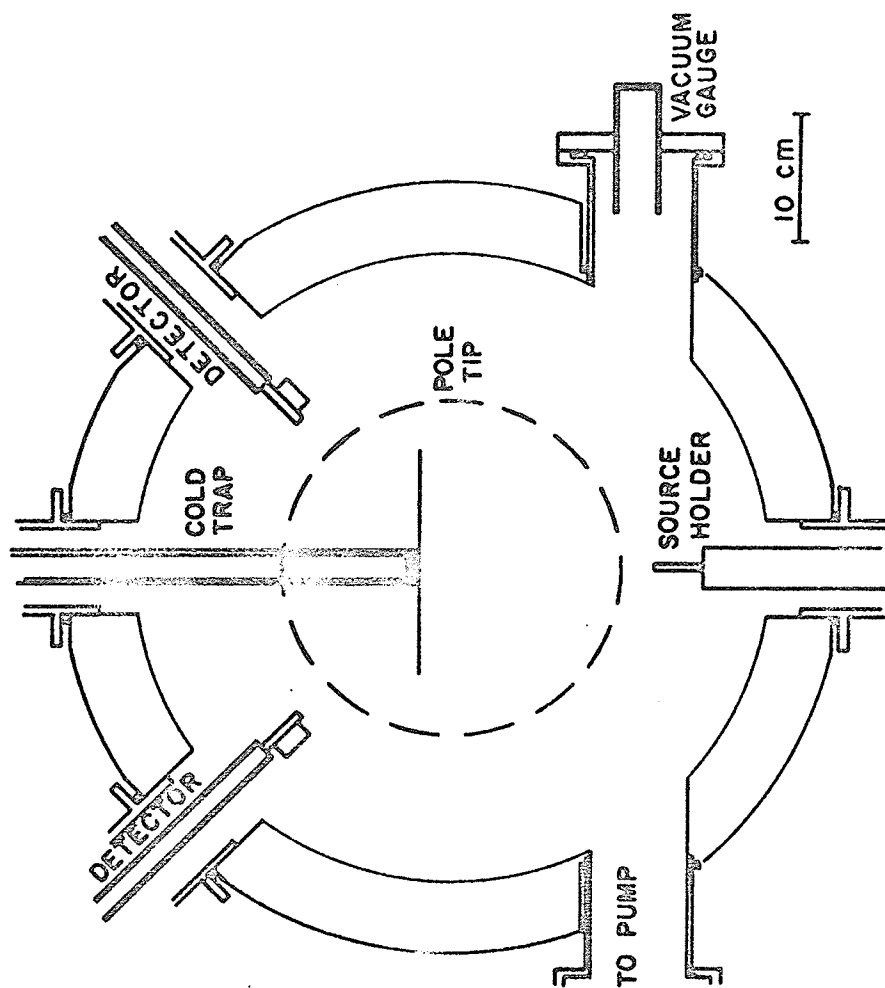
reported by Pinho,[17] Hagee[15] and Leang.[16] Table III-2 shows the relative intensities, normalised to $I_\gamma(283.65) = 100.0$. Also listed are the relative intensities (normalised to the same line) as reported by Pinho.[17]

III.4 CONVERSION ELECTRON SPECTRA

The conversion electrons have been examined using a trochoidal spectrometer which was designed and built at this University. The principle and operation of this spectrometer has been discussed elsewhere[22], and will not be given in detail here. Essentially, conversion electrons emitted by the source are spiralled along the fringing field of an electro-magnet having circular pole faces, and travel in a trochoidal path until they are intercepted by a surface barrier electron detector placed in the spectrometer, as shown in Figure III-6. The alpha particles, emitted as a result of the decay of ^{231}Pa, drift in the opposite direction since they have a charge opposite to that of the electrons, and hence are not detected. Thus the radiation damage of the electron detector due to the alpha particles is avoided.

It should be pointed out that a great advantage of using this spectrometer is that practically all the electrons emitted (irrespective of the direction of

Figure   III-7

Conversion electron spectrum of

^{227}Ac

COUNTS PER CHANNEL

CHANNEL NUMBER

243·15 K

255·76 K
260·23 K

273·15 K
277·10 K

283·65 K

300·02 K
302·65 K

312·94 K

243·15 L   327·26 K
330·06 K

340·77 K
260·23 L   354·57 K
357·21 K

283·65 L

379·41 K   300·02 L
302·65 L

407·80 K   312·94 L,   300·02M
302·65M

327·26 L
330·06 L

340·77 L,   330·06 M

354·57 L, 357·21 L

354·57 M, 357·21 M

379·41 L

379·41 M

407·80 L

407·80 M
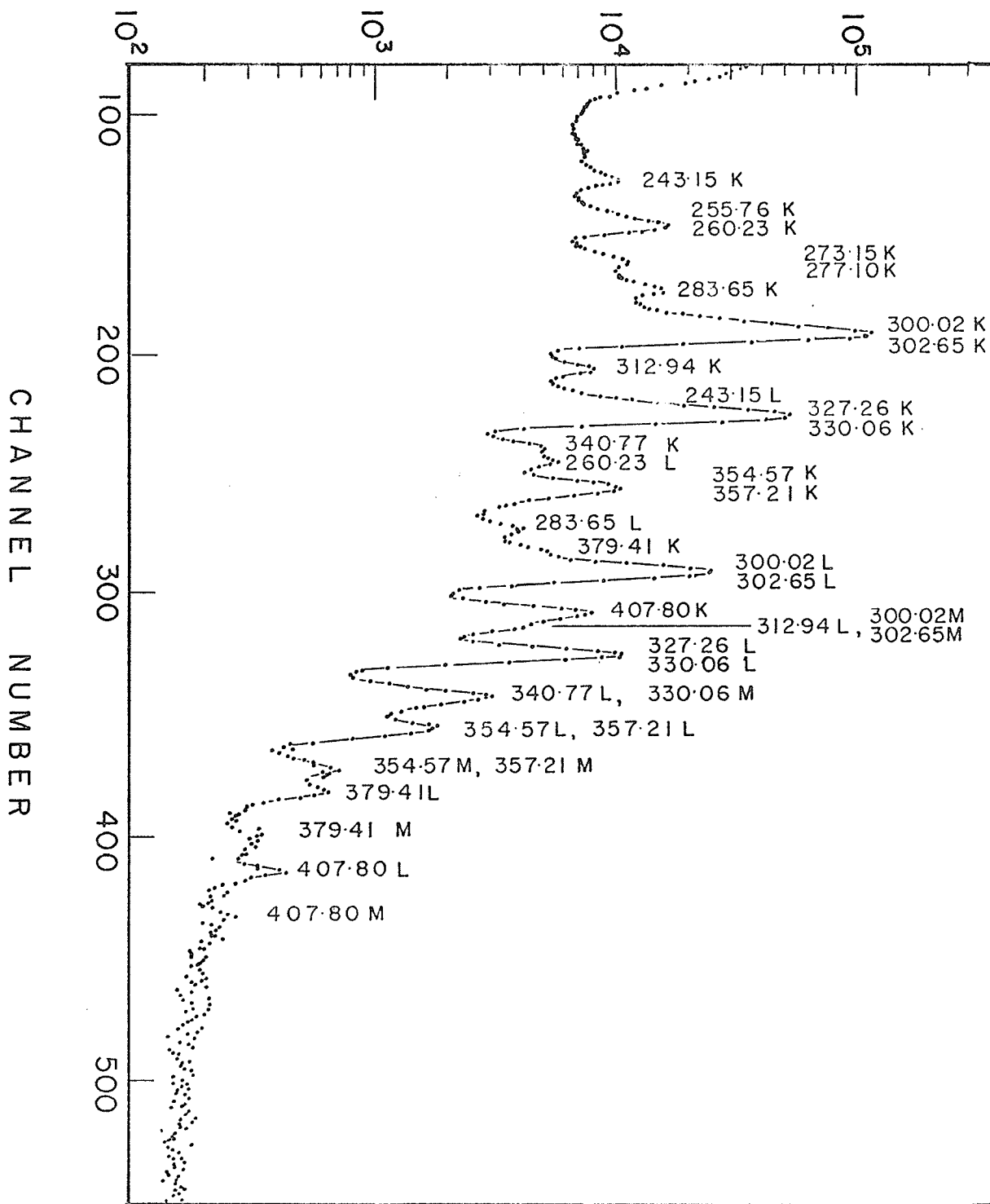
emission) arrive at the detector. Thus a strong source is not required.

The source mount for this spectrometer consists of a VYNS film[23] mounted on a rectangular aluminium frame whose external dimensions are 4.5 cm by 4.7 cm. A thin layer of gold is evaporated on the VYNS film, and a drop of ^{231}Pa in HCl is dropped onto the geometric centre of the film, and evaporated to dryness. Three different sources were prepared in this manner and four different runs were made.

A typical conversion electron spectrum of ^{227}Ac is shown in Figure III-7. The energy resolution is 6.0 keV at 300.0 keV; this is deemed satisfactory in view of the fact that dropped sources were used. The spectrum is very complicated, as expected, and numerous unwrapping procedures are required. Such unwrapping processes have been carried out by hand, since it is impractical to try numerical unwrapping, as too many parameters would be involved.

The detection efficiency of the trochoidal spectrometer has been absolutely calibrated[22] so that it is possible to determine absolutely the number of electrons emitted per second N_e from the area under the conversion electron peak observed in a given time. After an electron spectrum is obtained, the source is

Figure III-8

Plot of α_K versus energy E

α_K

E1   E2   M1

ENERGY (keV)
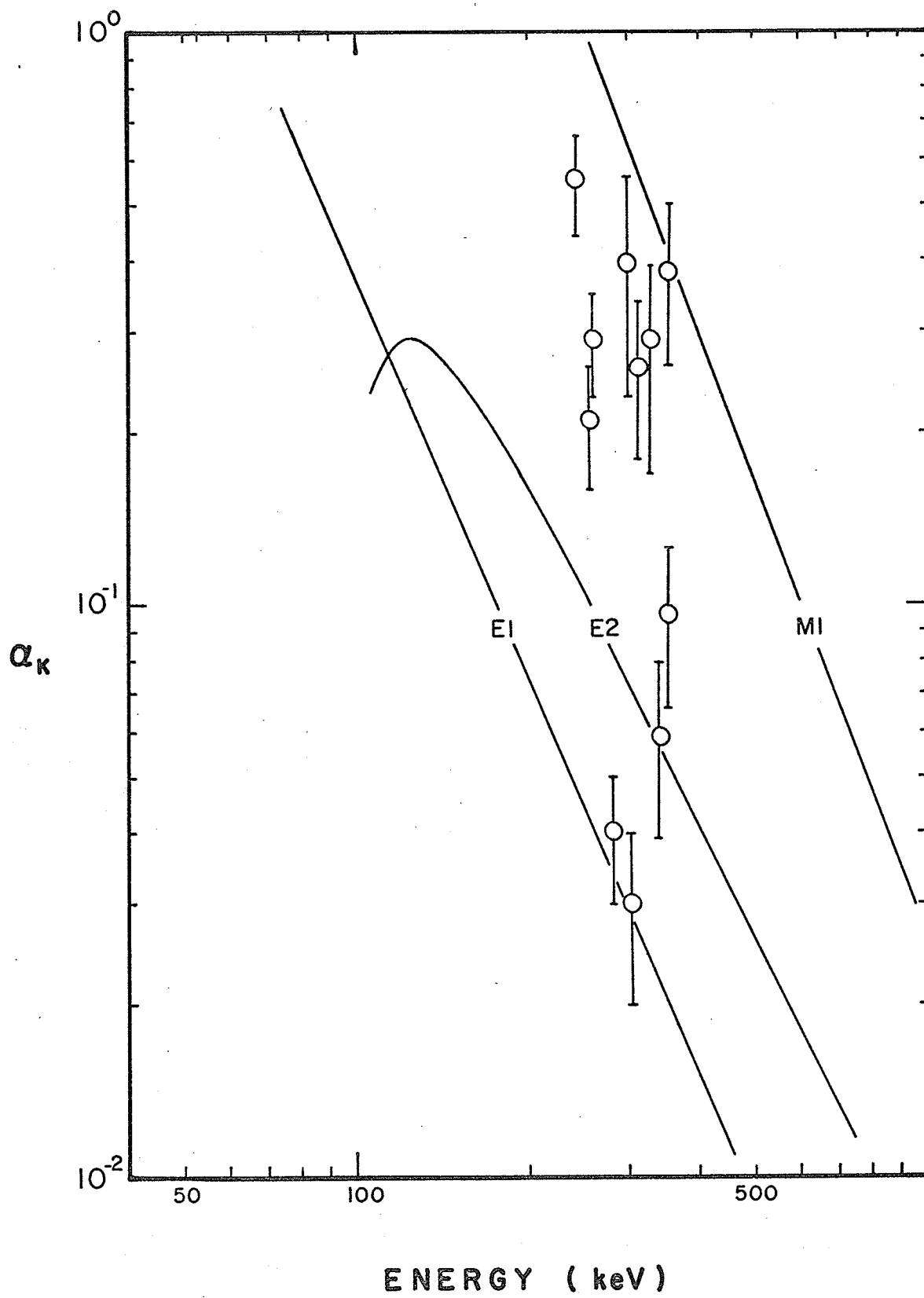
Table   III-3

K - conversion coefficients

of

^{227}Ac

E_γ (keV)	Run 1	Run 2	Run 3	Run 4	Mean		Pinho	Pinho et al		Hagee
243.15		0.59	0.50		0.54	± 0.14				
255.76		0.214	0.21		0.21	± 0.05				
260.23		0.29	0.29		0.29	± 0.07	0.23	0.62	± 0.16	
283.65	0.041	0.040	0.033	0.044	0.04	± 0.01	0.032	0.04	± 0.01	
300.02	0.39			0.31	0.35	± 0.09	0.26	0.39	± 0.06	
302.65	0.028			0.033	0.030	± 0.010	0.024	0.038	± 0.010	
312.94	0.28	0.27	0.24	0.25	0.24	± 0.08	0.25	0.47	± 0.16	1.78
330.06	0.29	0.27	0.25	0.27	0.27	± 0.07	0.25	0.41	± 0.05	0.412
340.77	0.052	0.067			0.060	± 0.020	0.2	0.054	± 0.020	0.222
354.57	0.096				0.10	± 0.02		0.14	± 0.05	
357.21	0.38				0.38	± 0.10		0.39	± 0.10	

removed from the spectrometer, and is put in front of a gamma ray detector whose absolute detection efficiency is known. Hence it is possible to determine N_γ , the absolute number of photons of a particular transition per second. Thus, for a given transition, the internal conversion coefficient α_k can be determined, knowing N_γ and N_e. Table III-3 lists the results of the four runs as well as those reported by Pinho[5,17] and Hagee[15] The agreement between the present work and Pinho's earlier data[5] is generally good. There are some discrepancies with that by Pinho et al[17] and Hagee[15].

The α_k for the 243.15 and 255.76 keV transitions are here reported for the first time to be 0.54 ± 0.14 and 0.21 ± 0.05 respectively. The 243.15 keV gamma ray de-excites the 273.15 keV level to the 30.01 keV level. The spins and parities of these levels are (5/2-) and 5/2- respectively (See level scheme in Figure III-22 in Section III.6). Thus, this transition with an α_k of 0.54 is very probably M1(39%)+E2(61%). The 255.76 keV gamma ray corresponds to a gamma transition from the 329.99 keV level (3/2-) to the 74.11 keV level (7/2-). An α_k of 0.21 suggests very strongly that this transition is E2+M1, specifically, 87%E2+13%M1. A summary of the conversion electron data is shown in Figure III-8.

III.5 GAMMA-GAMMA COINCIDENCE

Gamma-gamma coincidence work has been carried out employing the circuit as described in Chapter I. Because of the complexity of the spectrum, detectors of high resolution are necessary. In the present case, an Ortec Ge(Li) X-ray detector and an Ortec 35 cc Ge(Li) detector are used. Their resolutions are 290 eV at 6.5 keV and 3.0 keV at 1.33 MeV respectively. The coincidence work was carried out in the following manner. First, the 35 cc detector was used as the gating detector on channel 1. The SCA was set to gate on the strong lines in the 'high' energy region, namely those in the region between 230 to 570 keV. The X-ray detector at channel 2 was used to look for gamma rays in coincidence in the region between 20 to 100 keV. Then the two detectors were interchanged, with the X-ray detector being used as the gating detector in channel 1 and the 35 cc in channel 2. The advantage of doing this is that the two sets of data obtained may be checked against each other for consistency. Two large volume Ge(Li) detector were not used in both channels 1 and 2 because cascades consisting of high energy gamma rays are unlikely to occur in the present decay scheme. Two Ge(Li) X-ray detectors were not used in both channels because the detection efficiency would be too low. The method of removing the random coincidences and revealing the enhanced (i.e. coincident) lines is given on page 38 of Chapter I.

Figure III-9

Anti-scattering shield
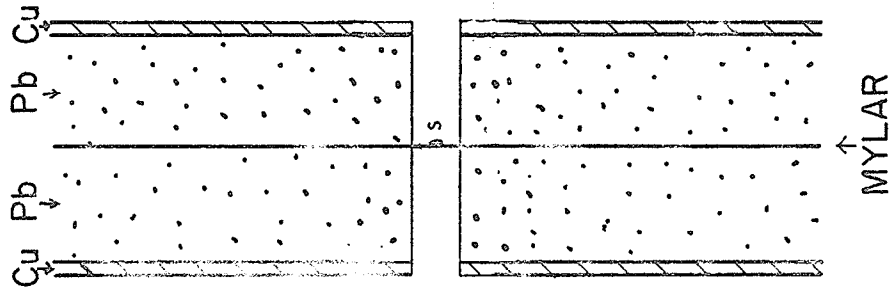
In order to minimize the effect of back scattering by one detector into the other, the source used for coincidence work was deposited on a piece of mylar film mounted in an anti-scattering shield as shown in Figure III-9. It should be noted that copper sheets were used to line the shield so as to absorb any lead X-rays that may be produced by fluorescence.

The counting time of each coincidence run was 7-10 days, and twelve gates were used. To avoid losses of activity in the purification processes, the same source as was used for some of the singles runs served for the coincidence studies. It was realized that ^{227}Th would have grown in but it was thought that its radiations would not complicate the analysis of the coincidence data. This proved to be only partially true, for the tails of some of the stronger lines from the ^{227}Th decay were found to be effective in opening the gates. This was enhanced by the gate widths used (up to 4 keV) for the various spectra on which the gates were set did not have such good resolution as was obtained for the singles runs, owing to the more complex electronic circuitry employed for the coincidence work. However, detailed analysis enabled unambiguous identification of the coincident radiations in the decay of ^{231}Pa.

To comprehend fully the discussion on the

Figure III-10

Coincidence spectrum with the

46.32 keV gamma ray
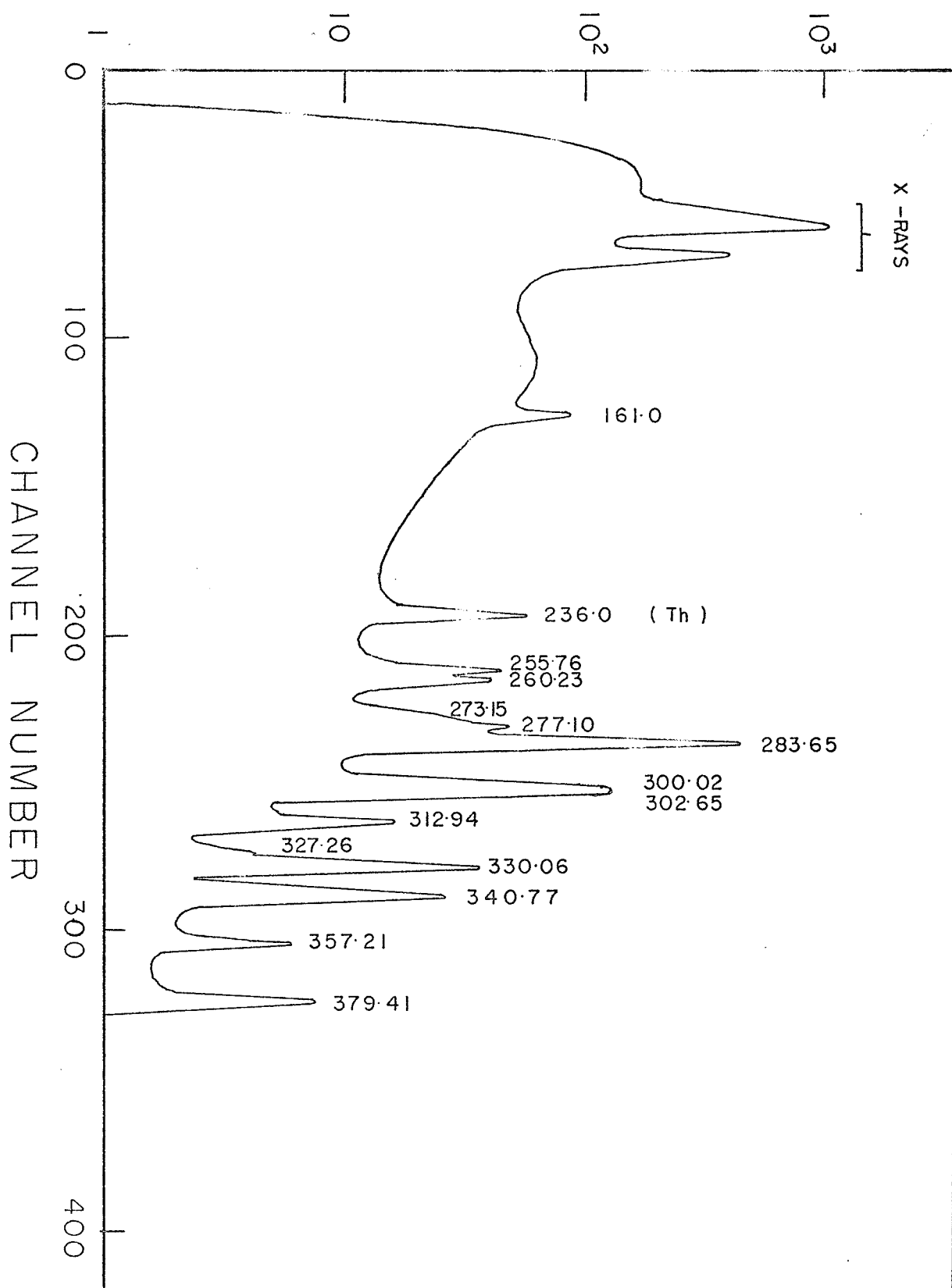
coincidence data, reference should be made, whenever
necessary, to the decay scheme as shown in
Figure III-23.

46.32 keV Gate :

Figure III-10 shows the coincidence spectrum when
the gate is set on the 46.32 keV line. The enhanced
lines include those whose energies are: 161.0, 236.0,
255.76, 260.23, 273.15, 277.10, 283.65, 312.94, 340.77
and 379.41 keV. Of these only those at 161.0, 260.23,
283.65, 340.77 and 379.41 keV are in true coincidence
with the gate. Although the lines at 161.0 and
260.23 keV do not feed the 46.32 keV level directly,
they are enhanced nevertheless, being in cascade with
the gate (46.32 keV gamma ray) through the 42.41, 38.19
and 63.60 keV transitions. Lines at 391.0 and
570.0 keV are expected to be enhanced, but they are too
weak to show up. The rest of the enhanced lines can be
accounted for on the grounds that due to the complexity
of the spectrum, it was not possible to obtain a clean
gate. In the present case, some pulses, corresponding
to the 50.2 keV gamma ray (the strongest transition[27] in
the decay of [227]Th) and the 50.68 keV from the decay of
[231]Pa leaked into the SCA and brought about the
enhancement of some of the lines. The line at 236.0 keV
is in coincidence with the 50.2 keV line which comes

Figure III-11

Coincidence spectrum with the

52.66 keV gamma ray
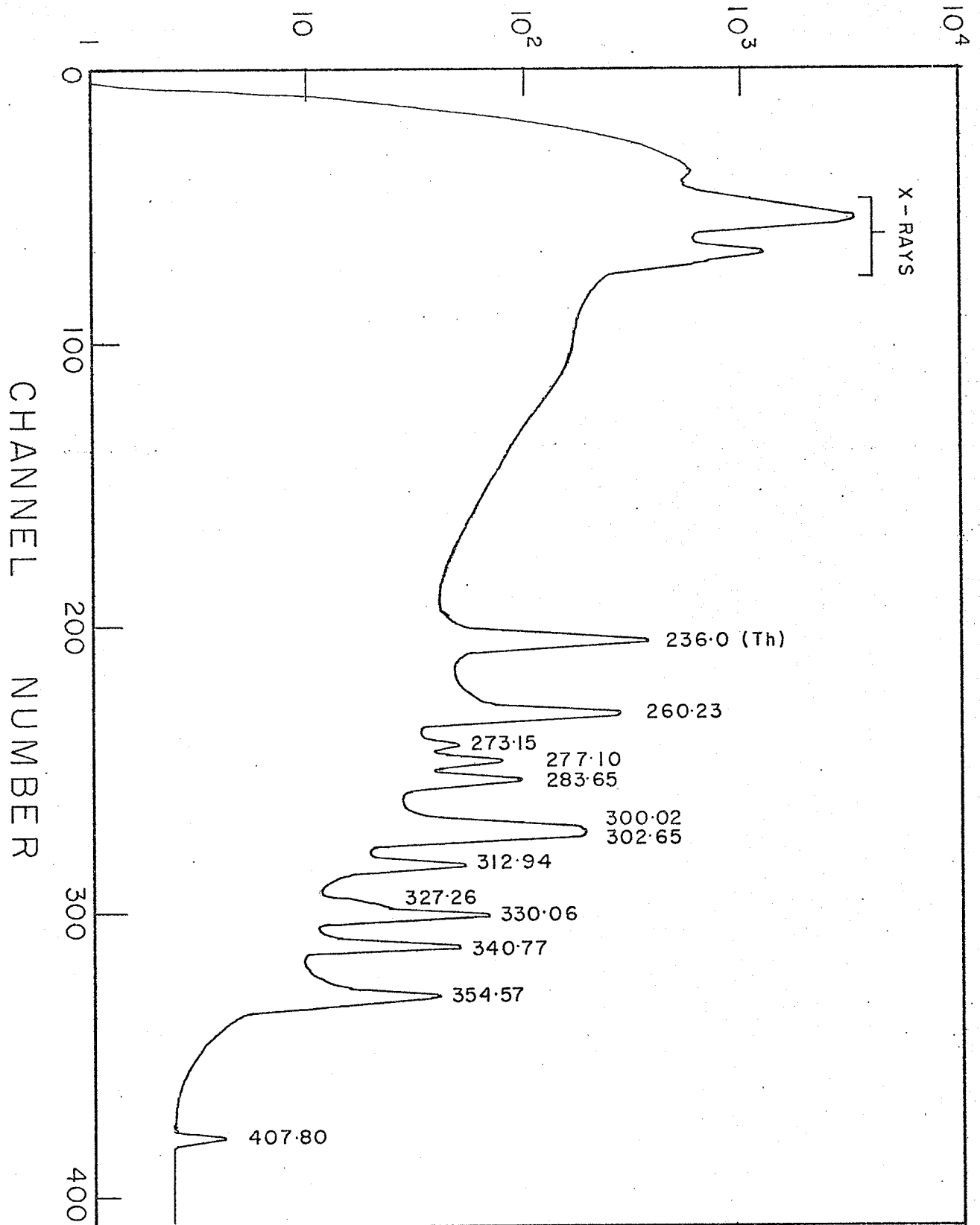
Figure III-12

Coincidence spectrum with the

54.56 keV gamma ray
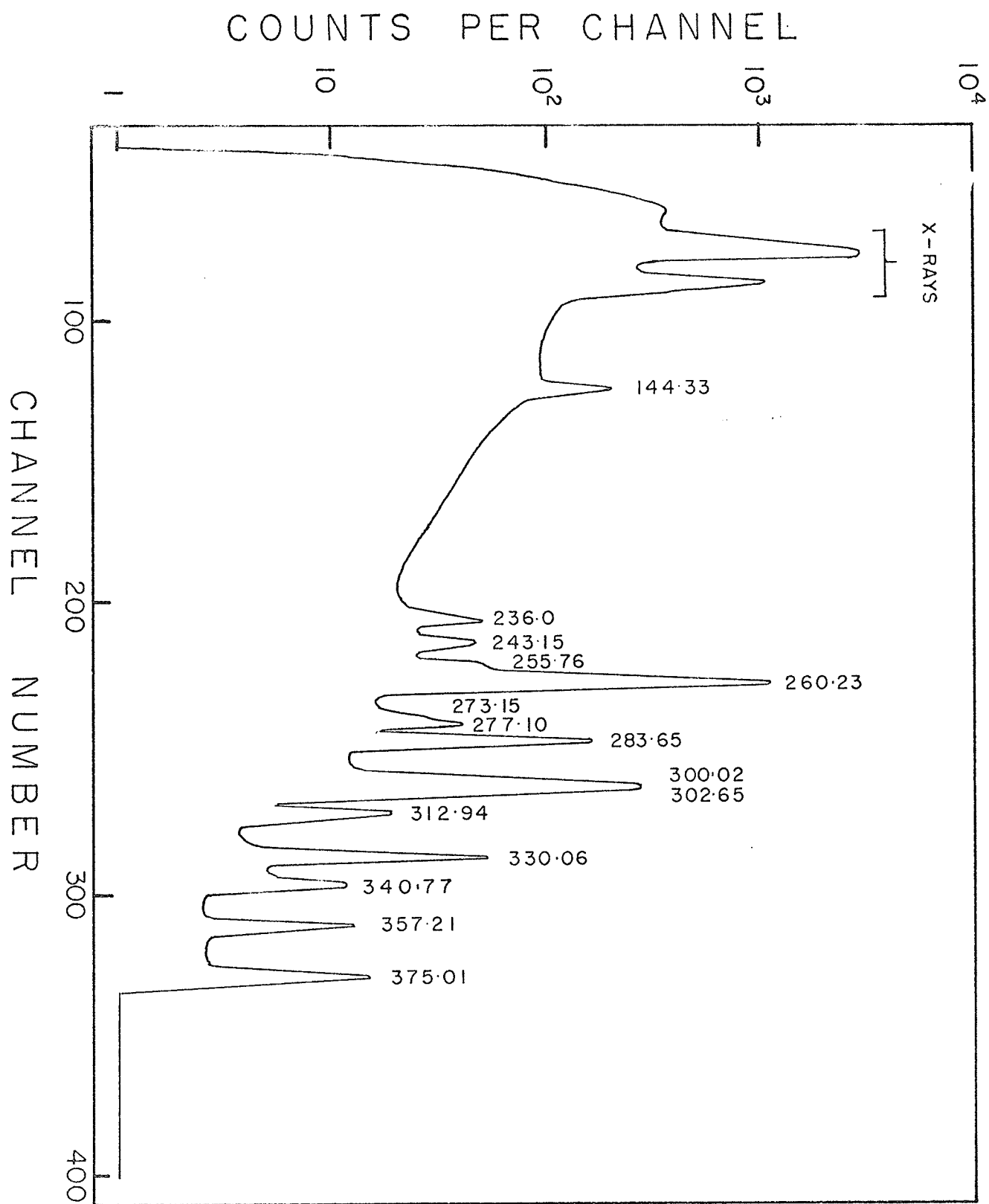
from ^{227}Th. The rest of the lines (namely, those at 255.76, 273.15, 277.10, 312.94, 340.77 and part of 260.23 keV) can be attributed to their being in cascade with the 50.68 keV line from ^{231}Pa decay. These gamma rays in coincidence with the 50.2 and 50.68 keV transitions are also observed when the gate is set on the 52.66 keV gamma ray (see below).

52.66 keV Gate :

The spectrum in coincidence with the 52.66 keV line is shown in Figure III-11. The enhanced lines occur at 144.33, 236.0, 260.23, 277.10, 312.94, 340.77 and 354.57 keV. Of these, the 236.0 keV transition is in cascade with the 50.2 keV line in ^{227}Th, while all the others, except the 144.33 and 260.23 keV lines, are in cascade with the 50.68 keV line in the ^{231}Pa decay. The 144.33 and 260.23 keV transitions are in cascade with the 52.66 keV gate.

54.56 keV Gate :

When the gate is set on the 54.56 keV line, the spectrum obtained is shown in Figure III-12. The enhanced lines are those at 144.33, 260.23, 273.15, 277.10 and 375.01 keV. It should be noted that the weak 273.15 keV line, being a ground state transition, is not expected to be enhanced, but its presence can be

Figure III-13

Coincidence spectrum with the

(56.79 + 57.19) keV lines
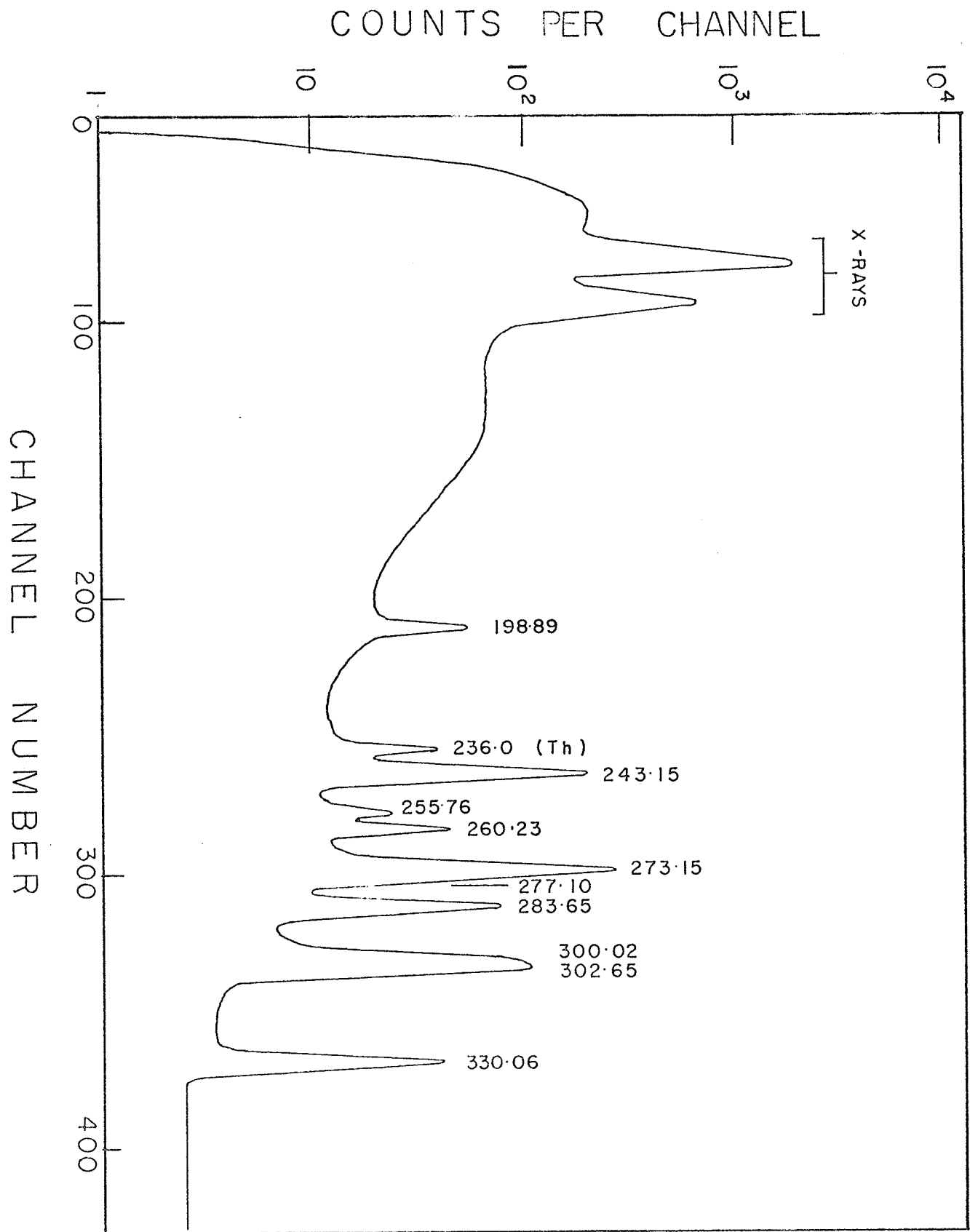
explained by the fact that some of the 56.79 keV photons are leaking into the SCA, thereby opening the gate, and the 273,15 keV line is in cascade with the 56.79 keV line. Also, the line at 260.23 keV may be due in part to the leakage of the 52.66 keV gamma ray into the gate, but this could not account for the enormous enhancement. This implies a genuine coincidence between the 54.56 and 260.23 keV transitions. This would require as a link, a transition between the levels at 126.85 and 84.55 keV, as shown in Figure III-23 The transition energy is 42.41 keV, and a gamma ray at this energy has been observed, so that such an assignment is reasonable, in view of the coincidence data. The line at 144.33 keV can be accounted for in a similar manner, being in cascade with the 54.56 keV gate via the 42.41 keV transition.

(56.79 + 57.19) keV Gate:

In Figure III-13 is shown the coincidence spectrum when the gate is set on the (56.79 + 57.19) keV lines. The lines that are enhanced include those at 198.9, 243.15, 255.76, 260.23 and 273.15 keV. The 56.79 keV transition is firmly established to be the transition from the 329.99 keV level to the 273.18 keV level. This is confirmed by the enhancement of the lines at 273.15, 243.15 and 198.89 keV, all of which de-excite

the 273.15 keV level. The 57.19 keV gamma ray, on the other hand, is known to de-excite from the 84.55 keV level to the 27.38 keV level. This is verified in the present work by the enhancement of the 2C0.23 keV line. (See Figure III-23). The 277.10 keV transition would be expected to be in coincidence with the 57.19 keV gamma ray through the 25.36 keV transition. however, the present data shows insufficient indication of the enhancement of the 277.10 keV line to give a definitive conclusion. An interesting feature in this set of data is the slight enhancement of the 255.76 keV line. This cannot be accounted for being in cascade with either the 57.19 keV gamma ray, which de-excites the 84.55 keV level, or with the 56.79 keV gamma ray, which de-excites the 329.99 keV level. This is an indication that there is a further transition above the 329.99 keV level whose energy is very close to 57.19 keV. Such a transition is found de-exciting the 387.16 keV level to the 329.99 keV level. This transition would bring about the enhancement of the 255.76 keV line, as is observed here. In fact, one expects to see the lines at 255.76, 283.65, 300.02, 302.65 and 330.06 keV appear enhanced but in the ratio in which they appear in the singles spectrum. However, in view of the slight enhancement of the 255.76 keV

Figure III-14

Coincidence spectrum with the

74.08 keV gamma ray
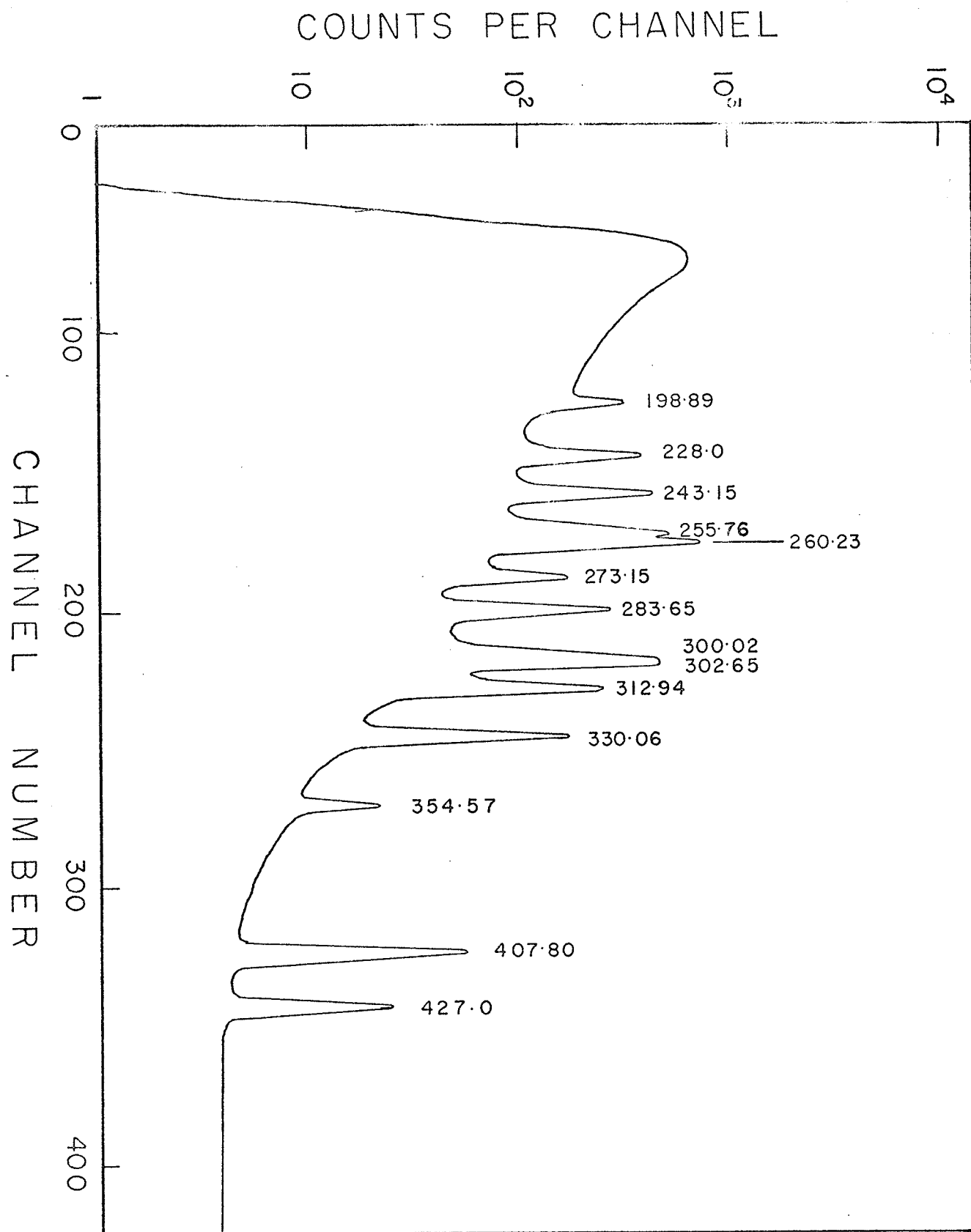
line, the enhancement of the other lines would be more difficult to observe, since one would be looking for a small enhancement in a very strong line. In a later discussion, more evidence will be presented to support this transition from the 387.16 keV level to the 329.99 keV level.

74.08 keV Gate :

The next gate is set at the 74.08 keV gamma ray. The coincidence spectrum is shown in Figure III-14. The enhanced lines include those at 198.89, 228.0, 243.15, 255.76, 260.23, 273.15, 312.94 and 427.0 keV. The lines at 228.0 and 427.0 keV have not been reported previously by other workers, nor have they been observed in the singles spectrum in the present work. They are now placed in the decay scheme and would be in coincidence with the 74.08 keV transition. The interesting point about this set of data is that whereas the lines at 198.89, 255.76, 260.23 and 312.94 keV are expected to be enhanced, the ones at 243.15 and 273.15 keV are also enhanced, although they are not expected to be (See Figure III-23). This suggests that there is probably a transition (whose energy is very close to 74.08 keV) above the 516. keV level. This will be discussed in greater detail at the end of this Chapter (see Section III.6).

Figure III-15

Coincidence spectrum with the

(255.76 + 260.23) keV lines
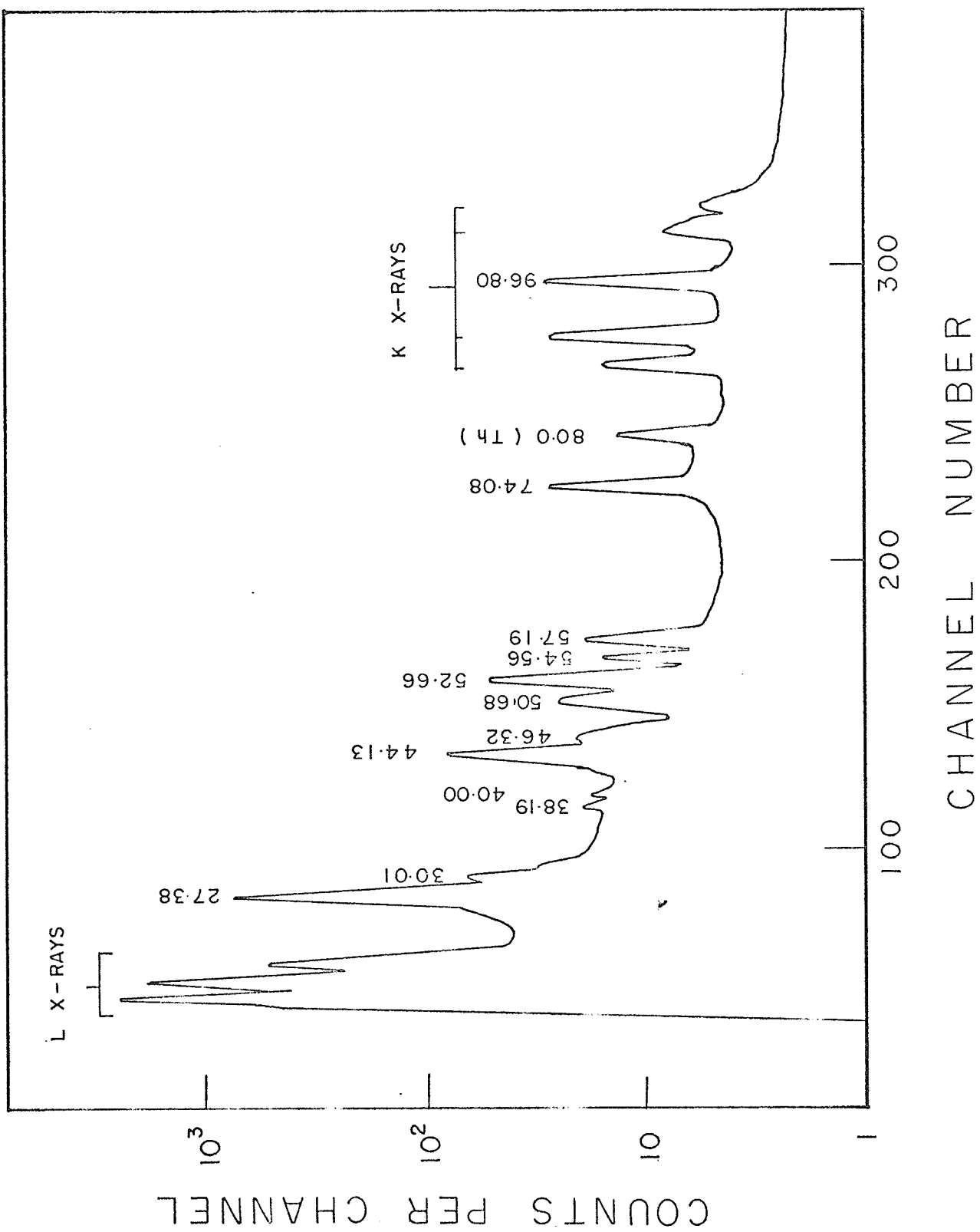
(255.76 + 260.23) keV Gate :

Next, the SCA is set to gate on the
(255.76 + 260.23) keV gamma rays. Such a wide energy
window is chosen because it is not possible to gate on
each of the gamma ray separately without getting
considerable interference from the other one.
Figure III-15 shows the coincidence spectrum obtained
with the composite gate. The lines at 30.01, 31.55,
44.13, 50.68, 52.66, 57.19, 74.08, 80.0 and 96.80 keV
are enhanced. It is immediately obvious from
Figure III-23 that the lines whose energies are 31.55,
50.68, 96.80, 52.66 and 30.01 are in cascade with the
260.23 keV transition. The line at 80.0 keV is less
well understood. A gamma ray at this energy is not
observed in a freshly prepared source, but after
leaving the source for a few months, a line at this
energy is readily observable. Thus, it seems that this
line might have originated from the radioactive decay
products of ^{227}Ac. In fact, ^{227}Th has a fairly intense
line ^{26,28} at 79.9 keV which is in cascade with several
gamma rays whose energies are about 260 keV (254.7,
262.7 and 270.0 keV). It is quite possible that the
line observed here is in fact from the ^{227}Th decay. The
rest of the enhanced lines (e.g. those at 74.08, 44.13,
and 57.19 keV) can be attributed to being in cascade

Figure III-16

Coincidence spectrum with the

283.65 keV gamma ray
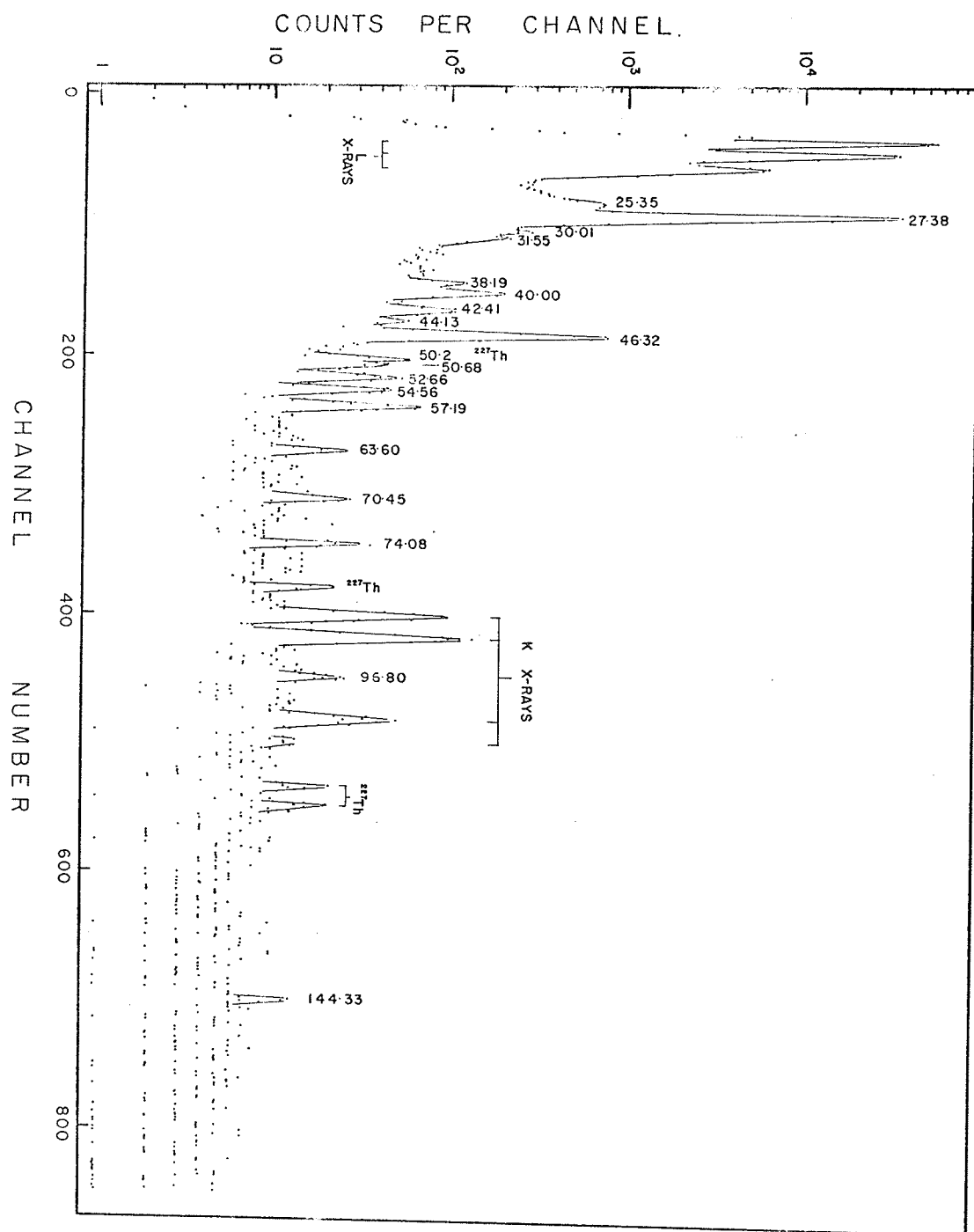
with the 255.76 keV line.

283.65 keV Gate :

The next gate is set at 283.65 keV, and the spectrum in coincidence with this gamma ray is shown in Figure III-16. The enhanced lines occur at 24.6, 27.38, 30.01, 30.87, 40.00, 42.41, 43.08, 46.32, 50.68, 57.19 and 70.45 keV. Of these, only the one at 43.08 keV is not placed in the level scheme. A very important result of this investigation is that as the 283.65 keV gamma ray de-excites to the 46.32 keV level, and the lines at 27.38 and 30.01 keV are observed to be enhanced, there have to be transitions from the 46.32 keV level to the 30.01 and 27.38 keV levels, the transition energies being 16.5 and 18.9 keV respectively. It should be noted that gamma rays at these energies are not observed in the present work, since they, if present, would be masked by the intense L X-rays. Further, transitions at these energies would be very strongly converted. In fact, the conversion electrons corresponding to these transitions have been reported[4,17,18], and the present work seems to substantiate this report.

(300.02 + 302.65) keV Gate :

The next gate is set on the (300.02 + 302.65) keV

Figure III-17

Coincidence spectrum with the

(300.02 + 302.65) keV lines
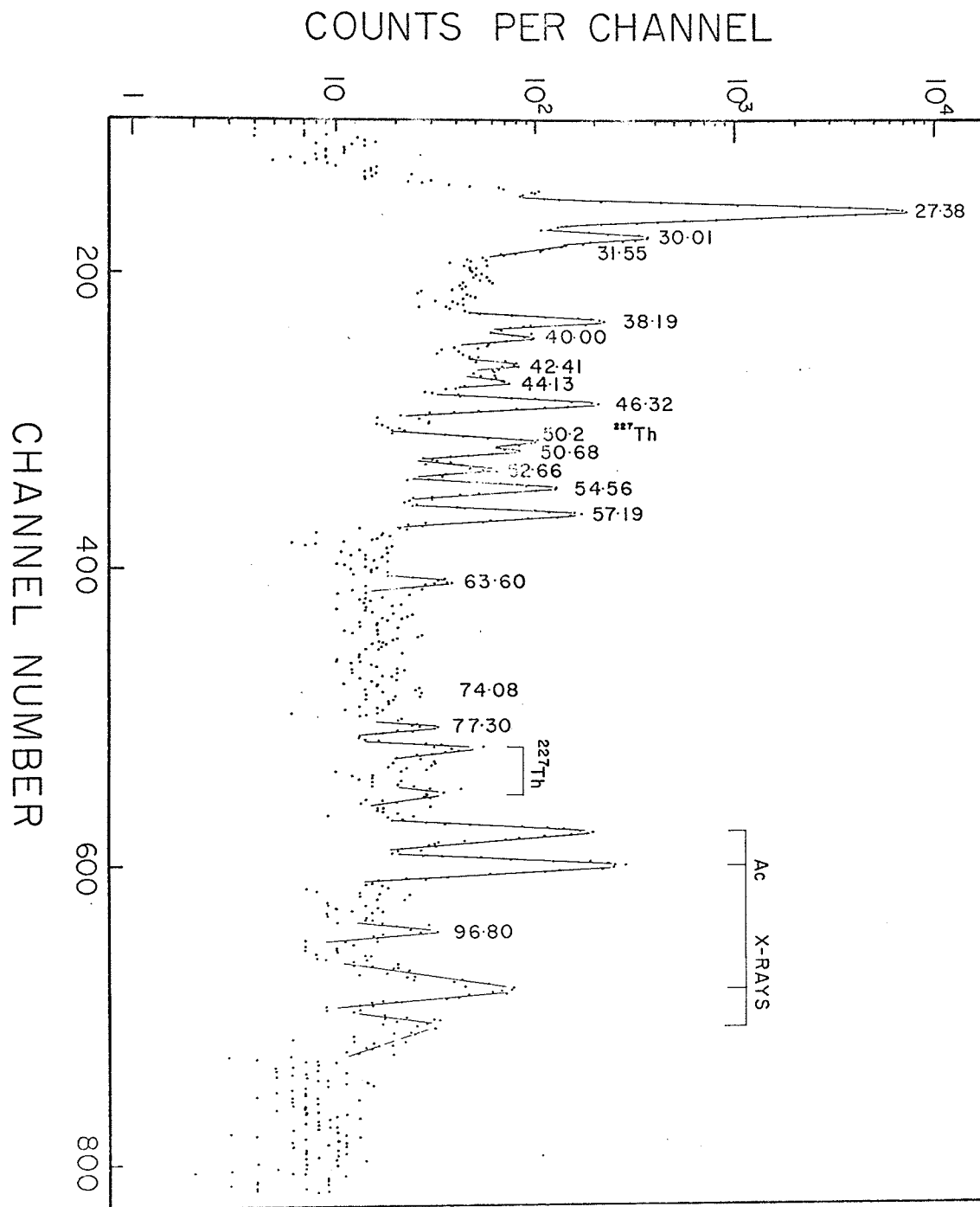
Figure III-18

Coincidence spectrum with the

312.94 keV gamma ray
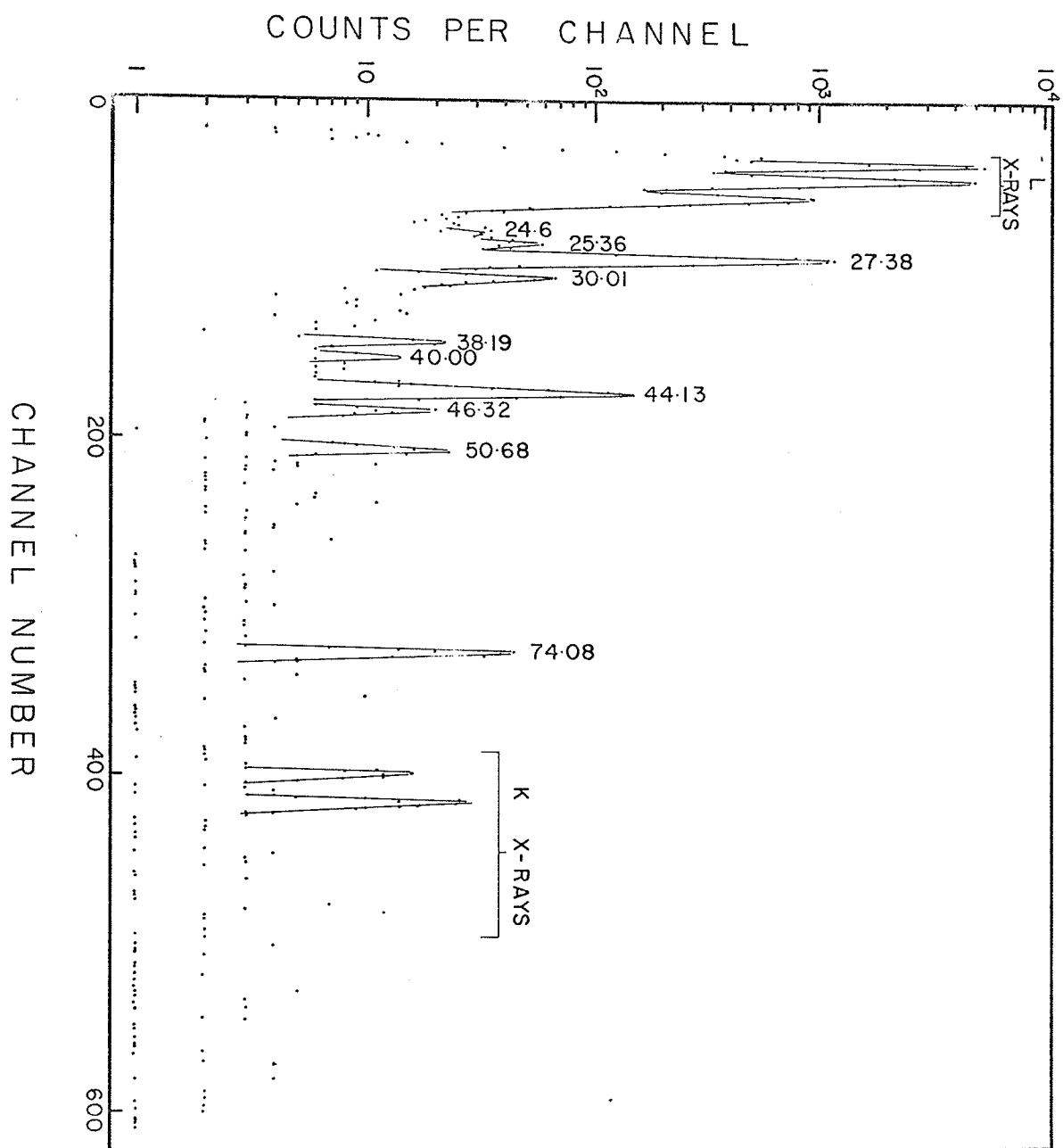
doublet. The coincidence spectrum is shown in Figure III-17. The enhanced lines are found at 27.38, 30.01, 38.19, 40.00, 42.41, 46.32, 50.68, 54.56 and 57.19 keV. The present data confirms the fact that there are two gamma transitions whose energies are very close to 302.65 keV, as suggested by Pinho. One transition is very well established and de-excites the 329.99 keV level to the 27.38 keV level. The other transition de-excites the 387.19 keV level to the 84.55 keV level (See Figure III-23). The existence of this transition is verified by the enhancement of the gamma rays at 57.19, 54.56, 38.19 keV which de-excite the 84.55 keV level. The presence of this transition also explains the enhancements of the gamma rays at 46.32 and 30.01 keV.

312.94 keV Gate :

Figure III-18 shows the coincidence spectrum obtained when the gate is set on the 312.94 keV gamma ray. The lines at 30.01, 44.13, 50.68 and 74.08 keV are enhanced here. This is consistent with the assignment that the 312.94 keV gamma ray correspond to the transition from 387.94 keV level to the 74.11 keV level, as shown in the level scheme (Figure III-23). The lines at 31.55, 40.00 and 42.41 keV are expected to be enhanced also. However, with the present data they

Figure III-19

Coincidence spectrum with the

(327.26 + 330.06) keV lines
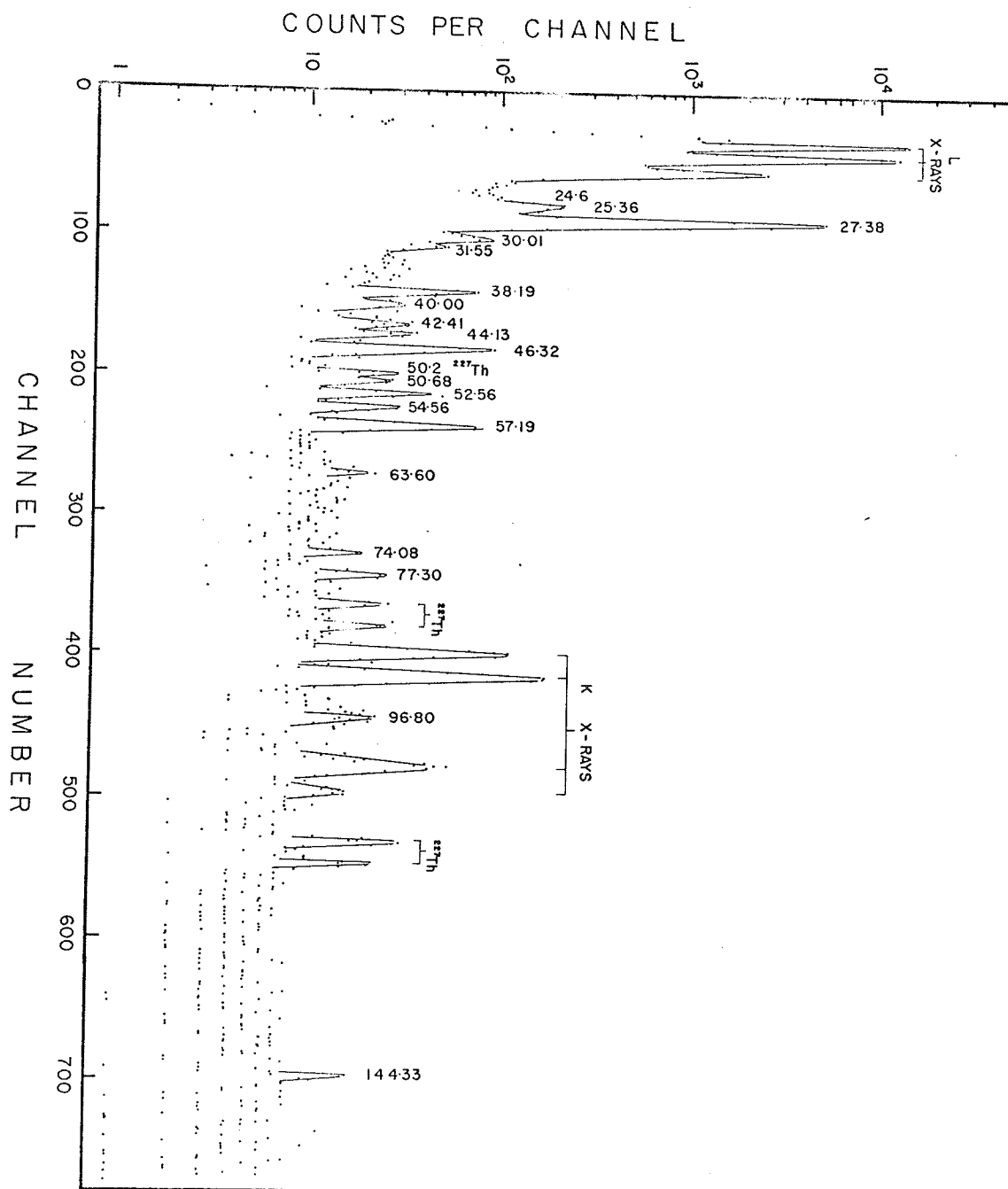
Figure III-20

Coincidence spectrum with the

340.77 keV gamma ray
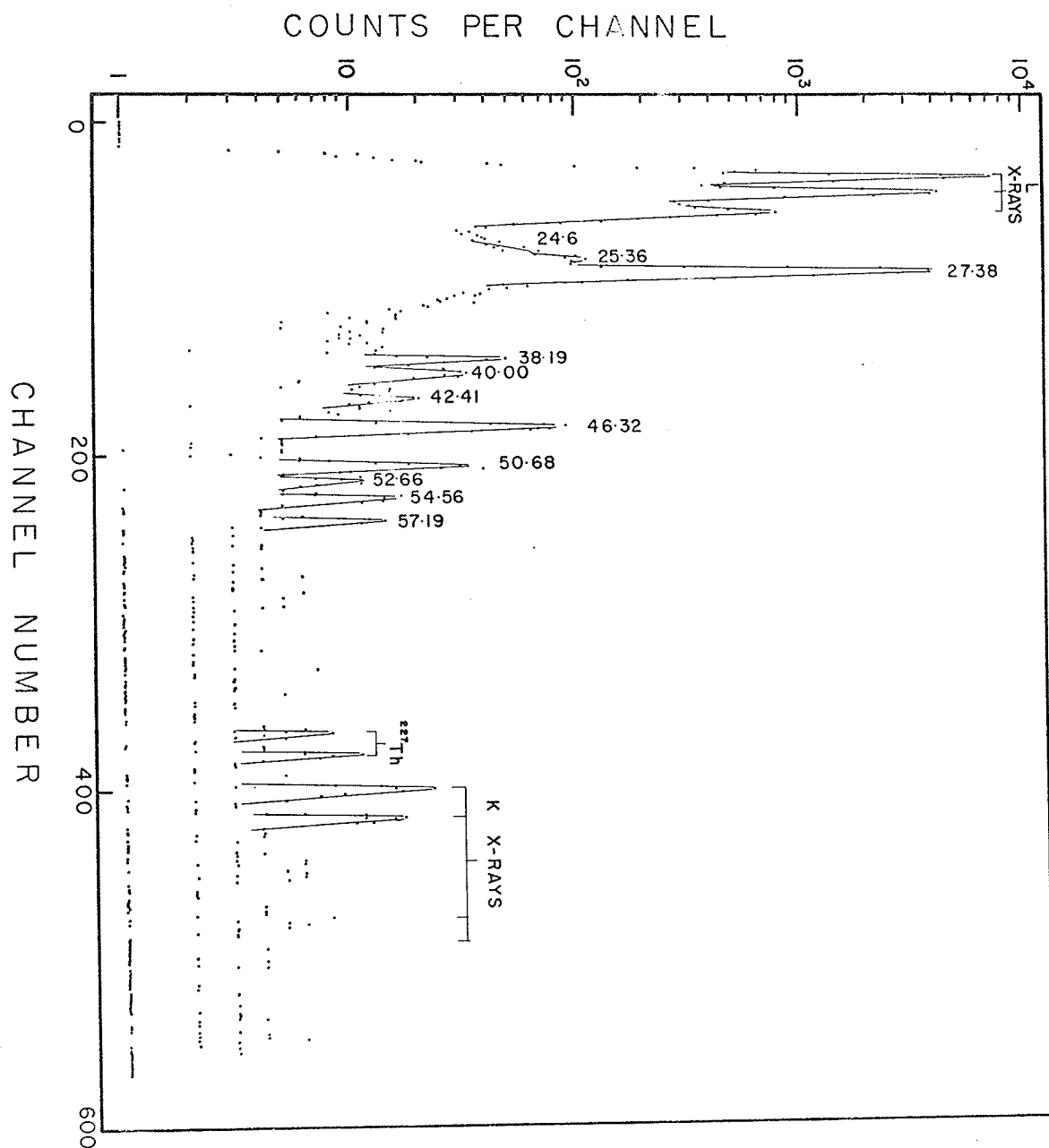
are too weak to show any enhancement they might have.

(327.26 + 330.01) keV Gate :

Next, the gate is set on the (327.26 + 330.01) keV gamma rays. It should be noted that the former line (327.26 keV) is very weak compared to the latter one (330.01 keV). In fact the 330.01 keV gamma ray is almost 40 times more intense than the 327.26 keV line. Figure III-19 shows the coincidence spectrum. The enhanced lines include those at 24.6, 27.38, 31.55, 50.68 and 57.19 keV. The data confirms the placing of the 57.19 keV transition between the 387.16 keV and the 329.99 keV levels. It should be mentioned that there is a slight evidence for the enhancement of a transition at about 144 keV. This cannot be the 144.33 keV transition, but this may signify a transition feeding to or above the 354.6 keV level. The present data is indecisive.

340.77 keV Gate :

Figure III-20 shows the coincidence spectrum obtained when the SCA is set to gate on the 340.77 keV gamma ray. The enhanced lines include those at 27.38, 40.00, 46.32 and 50.68 keV. Refering to Figure III-23, the line at 31.55 keV is expected to be enhanced, but in the present data, it is too weak to reveal its

114

Figure III-21

Coincidence spectrum with the

(354.54 + 357.21)keV lines
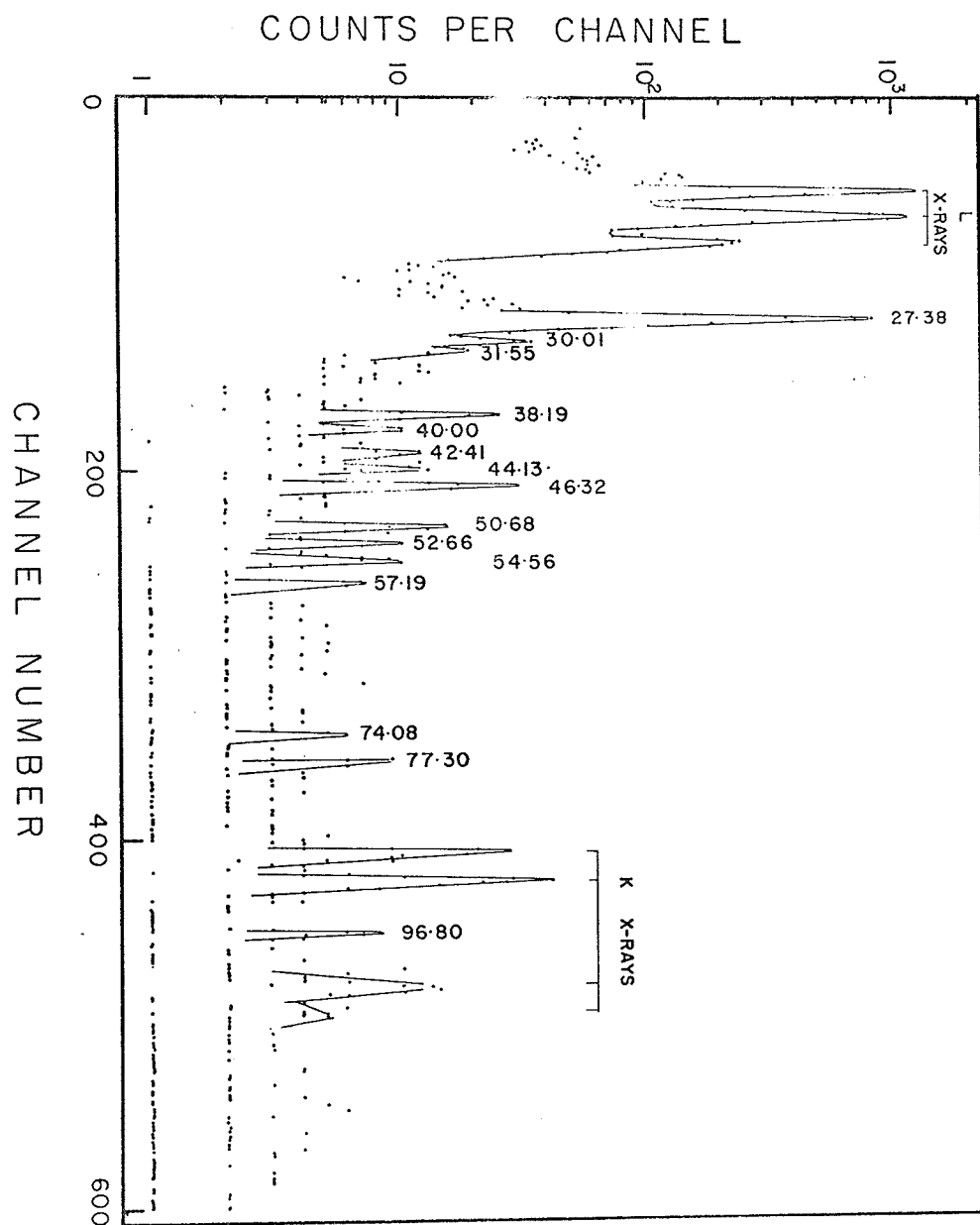
Figure III-22

Energy window for the

(354.54 + 357.21) keV gate
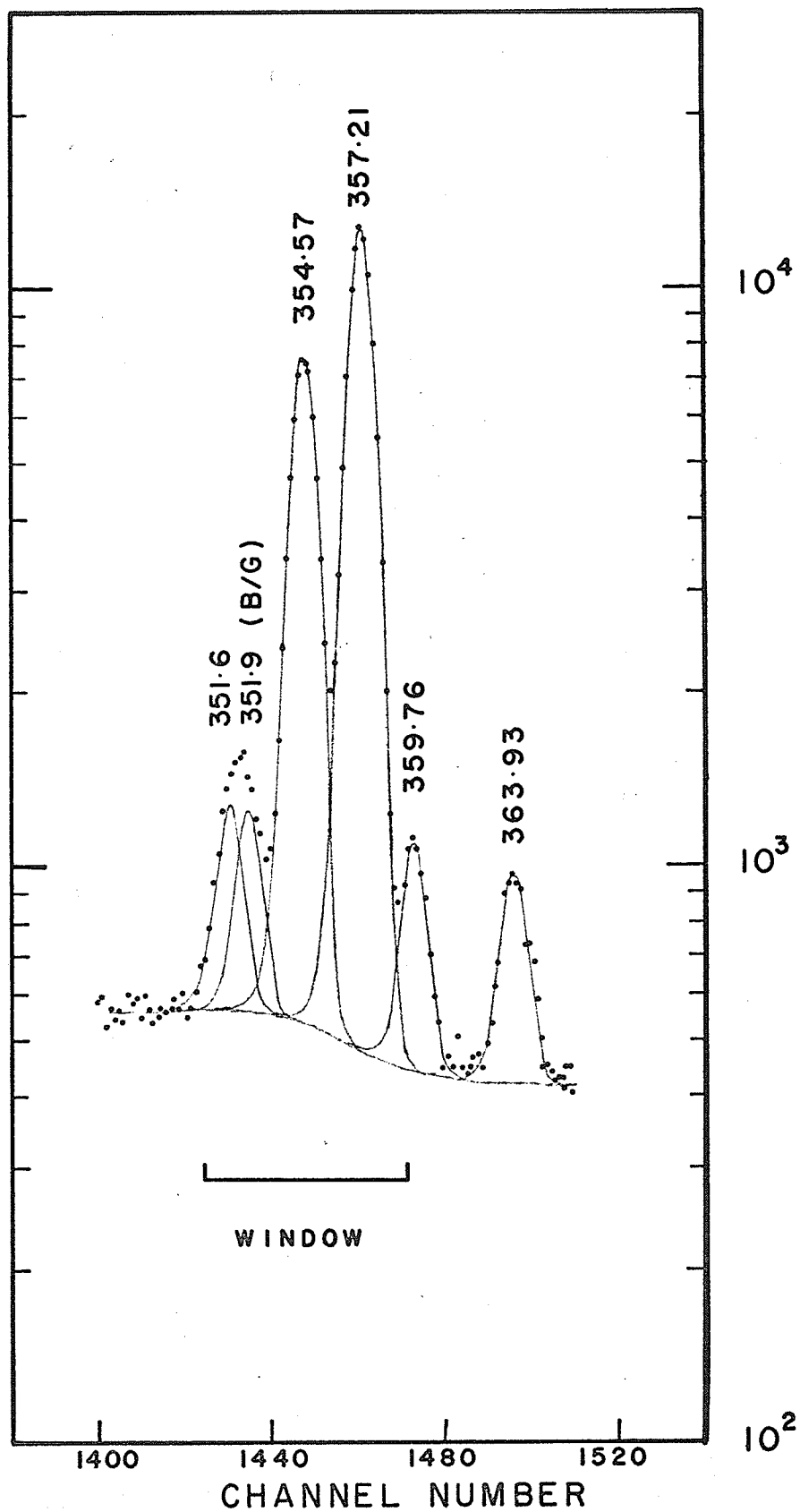
Table III-4

^{231}Pa coincidence table

Coincident Gamma ray	Gate											
	46.32	52.66	54.56	57.19	74.08	255.76 260.23	283.65	300.02 302.65	312.94	327.26 330.06	340.77	351.57 357.21
24.6							x			x		
27.38							x	x		x	x	
30.01						x	x	x	x			x
30.87							x					
31.55						x				x		
38.19								x				
40.00							x	x			x	
42.41							x	x			x	x
43.08							x					
44.13						x			x			
46.32							x	x			x	
50.68						x	x	x	x	x	x	x
52.66						x						
54.56								x				
57.19						x	x	x		x		
70.45							x					
74.08						x			x			
96.80						x						
144.33		?	x									
161.0	x											
198.89				x	x							
228.0					x							
243.15				x	x							
255.76				x	x							
260.23	x	x	x	x	x							
273.15				x	x							
277.10			x									
283.65	x											
312.94					x							
340.77	x											
375.01			x									
379.41	x											
427.0					x							

presence.   The 42.42 keV transition is that which feeds
the 387.16 keV level.

(354.57 + 357.21) keV Gate :

Figure III-21 shows the spectrum in coincidence
with the (354.57 + 357.21) keV gamma rays.   It should
be noted that the gate consists of, in actuality, a
group of several lines, as shown in Figure III-22.
This figure is the CUTIPIE analysis of the gamma ray
spectrum in the region 350-360 keV.   The spectrum is
taken with a Ge(Li) X-ray detector whose resolution is
290 eV at 5.9 keV. Obviously, all the four gamma rays
(eg. 351.6, 354.57, 357.21 and 359.75 keV) open the
gate. However in the present case, the contributions
from the 351.6 and 359.75 keV lines consitute less than
1 % of all the gating pulses, so that for all practical
purpose, they can be ignored. The enhanced lines are
those at 30.01, 42.41 and 50.68 keV.   It should be
noted that the line at 70.45 keV is also expected, but
is too weak to show up. Again the 42.41 keV transition
is that feeding the 387.16 keV level.

III.6 DISCUSSION

The coincidence data is summarised in Table III-4.
The data is self-consistent. From Table III-4, it is
evident that the line at 42.41 keV is enhanced with

118

Figure III-23

Decay scheme for ^{231}Pa decay
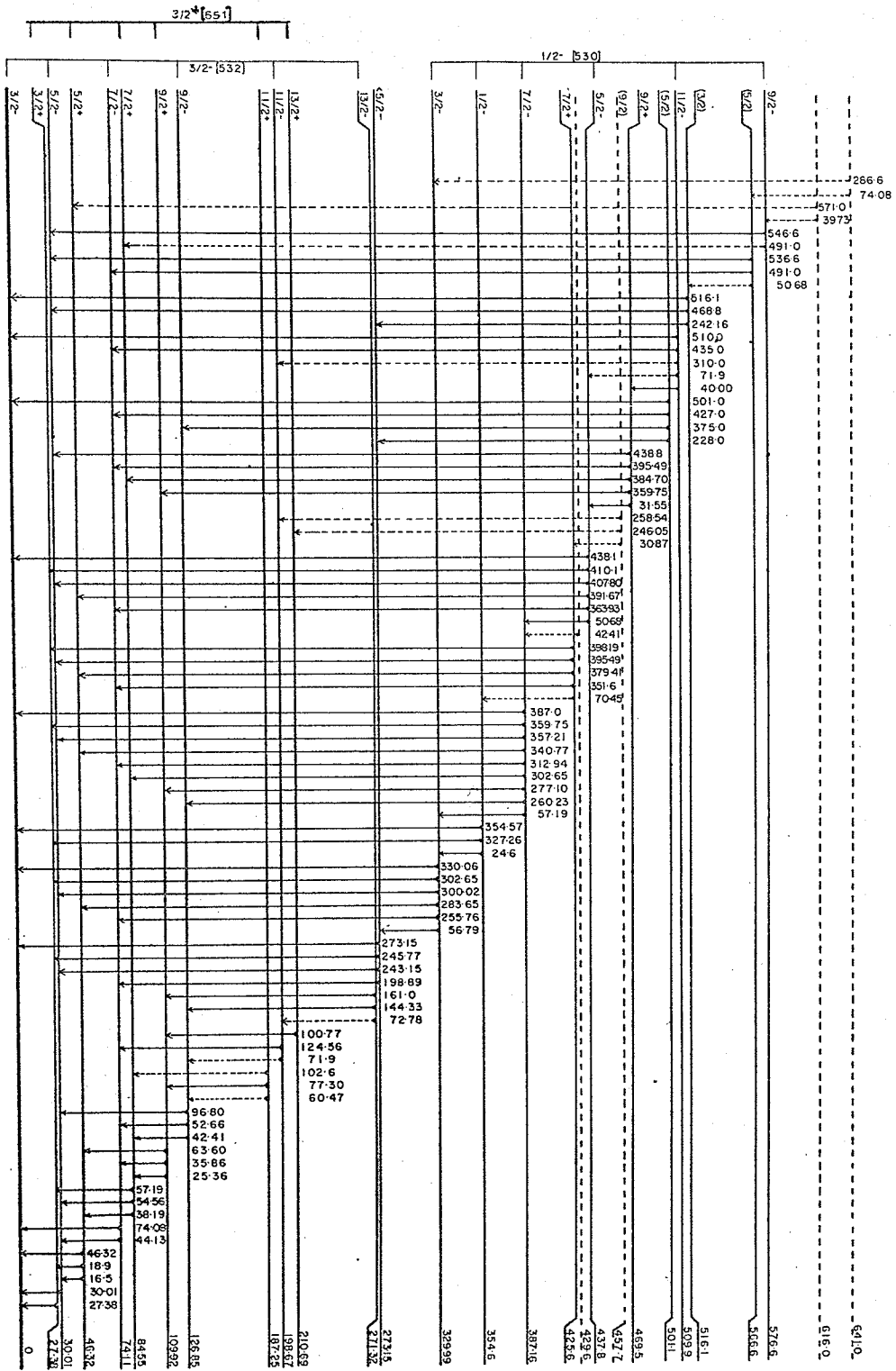
practically every line in the high energy region. It is therefore suggested that there should be an additional level above the existing 387.16 or 437.76 keV levels. In the present work, a level at 429.6 keV is suggested to accomodate this gamma ray, as shown in the level scheme in Figure III-23.

A second level is suggested at 457.7 ± 2.0 keV. This suggestion does not arise from the coincidence data, but is put there because it can accomodate four gamma rays that were not previously placed in the decay scheme. Further, the closeness of this level to the 469.5 keV level does not exclude the possibility that it is very weakly fed by alpha decay, but is not observed due to the relatively poor resolution of the alpha particle spectrometers.

Another level is suggested at about 641 keV, as shown in Figure III-23. Lange et al[13] has reported having observed a very weak alpha group (about 0.001%) whose energy is 4.41 ± 0.01 MeV in the decay of ^{231}Pa. This would mean a level at 635 ± 10 keV above the ground state. The present data seems to support this finding (See coincidence data gating on the 74.08 keV gamma ray), except that the energy of this level is adjusted to be 641.0 ± 2.0 keV, based on the energies of the gamma rays and othe other existing levels. This

level can also accomodate the 280.6 keV transition, which has been observed but not previously placed in the level scheme with certainty. It should be noted that this transition is based entirely on the energy agreement between the energy of the gamma ray and the energy difference between the levels.

Lines at 71.9, 102.6, 310.0 and 387.0 keV have been reported by Pinho[7] but are not observed in the present work. Also, three new transitions (161.0, 228.0 and 427.0 keV) are reported here for the first time. All three are observed only in coincidence experiments. All save one (43.08 keV) of the 73 gamma rays observed in the present work have been placed in the decay scheme.

In the present work, the sources available were too weak to permit any angular correlation work to be carried out. Thus the spins quoted in Figure III-23 are those reported by Pinho[7] In his paper, a spin of 1/2 is suggested for the 501.1 keV level. In the present work, however, it is felt that in view of the gamma rays (228.0, 275.1, 427.0 and 501.0 keV) de-exciting this level to levels whose spins are 5/2, 9/2, 7/2, and 3/2 respectively, a spin of 5/2 seems more reasonable than 1/2. A spin of 5/2 is thus assigned to this level.

The rotational properties of this nucleus have been investigated by Hagee[13] and Pinho.[17] The ground state parity has been shown to be odd,[15] contrary to the even parity as suggested by Baranov et al.[14] The ground state of ^{227}Ac has been unambiguously assigned as the 3/2-(532) Nilsson state. The first four members of this rotational band are firmly established to occur at 0, 30.01, 74.11 and 126.85 keV. The other members of this band are less well understood, but it seems that the levels at 198.78 and 271.3 keV correspond to the 11/2 and 13/2 members of this band.

The Nilsson state of 3/2+(651) is assigned to the 27.38 keV level. Other members of this band include those at 46.32 (5/2+), 84.55 (7/2+), 109.92 (9/2+), 187.25 (11/2+) and 210.69 (13/2+) keV. A more interesting band occurs at 329.99 keV. This level has been firmly established to be the origin of the the 1/2-(530) band. The 1/2, 3/2, 5/2 and 7/2 members occur at 354.60, 329.99, 437.76 and 387.16 keV respectively. The interesting feature is that the 1/2 and 5/2 members of this band have energies higher than that of the 3/2 and 7/2 members. This is probably due to the coriolis coupling between this band and other rotational bands.

Other possible rotational bands have been looked

for by other workers[13,17] but they have met only partial
success.

CHAPTER IV

THE DECAY OF ^{231}Th

IV.1 INTRODUCTION

^{231}Th, a beta emitter of 25.52 hour half-life, is the immediate decay product of ^{235}U. In classical radioactive terminology, ^{231}Th was known as "UY". Its early history and its relation in the ^{235}U decay chain, have appeared in some detail in the literature[1,2].

^{231}Th can be isolated from ores containing ^{235}U or produced by the ^{230}Th$(n, \gamma)^{231}$Th reaction. The investigation of the radiations from ^{231}Th dates as far back as 1932,[3] and the accepted decay scheme has increased in complexity[4-6] with the passage of time and with the increasing number of investigations.

IV.2 SOURCE PREPARATION

In the present work, ^{231}Th was prepared from the 7.13×10^{8} year ^{235}U in the following way[7]. Since ^{231}Th has a half life of about one day, it will be in secular equilibrium with its parent (^{235}U) in a matter of days. 2.5 grammes of 93% enriched ^{235}U was loaded onto a 200x13 mm ion-exchange column packed with Amberlite AG1x8 resin using 12M HCl. The source was

left to stand for the ^{231}Th to grow for two or three days, after which the ^{231}Th was eluted from the column using 50 ml of 12M HCl. In the earlier part of this work, thorium was removed from the eluant by hydrolytic co-precipitation with iron as a carrier. However, difficulty was encountered when attempts were made to remove completely the carrier(Fe). The sources obtained as a result were too poor for low energy gamma ray studies. An alternative procedure was adopted subsequently. The eluant containing ^{231}Th was evaporated to dryness, and any organic material that might be present was oxidized by treating the residue with a few drops of hot HNO_3 and H_2O_2. The residue was then re-dissolved in a few drops of 12M HCl, and the solution was passed through a second 60x8 mm resin column to remove any contaminants that might be present. The eluant, containing only ^{231}Th, was again evaporated to dryness, and then re-dissolved in a few drops of HNO_3.

The solution of ^{231}Th was evaporated on a piece of mylar backing whose thickness was 0.71 mg/cm^2. After the source was dried completely, it was covered with a second piece of mylar of the same thickness for radiation safety, and was then ready for counting.

Sources produced this way appeared as faint white

Figure IV-1

X-ray spectrum of inert impurities
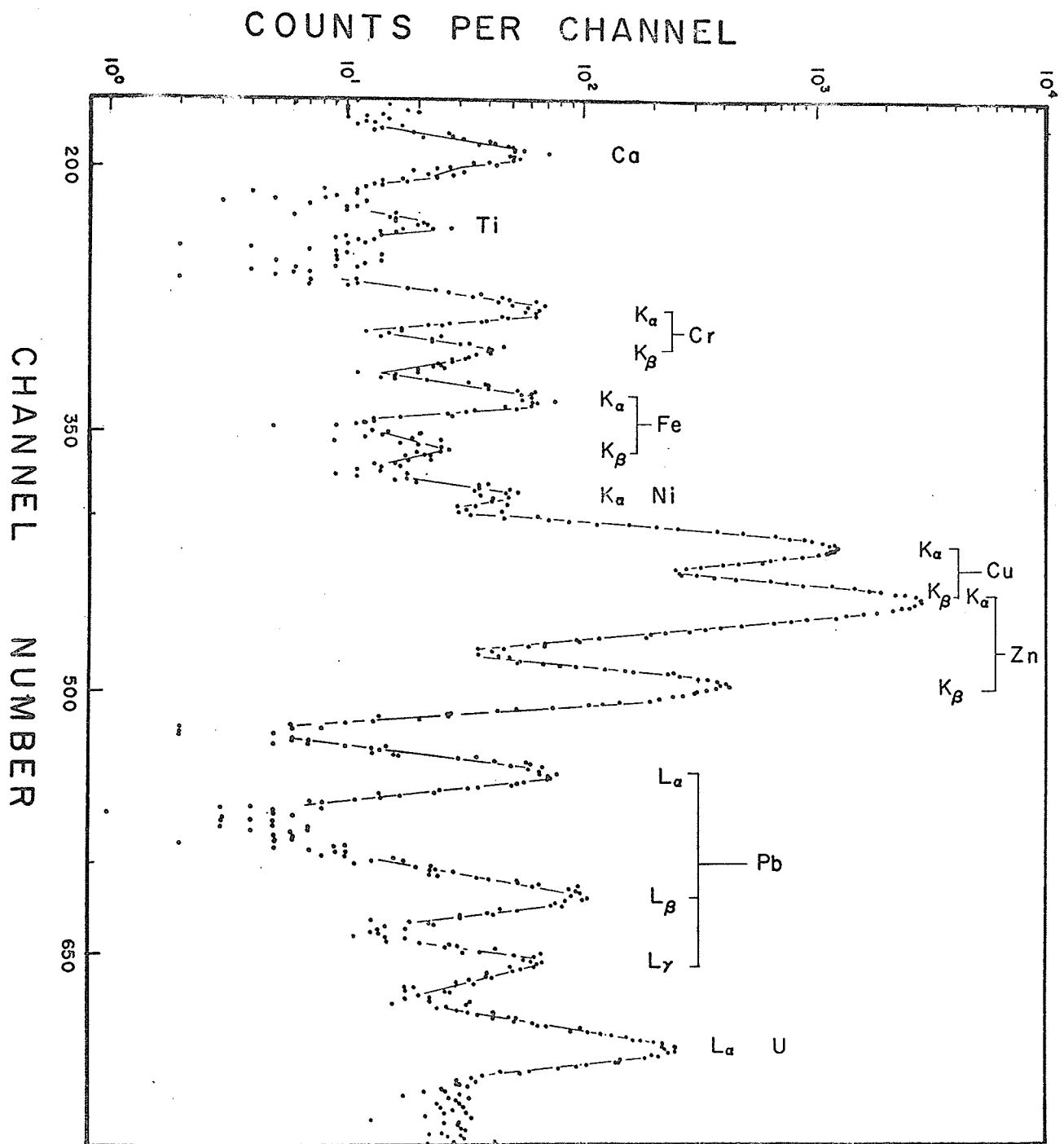
stains, and were generally quite acceptable for gamma ray work in the energy range of 10-400 keV. As a matter of secondary interest, an X-ray fluorescence experiment was performed on a source to determine its possible contaminants. The source used had been left to stand for a period of 12 months so that for all practical purpose, it could be regarded as free of the activities of ^{231}Th. A beam of tungsten (W) X-rays from a TuR-M60 X-ray machine operating at 50 KV and 20 ma was used to excite the characteristic X-rays of the contaminants. The spectrum, taken with a Kevex Si(Li) X-ray detector (whose resolution at 6.5 keV was 290 eV) is as shown in Figure IV-1. The contaminants were identified to be Ca, Ti, Cr, Pb, Fe, Cu, Zn, Ni and not surprisingly uranium. Unfortunately the system was not calibrated[8] so that it was not possible to obtain the absolute abundance of these elements. The presence of traces of Uranium was due to the fact that some uranium was washed off the first column with the thorium; a further confirmation of the presence of ^{235}U in the source material was indicated by the faint presence of its more intense gamma rays in the ^{231}Th spectra (See following section).

IV.2 GAMMA RAY SPECTRA

All the semi-conductor detectors mentioned in

Figure IV-2

Gamma ray spectrum of ^{231}Th decay

(3 - 60 keV)
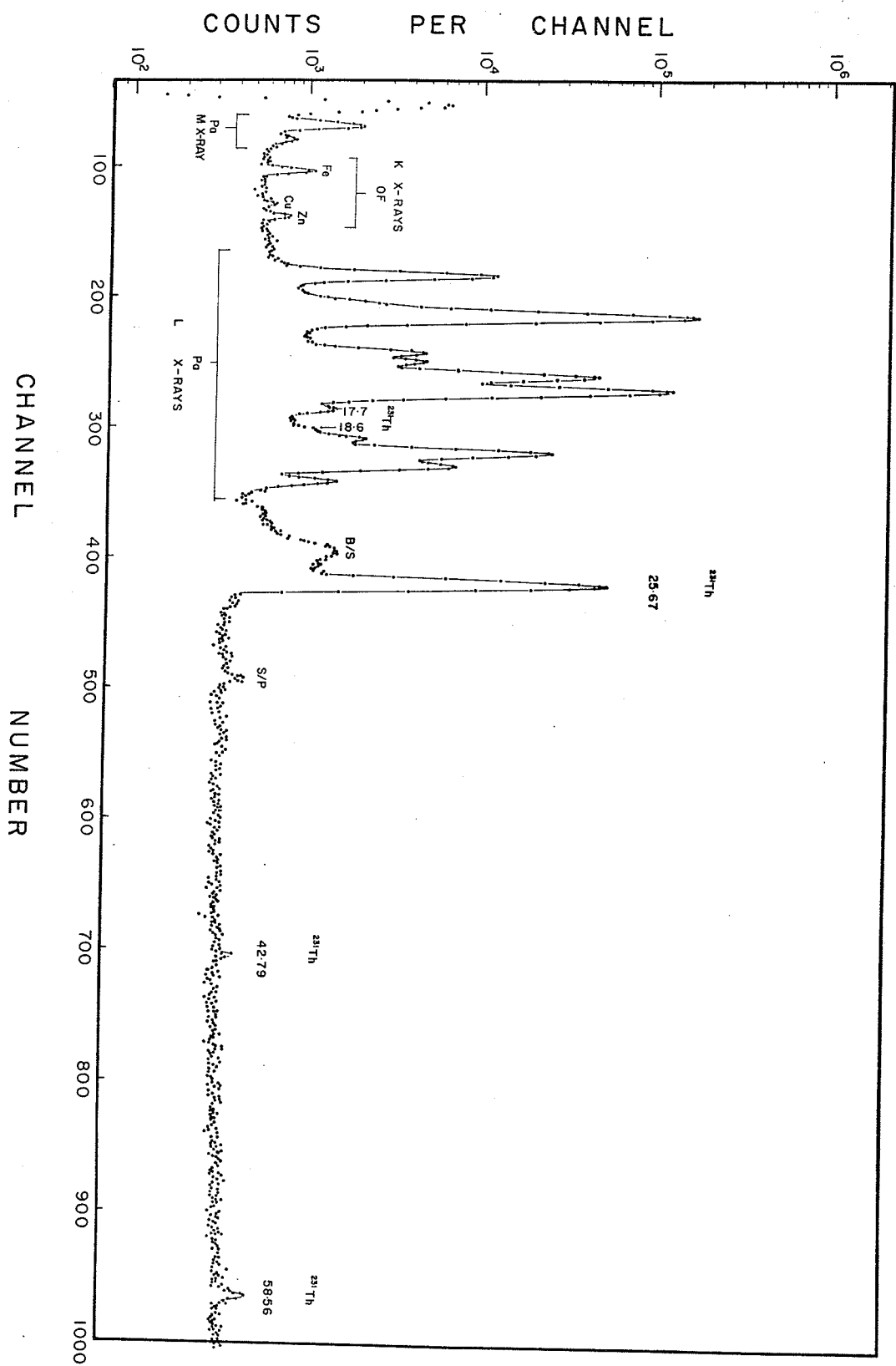
Figure IV-3

Gamma ray spectrum of ^{231}Th decay

(20-320 keV)
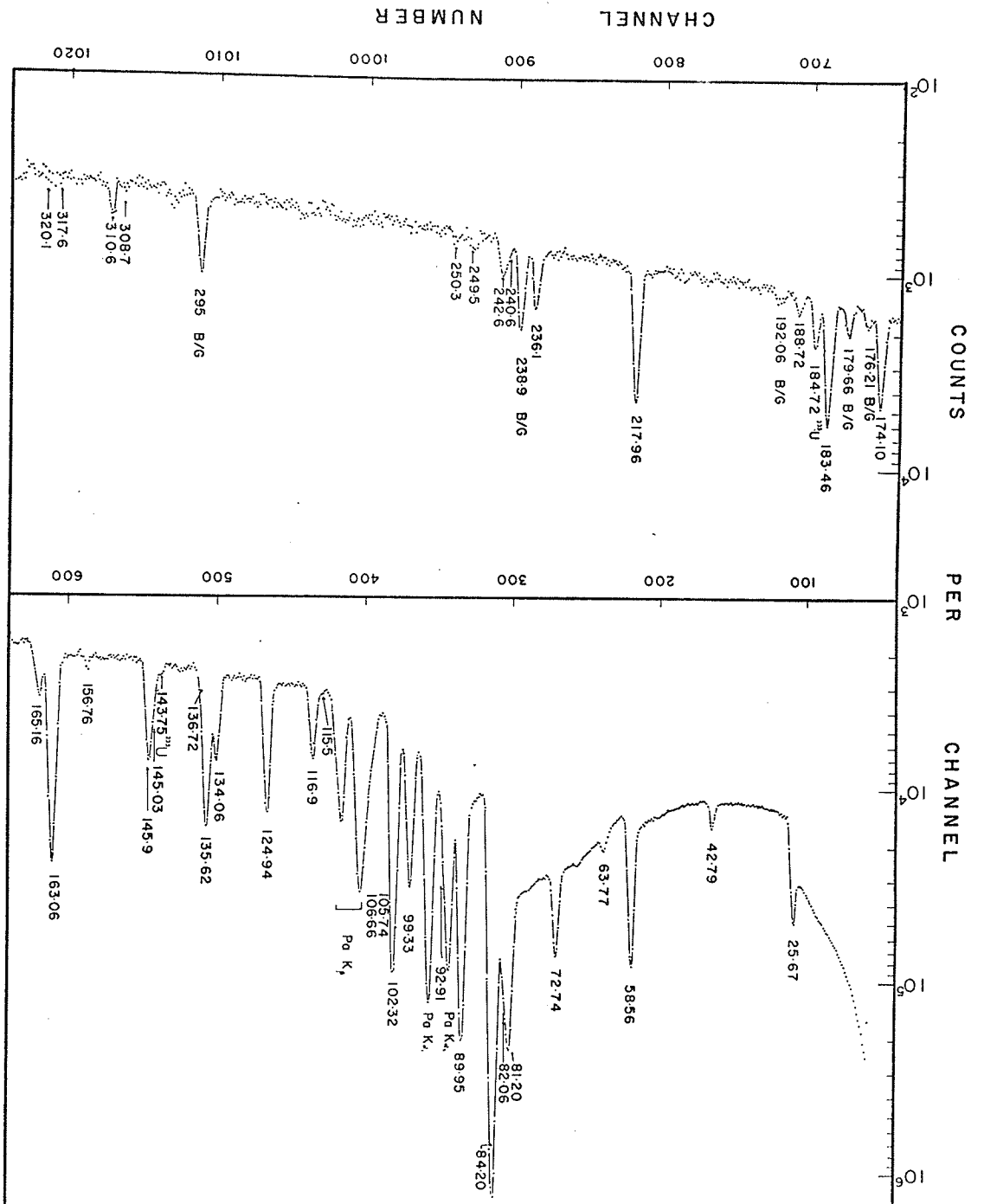
Chapter I were used to examine the gamma rays emitted as a result of the ^{231}Th decay. The Si(Li) X-ray detector having a resolution of 240 eV at 6.5 keV was particularly useful in examining the L X-ray region (up to 30 keV). Figure IV-2 shows a portion of the spectrum in this energy region. The only true gamma rays belonging to the ^{231}Th decay are those at 17.6, 18.4, 25.67, 42.79 and 58.56 keV. The line at 25.67 keV is the strongest gamma transition in the entire decay. All the other peaks can readily be identified as the various components of the L X-rays of Pa. The weak lines in the region between 7 and 9 keV are the X-rays of the various stable comtaminants mentioned earlier.

Figure IV-3 shows a portion of the gamma ray spectrum of ^{231}Pa following the beta decay of ^{231}Th. This spectrum is taken with the 50 cc Ge(Li) detector whose resolution is 2.0 keV at 1.33 MeV. The photopeaks beyond 350 keV (See Figure IV-4) come from the background radiation. Thus it can be concluded that there are no gamma transitions beyond 350 keV coming from the ^{231}Th decay. In the region 40 to 320 keV, the most intense gamma ray is found at 84.20 keV. The weak lines at 92.91, 115.5, 116.9 and 136.72 keV should be noted. The line at 185.7 keV is due to the presence of

traces of ^{235}U in the source material.

An inherent problem associated with using semi-conductor detectors (particularly large volume detectors) is accidental summing between the incident gamma rays. Two intense gamma rays of different energies can enter the detector simultaneously, giving rise to a spurious sum peak whose energy is equal to the sum of that of the two gamma rays. This summing effect is particularly obvious if the source is strong, and is put very close to the detector window so that the window subtends a large solid angle at the source. Summing may also occur when Ge(Li) X-ray detectors are used, since the L X-rays of heavy elements are usually very strong, and summing between the stronger gamma rays and the L X-rays are often seen. In order to ascertain that the relative intensity of the photopeaks obtained in an experiment is correct, it is necessary to ensure that sum peaks are eliminated as far as possible. One easy way to achieve this is by taking the gamma ray spectrum through a properly chosen filter. In this case, it is of course necessary to compensate for the attenuation due to the presence of the filter.

In the present work, two different types of filters were used. In the region above 40 keV, most of

131

Figure IV-4

Gamma ray spectrum of ^{231}Th decay,

taken through a Pt filter

COUNTS PER CHANNEL

CHANNEL NUMBER

10 10^2 10^3 10^4 10^5 10^6

100

42·79

58·56

72·74

Pt X-RAYS

81·20
82·06
84·20

89·95

92·91

200

Pa X-RAYS

99·33
102·32

105·74
106·66

111·5
116·9

124·94

134·06
135·62
136·72

145·03
145·62

300

163·06

165·16
169·52
174·10

183·46

235U
188·72

400

217·96

236·2

240·6
242·6
B/G

249·5
250·3

267·6
B/G

500

B/G

B/G
B/G

310·6

317·6
B/G

600

B/G
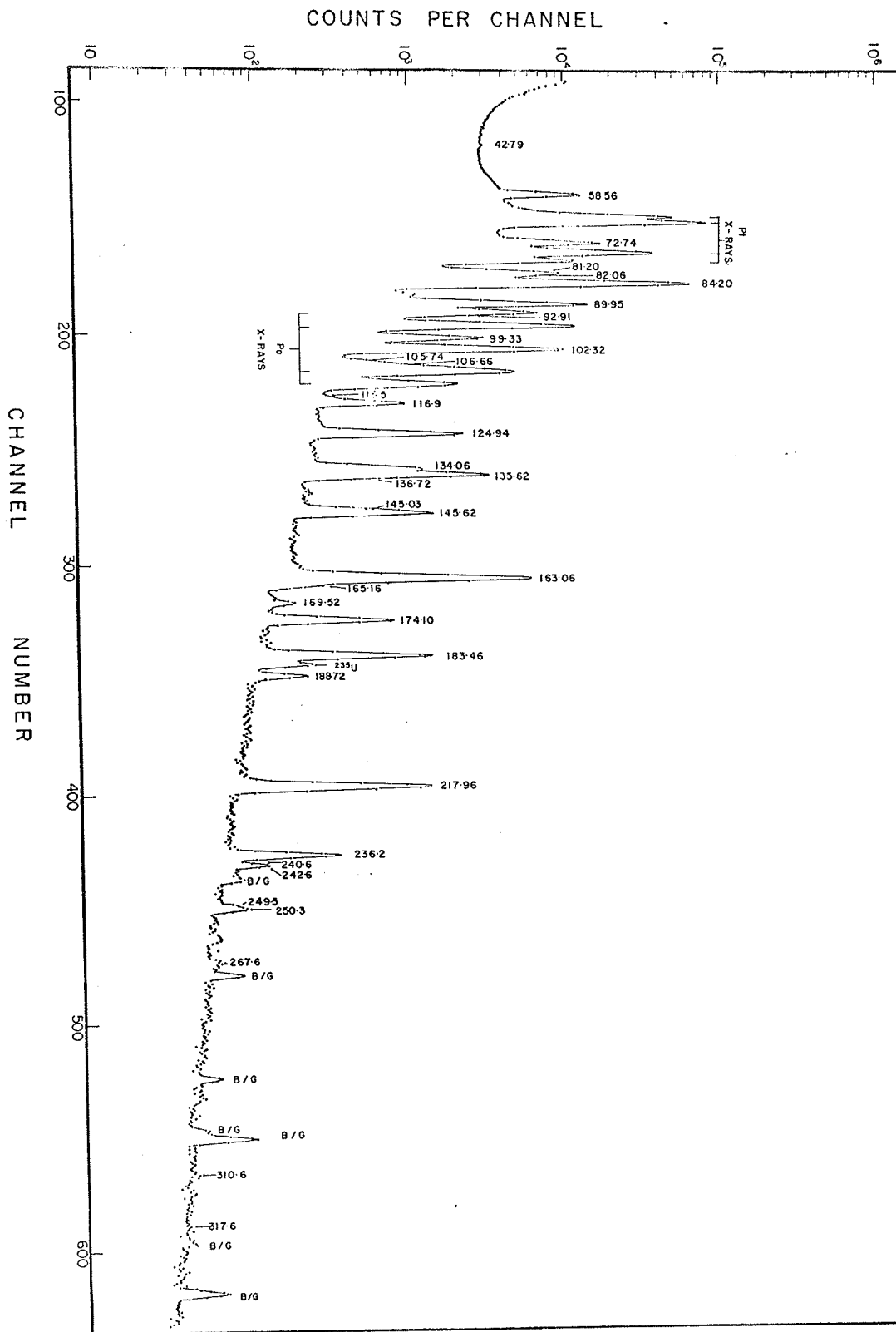
Figure IV-5

Attenuation curve of the Pt filter
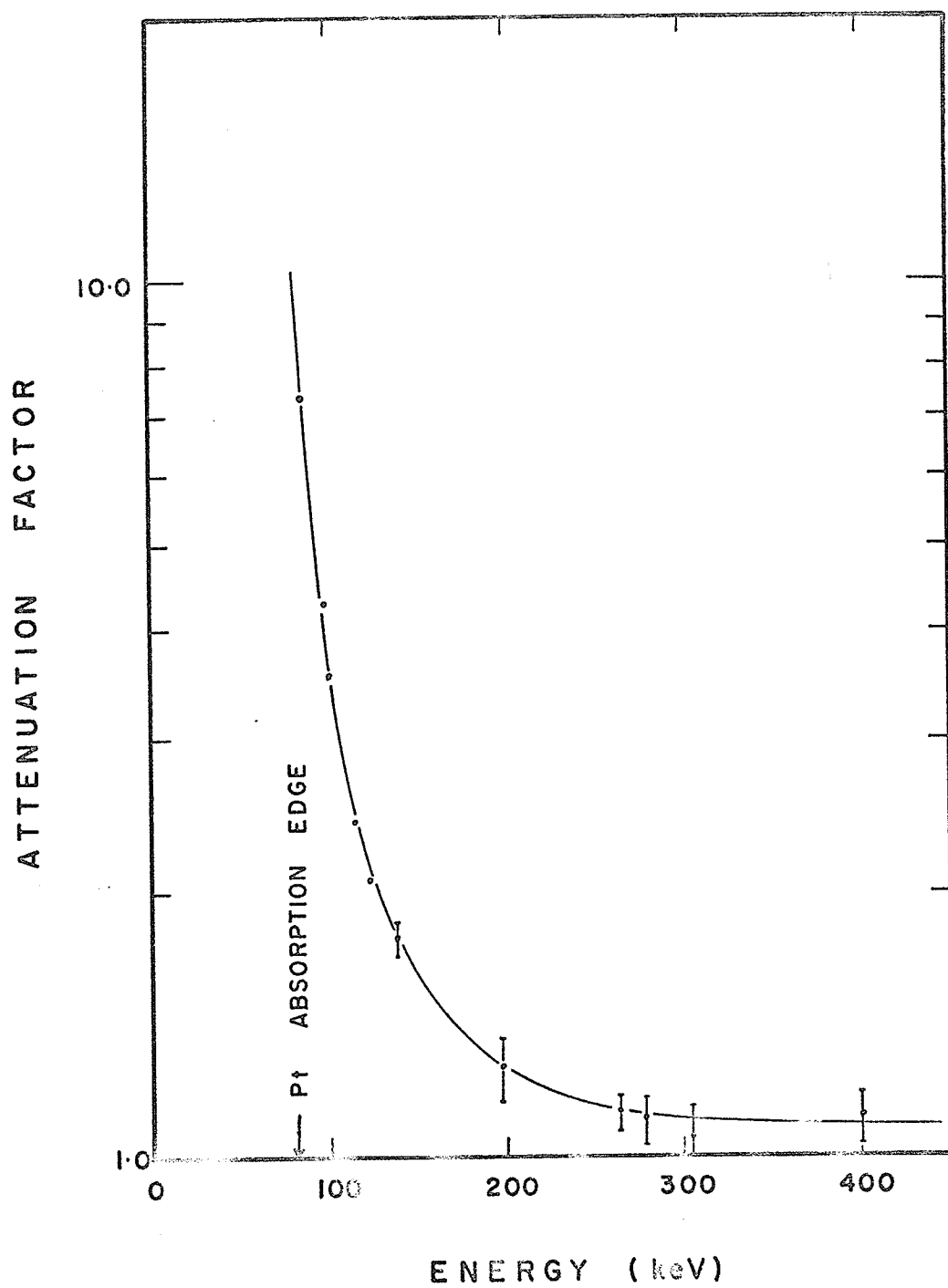
Figure IV-6

Attenuation curve of a Mo filter
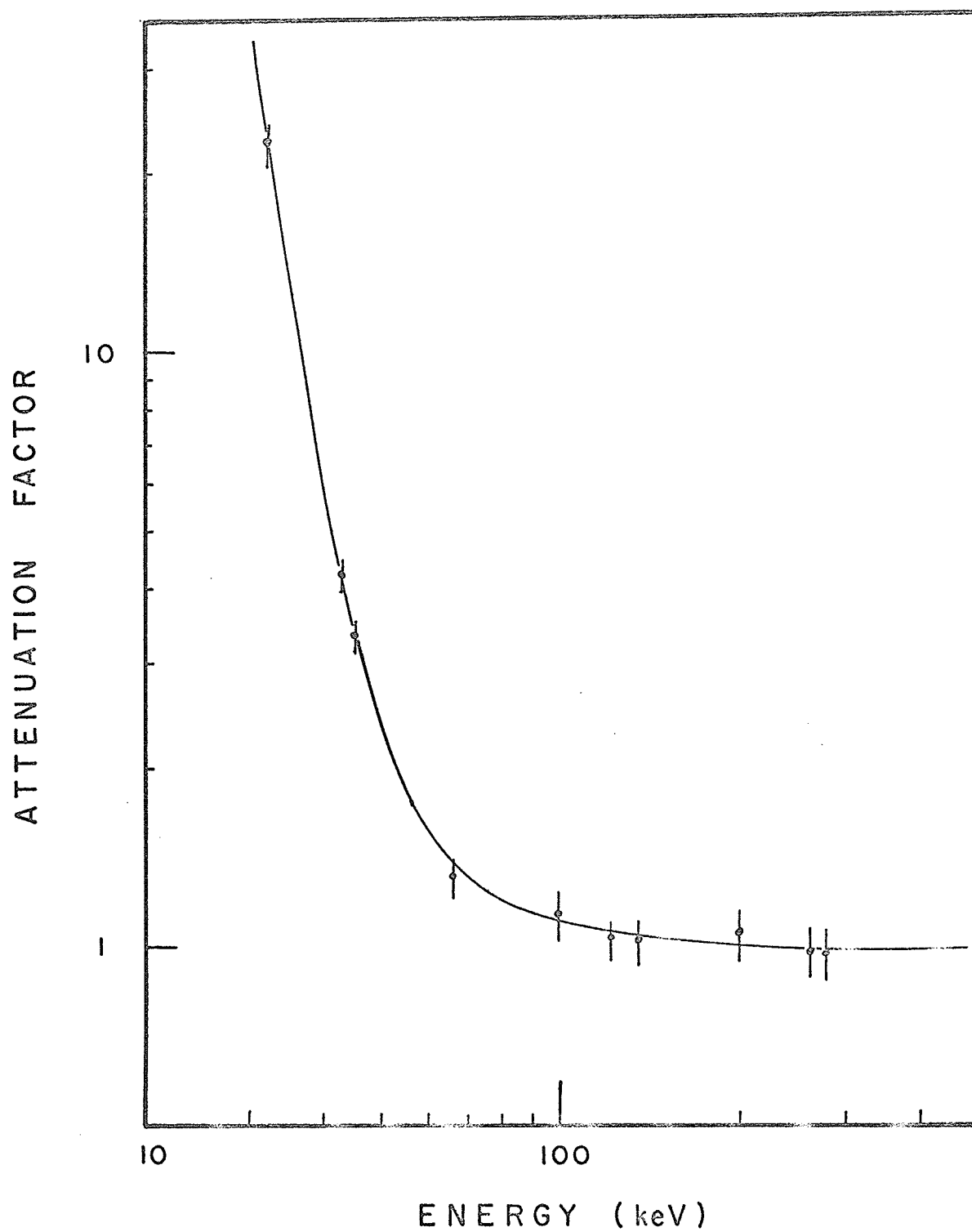
Figure IV-7

Gamma ray spectrum of ^{231}Th decay,

taken through the Mo filter

COUNTS PER CHANNEL

CHANNEL NUMBER

25·67

42·79

58·56

63·77
Au

Au X-RAYS

72·74

81·20 82·06 84·20

89·95

92·91

Pa

X-RAYS

99·33

102·32

105·74 106·66

115·5 116·9

124·94

134·06 135·62

136·72

B/G

145·03 145·9

B/G

163·06

165·16

169·52

174·10

183·46

235U

188·72

217·96

236·2
B/G
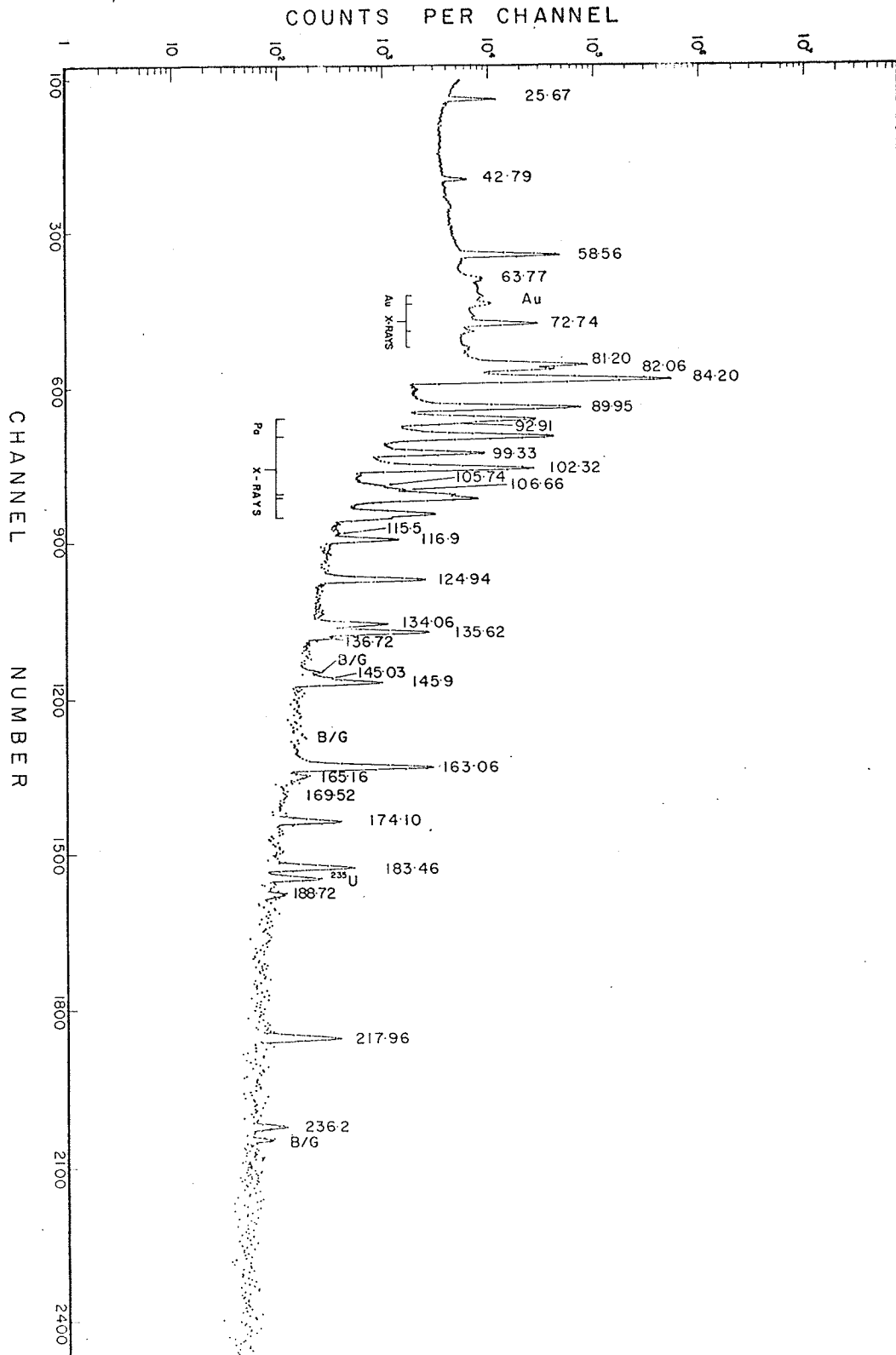
the summing occurs between the strong 84.20 keV gamma ray with the other photopeaks. A platinum filter of thickness (0.27 ± 0.02) gm/cm^2 was used between the source and the 50 cc detector. The resultant spectrum is shown in Figure IV-4. The K-absorption edge of platinum occurs at 78.381 keV[9] so that the gamma rays in the region of 80 to 100 keV were very heavily attenuated, thereby drastically reducing the possibility of their summing with the rest of the spectrum. An attenuation curve for this filter (see Figure IV-5), obtained experimentally using the photopeaks[10] of ^{75}Se, was used to correct for the attenuation of the gamma rays from the ^{231}Th decay due to this filter. The resultant relative intensities (relative to $I_\gamma(84.20) = 100.0$) are shown in Table IV-1.

The low energy region was similarly re-examined using the Ortec Ge(Li) X-ray detector, and the undesirable L X-rays, together with the 25.65 keV gamma ray, were attenuated using a molybdenum filter of thickness (0.20 ± 0.02) gm/cm^2. The attenuation curve of molybdenum (K absorption edge at 20.0039 keV)[9] is shown in Figure IV-6, and the gamma ray spectrum taken through this filter, is shown in Figure IV-7. The result of the analysis is shown in column 4 in

Energy	No Filter	Brown	No Filter	Pt Filter	Weighted Mean
25.67	204.3	202.0			204.3
42.79	1.59	0.87	1.03		1.12
58.56	8.21	7.2	7.45	7.86	7.61
63.77	0.25		0.23	0.17	0.22
72.74	3.83	4.0	3.64		3.67
81.20	13.1	14.2	13.70	13.43	13.52
82.06	6.8	7.2	5.85	6.60	6.42
84.20	100.0	100.0	100.00	100.0	100.0
89.95	14.8	15.3	14.68	16.5	15.33
92.91	1.0	1.1	0.81	0.99	0.93
99.33	2.0	2.1	2.06	2.14	2.07
102.32	6.8	6.7	6.86	6.93	6.86
105.74	0.14	0.14	0.13		0.13
106.66	0.34	0.34	0.33		0.33
115.5	0.017	0.041	0.014	0.013	0.014
116.9	0.38	0.39	0.37	0.37	0.37
124.94	0.86	0.95	0.97	0.95	0.95
134.06	0.35	0.42	0.43	0.40	0.41
135.62	1.09	1.3	1.35	1.32	1.31
136.72	0.04	0.09	0.03	0.07	0.05

Energy	No Filter	Brown	No Filter	Pt Filter	Weighted Mean
145.03	0.11	0.012	0.09	0.09	0.09
145.90	0.48	0.58	0.55	0.49	0.53
163.06	2.24	2.6	2.49	2.49	2.47
165.16	0.1	0.06	0.06	0.066	0.066
169.52	0.03	0.03		0.02	0.02
174.10	0.38	0.31	0.39	0.28	0.34
183.46	0.48	0.57	0.57	0.49	0.55
188.72	0.1	0.08		0.044	0.05
217.96	0.64	0.67	0.64	0.63	0.64
236.1	0.14	0.18		0.14	0.14
240.6	0.004	0.005		0.008	0.007
242.6	0.016	0.013		0.015	0.015
249.5	0.01	0.01		0.009	0.009
250.3	0.01	0.011		0.011	0.011
267.6		0.023		0.019	0.019
308.7	0.01	0.008		0.007	0.008
310.6	0.05	0.054		0.049	0.049
317.6		0.002			
320.1		0.0035			

Table IV-2

^{231}Th gamma ray table

(C) Observed in coincidence only

Present Work		Brown	
E_γ	I_γ	E_γ	I_γ
17.7 ± 0.1	1.3 ± 0.5		
18.6 ± 0.1	0.6 ± 0.3		
25.67 ± 0.03	204.3 ±10.0	25.56	202. ± 20
42.79 ± 0.06	1.12 ± 0.20	42.80 ± 0.06	0.87 ± 0.10
44.2 ± 0.3	(C)		
45.8 ± 0.3	(C)		
47.4 ± 0.3	(C)		
58.56 ± 0.05	7.61 ± 0.47	58.47 ± 0.05	7.2 ± 0.7
63.77 ± 0.10	0.22 ± 0.04		
71.8	(C)		
72.74 ± 0.05	3.67 ± 0.23	72.66 ± 0.06	4.0 ± 0.4
73.23	(C)		
81.20 ± 0.04	13.5 ± 1.0	81.18 ± 0.05	14.2 ± 1.4
82.06 ± 0.05	6.42 ± 0.58	82.02 ± 0.06	7.2 ± 0.7
84.20 ± 0.03	100.0	84.17	100.0
89.95 ± 0.05	15.3 ± 1.0	89.94 ± 0.05	15.3 ± 1.5
92.91 ± 0.10	0.93 ± 0.18	93.00 ± 0.10	1.1 ± 0.1
99.33 ± 0.05	2.07 ± 0.13	99.30 ± 0.05	2.1 ± 0.2
102.32 ± 0.04	6.86 ± 0.42	102.30 ± 0.05	6.7 ± 0.7
104.1	(C)		
105.74 ± 0.15	0.13 ± 0.02	105.73 ± 0.10	0.14 ± 0.02
106.66 ± 0.12	0.33 ± 0.03	106.58 ± 0.10	0.34 ± 0.04
114.8 ± 0.3	(C)		
115.5 ± 0.2	0.014± 0.005	115.58 ± 0.20	0.041± 0.014

Present Work		Brown	
E_γ	I_γ	E_γ	I_γ
115.9	(C)		
116.9 ± 0.1	0.37 ± 0.03	116.91 ± 0.05	0.39 ± 0.04
124.94 ± 0.04	0.95 ± 0.04	125.10 ± 0.05	0.95 ± 0.09
134.06 ± 0.06	0.41 ± 0.03	134.14 ± 0.08	0.42 ± 0.05
135.62 ± 0.04	1.31 ± 0.09	135.77 ± 0.06	1.3 ± 0.1
136.72 ± 0.08	0.05 ± 0.01	136.78 ± 0.20	0.09 ± 0.03
145.03 ± 0.20	0.09 ± 0.01	145.15 ± 0.30	0.012± 0.003
145.9 ± 0.1	0.53 ± 0.06	146.00 ± 0.07	0.58 ± 0.06
163.06 ± 0.07	2.47 ± 0.15	163.16 ± 0.06	2.6 ± 0.3
165.16 ± 0.12	0.07 ± 0.02	164.94 ± 0.10	0.06 ± 0.03
169.52 ± 0.15	0.02 ± 0.01	169.58 ± 0.10	0.03 ± 0.01
174.10 ± 0.06	0.34 ± 0.03	174.19 ± 0.08	0.31 ± 0.03
183.46 ± 0.06	0.55 ± 0.05	183.47 ± 0.07	0.56 ± 0.06
188.72 ± 0.10	0.05 ± 0.03	188.77 ± 0.20	0.08 ± 0.01
217.96 ± 0.05	0.64 ± 0.06	218.00 ± 0.07	0.67 ± 0.07
236.2 ± 0.1	0.14 ± 0.07	236.17 ± 0.07	0.18 ± 0.02
240.6 ± 0.1	0.007± 0.001	240.4 ± 0.2	0.0050± 0.0005
242.6 ± 0.1	0.015± 0.007	242.60 ± 0.10	0.013± 0.006
249.5 ± 0.8	0.009± 0.004	249.8 ± 0.3	0.010± 0.002
250.3 ± 0.8	0.0 ± 0.004	250.5 ± 0.3	0.011± 0.002
267.6 ± 0.6	0. 0.007	267.80 ± 0.07	0.023± 0.006
308.7 ± 0.6	0. ± 0.004	308.9 ± 0.3	0.008± 0.001
310.6 ± 0.7	0.049± 0.010	311.0 ± 0.1	0.054± 0.005
317.6 ± 1.	0.007	318.0 ± 0.4	0.002± 0.0002
320.1 ± 1.0	0.007	320.2 ± 0.3	0.0035± 0.0002

Table IV-1.   The weighted mean of the relative intensities (relative to I_γ (84.20) = 100.0) are adopted as the relative intensities of the gamma rays coming from the [231]Th decay (see column 6 in Table IV-1).

The energies of the gamma rays were determined as described in Chapters I and II. Even though the non-linearity of the spectrometer was allowed for, highly accurate energy determination was difficult due to the numerous gamma rays grouped in a relatively small energy region. In the present work, an accuracy of no better than 30 eV was the best one could obtain for the lines at 25.65 and 84.20 keV. Table IV-2 lists the average gamma ray energies and relative intensities. Also listed in the same table are that reported by Brown[11,16] for comparison. Generally, the agreement is good within the experimental error quoted. In the singles gamma ray studies, no new gamma rays are observed in the present work beyond those listed by Brown, although several new gamma transitions were shown to exist by the gamma-gamma coincidence work which will now be described.
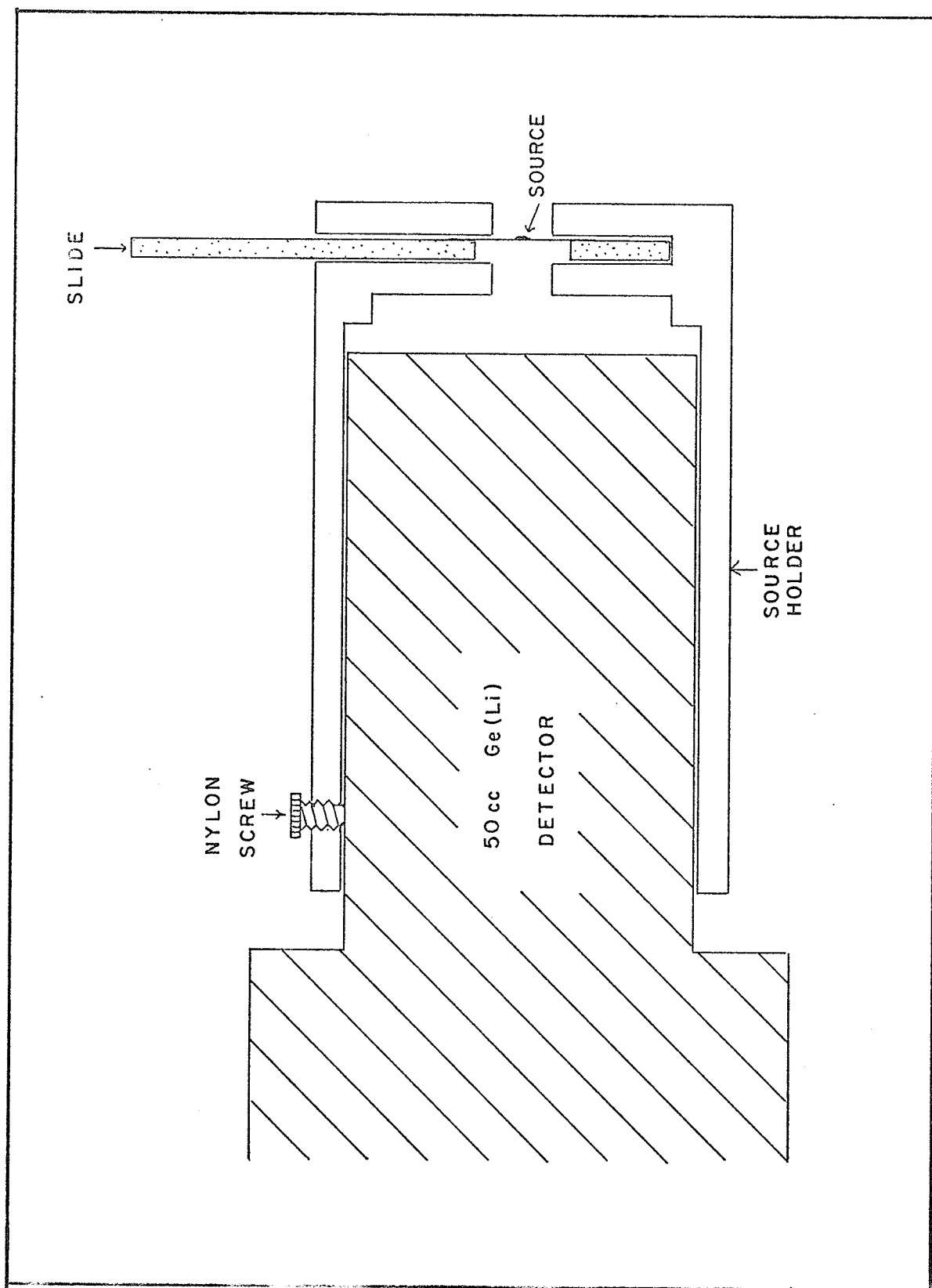
IV.4 GAMMA-GAMMA COINCIDENCE

Gamma gamma coincidence work was carried out, using the Ortec 35 cc Ge(Li) detector as the gating detector in channel 1, and the Nuclear Diode 50 cc

Figure IV-8

Source holder for ^{231}Th

Not drawn to scale

SLIDE

SOURCE

SOURCE
HOLDER

NYLON
SCREW

50 cc   Ge(Li)

DETECTOR

Ge(Li) detector in the other channel. Since the source has a half life of only 25.52 hours, it is necessary to change the source every two days in the coincidence experiments. In order not to disturb the geometry, a special source holder was constructed as shown in Figure IV-8. Essentially, it consisted of a lucite cylinder with one end closed, and could be snuggly fitted onto the aluminium covering case of the 50 cc detector. A circular aperture whose diameter was 2.0 cm, was cut at the geometric center of the end wall of the cylinder. The active material was evaporated to dryness on a piece of mylar glued to a lucite plate which could slide freely along the slots cut on the outside of the closed end wall of the cylinder. A stop was attached so that when the slide was in place, the active material was on the long axis of the detector and the gamma rays could enter the detector through the circular aperture. This simple device permits changing sources in a coincidence experiment without disturbing the geometry. A nylon fixing screw ensured that the position of the lucite cylinder relative to the detector remained fixed.

On the average, a coincidence experiment took four to five weeks. In order to minimize data collection time, the coincidence circuit was modified to permit

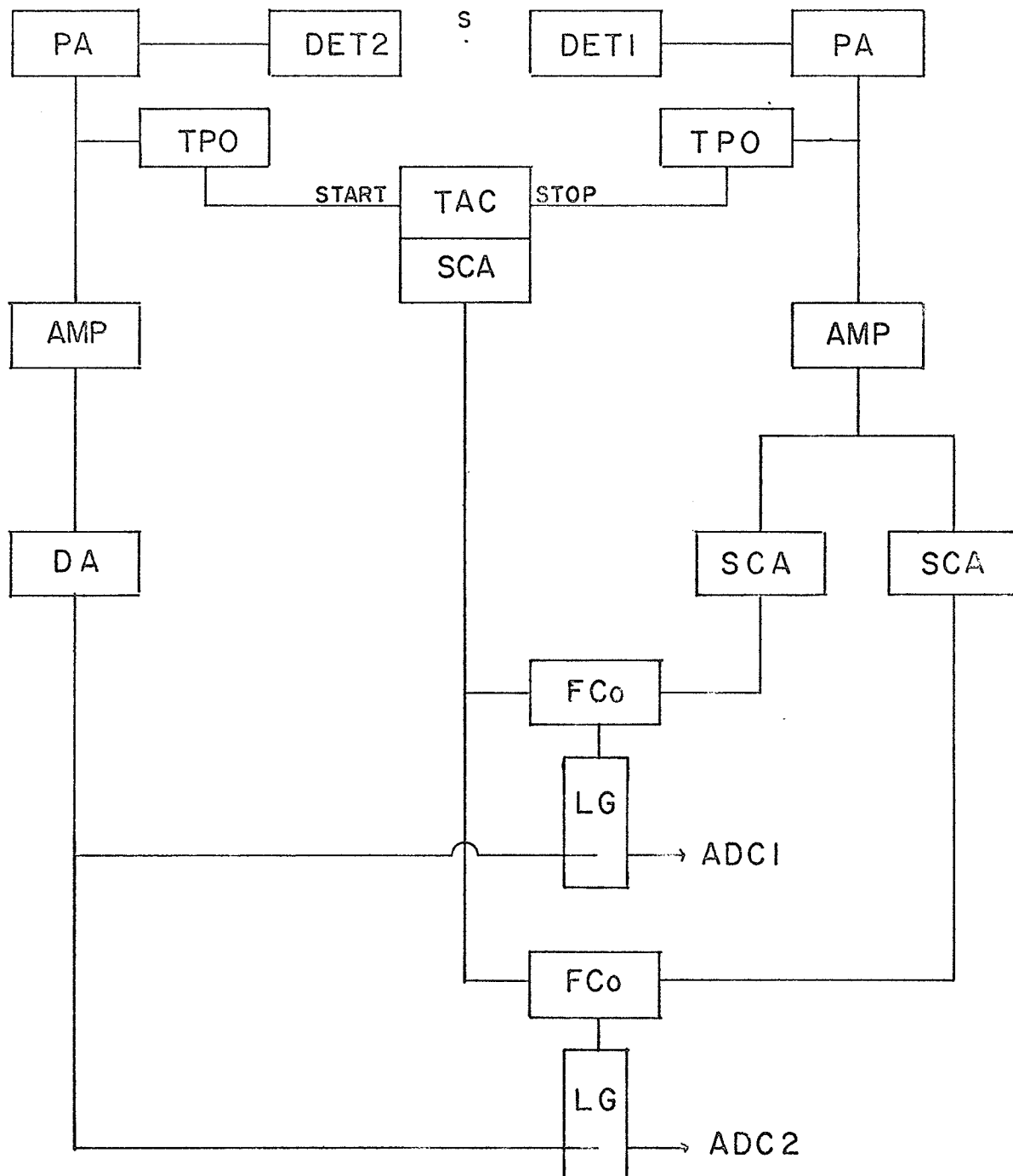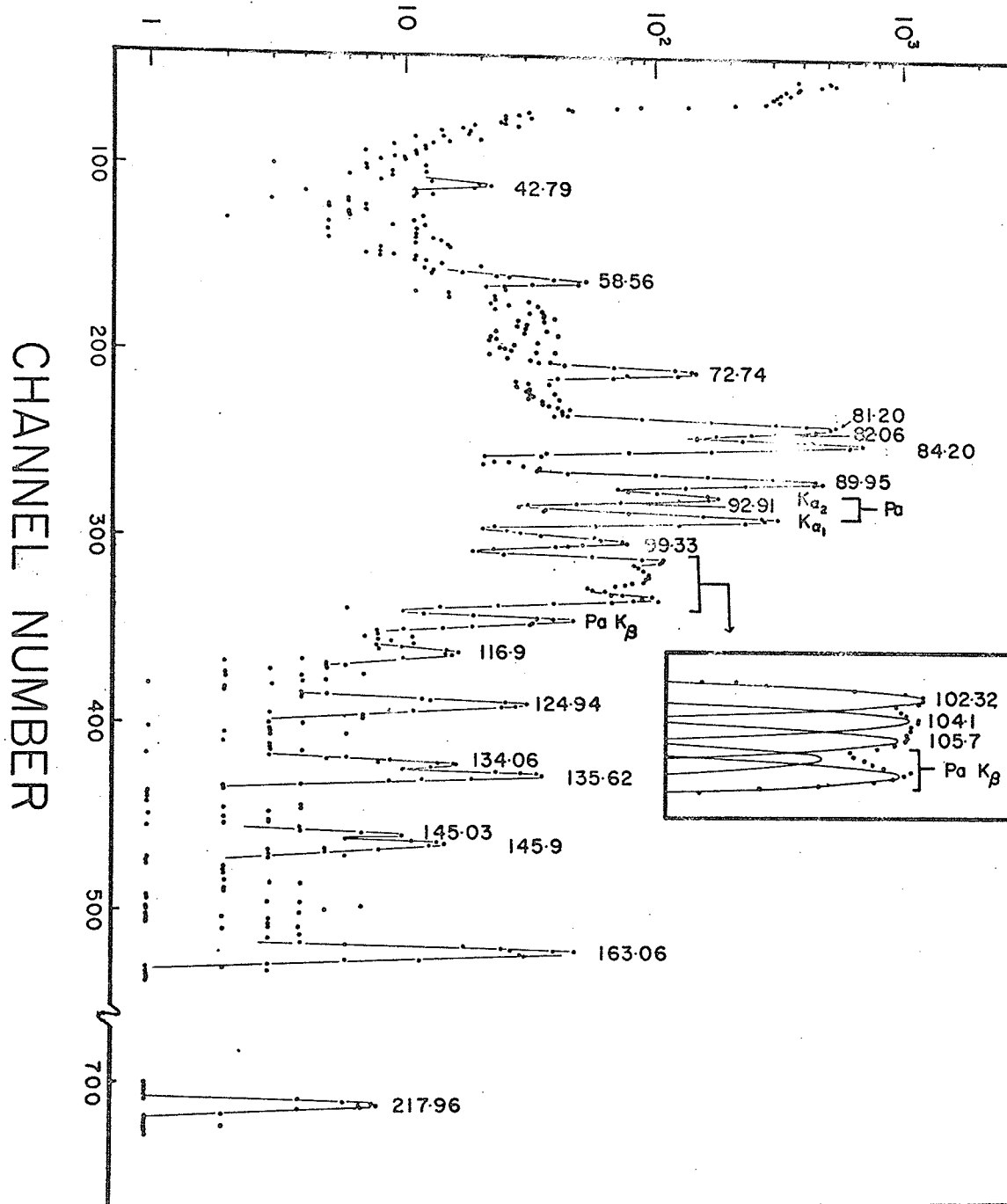Figure IV-9

Modified circuit for ^{231}Th

coincidence work

Figure IV-10

Coincidence spectrum with the

58.56 keV gamma ray

two separate coincidence spectra to be collected simultaneously. The modified circuit is shown in Figure IV-9.

Most of the more intense gamma rays were selected as gates, and the coincidence spectra collected. The gates selected were the the gamma rays at 58.56, 81.20, 82.06, 84.20, 89.95, and 102.32 keV.

58.56 keV Gate:

When the 58.56 keV gamma ray was selected as gate, the coincident spectrum is as shown in Figure IV-10. After analysis, the gamma rays that are in coincidence with the 58.56 keV gamma ray are 42.79, 72,74, 81.20, 82.06, 89.95, 104.1, 105.74, 116.9, 124.94, 134.06, 135.62, 136.72, 145.03, 145.9. 163.06 and 217.96 keV. The line at 84.20 keV occurs entirely due to random events. The interesting feature in this spectrum is a group of gamma rays in the region 102 to 108 keV. Sucessful unfolding revealed two gamma rays at 104.1 ± 0.5 and 105.9 ± 0.5 keV, which had not been previously observed (see insert). The peaks at 107.6 and 108.4 keV are the $K-M_{III}$ and $K-M_{IV}$ components of the Pa X-rays. Of all the gamma rays observed in coincidence with the 58.56 keV gate, only the line at 104.1 keV line does not have a certain place in the level scheme.

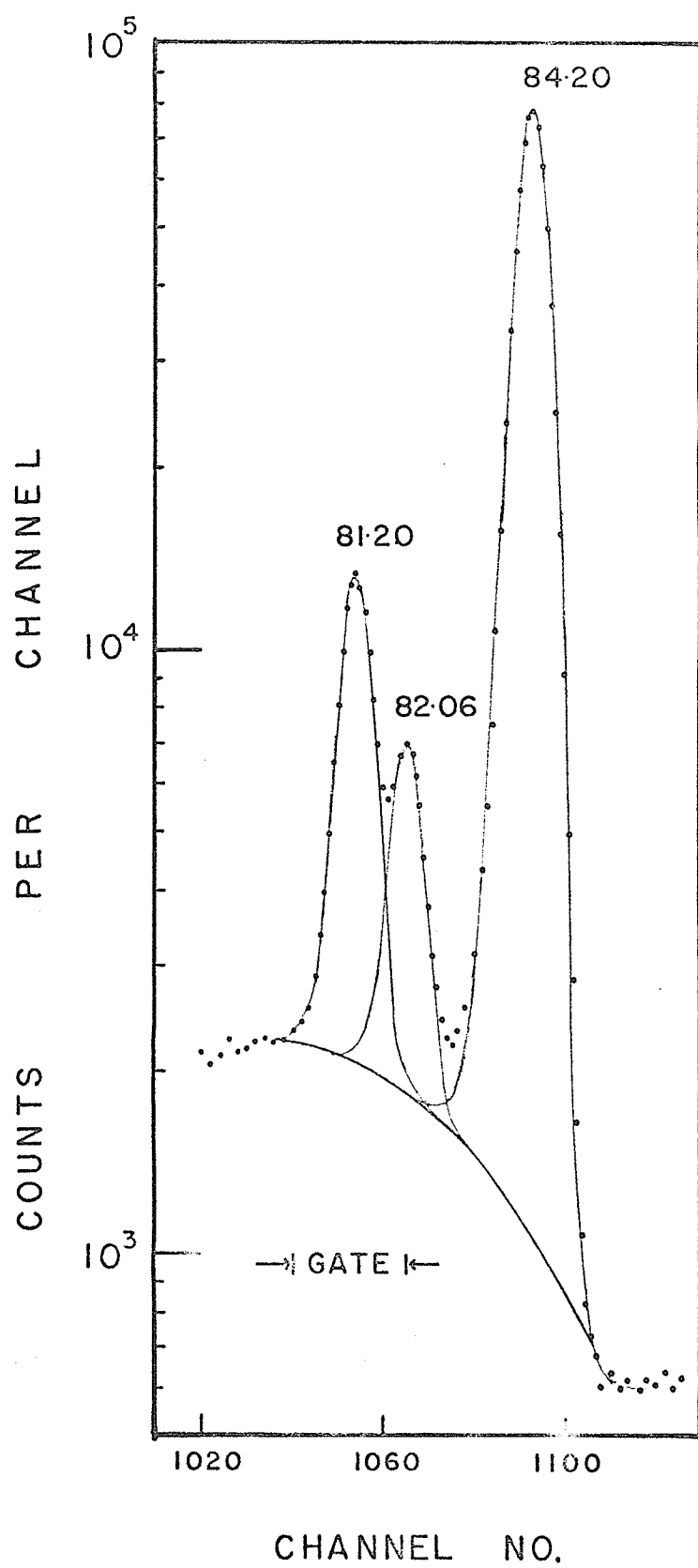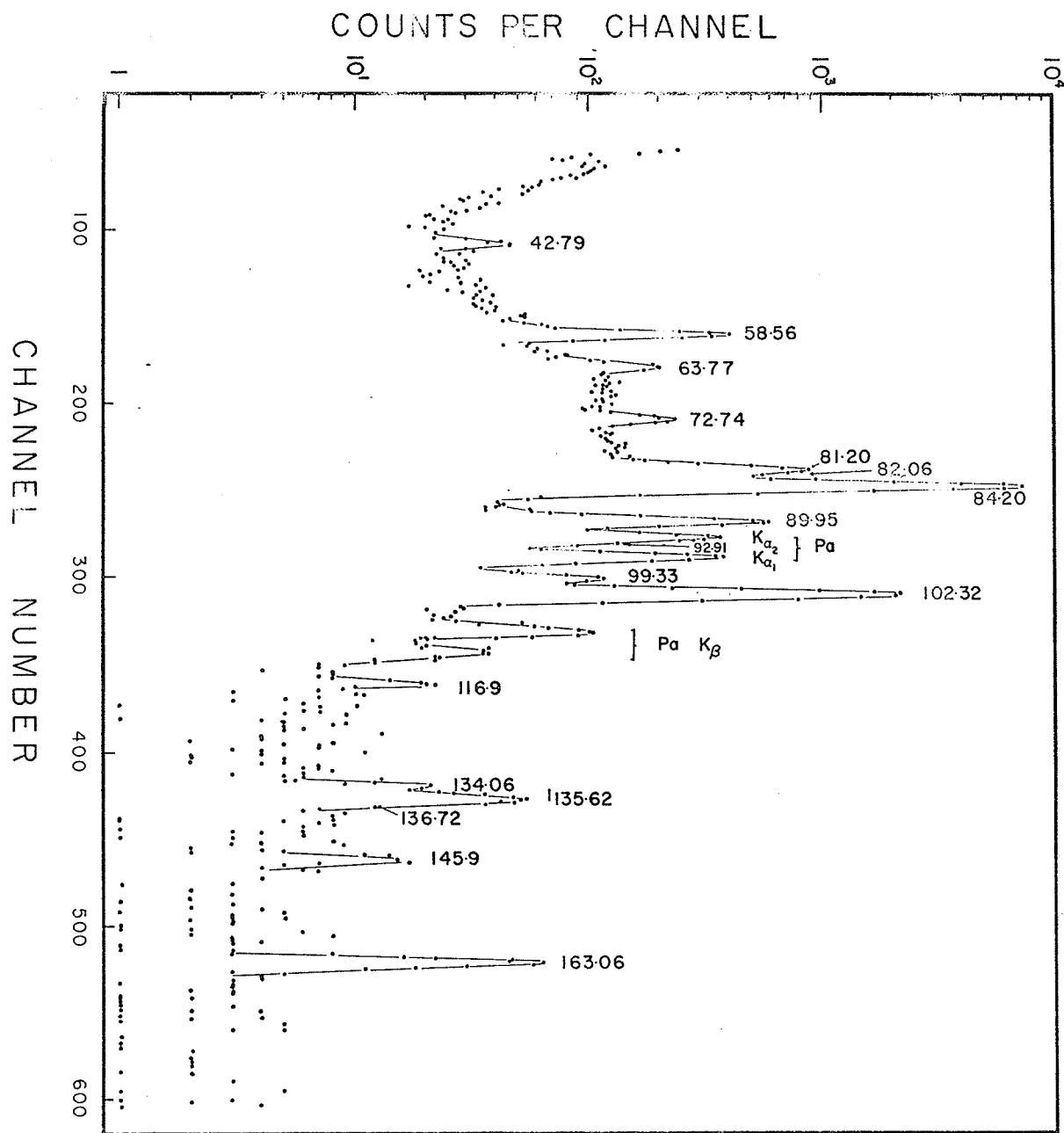Figure IV-11

Energy window of the

(81.20 + 82.06) keV gate

Figure IV-12

Coincidence spectrum with the

(81.20 ÷ 82.06) keV lines

(81.20 + 82.06) keV Gate:

Next, it is interesting to obtain the coincidence spectrum in coincidence with the 81.20 and 82.06 keV gamma rays, since they de-excite from the same level to two different levels which are only 1.0 keV apart. It is evident from Figure IV-3 that it is not possible to set the energy window on each of these two lines individually. In the present work, the SCA is set in such a way that about 80% of the gating pulses come from the 81.20 keV line, while the remaining 20% come from the other gamma ray, and a diagram of the energy window is depicted in Figure IV-11. The gate is so selected as to minimize the contribution from the unwanted pulses coming from the 84.20 keV gamma ray.

The coincidence spectrum is shown in Figure IV-12. The gamma rays in coincidence with the gate are 25.67, 42.79, 58.56, 63.77, 84.20, 92.91, 102.32, and 136.72 keV. It should be noticed that the 63.77 keV gamma ray is very weak in the singles spectra but is much enhanced here. The lines at 92.91 and 136.72 keV are shown to be enhanced only after numerical analysis. The 92.91 keV gamma ray observed in the present work is identical to the 93.1 keV line reported by Brown.

Figure IV-13

Coincidence spectrum with the

84·20 keV gamma ray

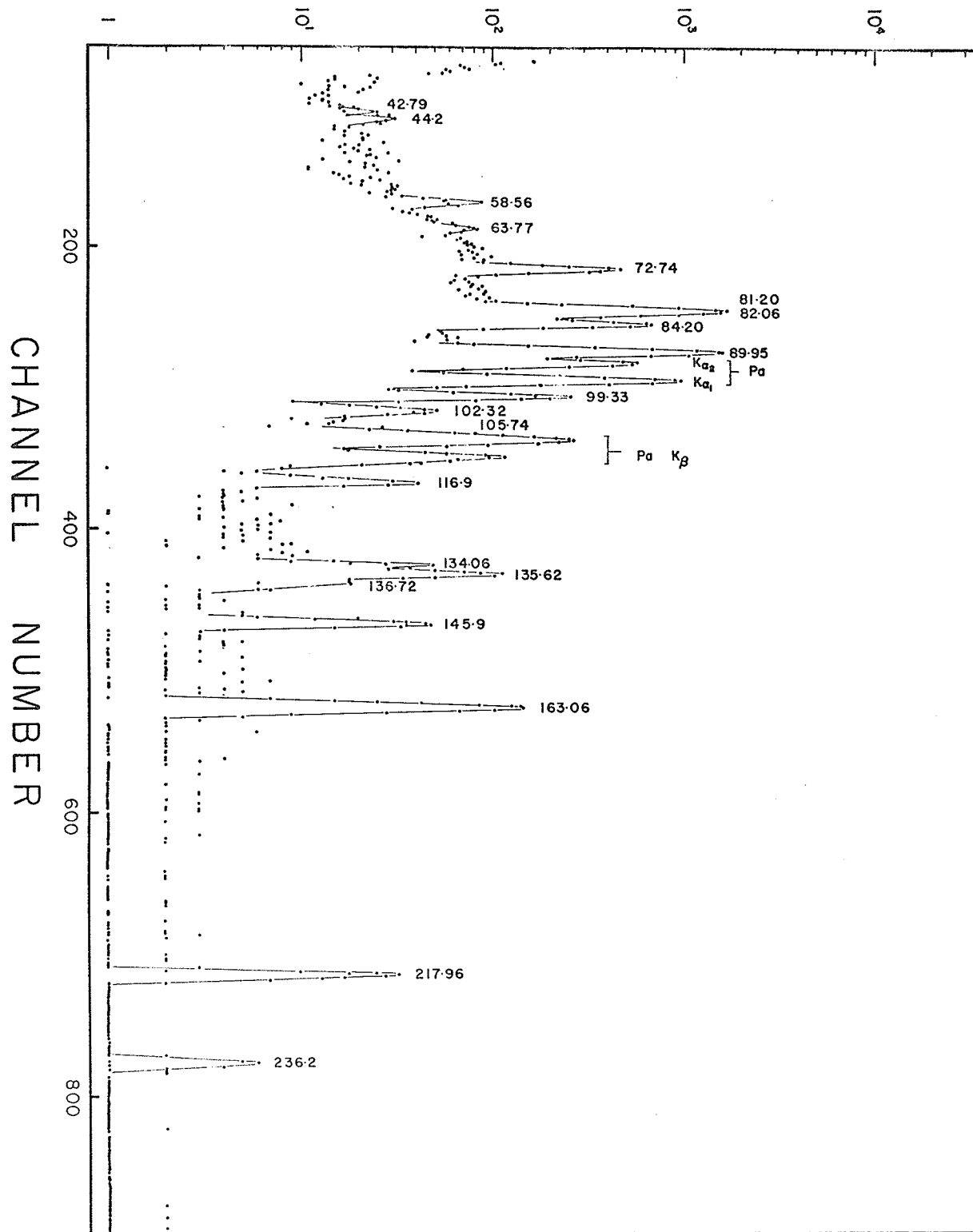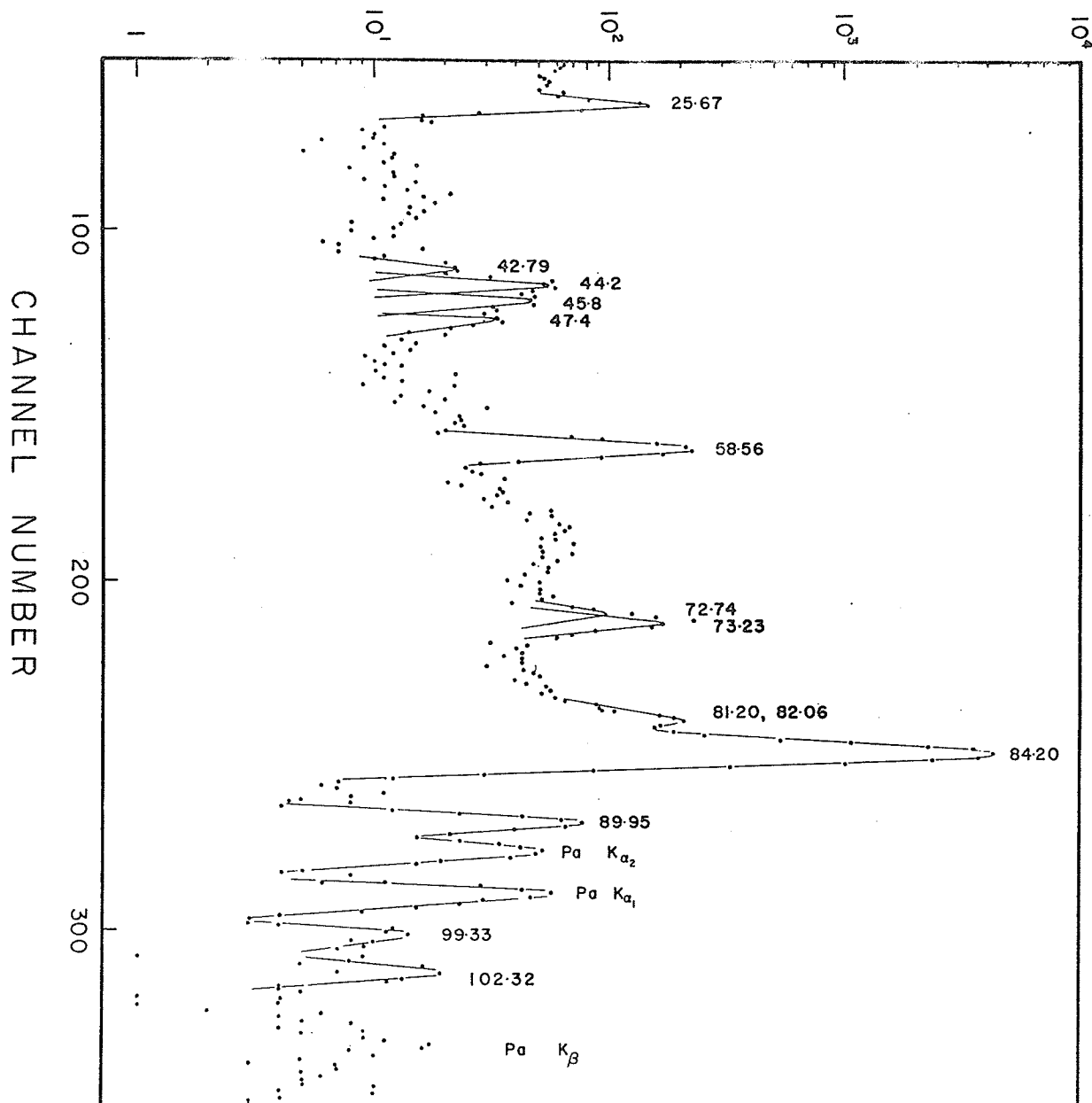Figure   IV-14

Coincidence spectrum with the

89.95 keV gamma ray

84.20 keV Gate

Figure IV-13 shows a coincidence spectrum collected when the gate was set on the 84.20 keV gamma ray. The enhanced lines include those at 44.2, 63.77, 72.74, 81.20, 82.06, 89.95, 99.33, 116.9, 134.06, 135.62, 136.72, 145.03, 145.9, 163.06, 217.96 and 236.2 keV. The interesting feature in this spectrum is the presence of a 44.2 keV line, which appeared only in coincidence spectra but not in singles spectra. It should be noted that the 84.20 keV gamma ray de-excites a level which has a half life of 41 nanoseconds.[18] However, this does not cause any problem here since the time resolution of the system is 65 nanoseconds.

89.95 keV Gate:

When the SCA is set to gate on the 89.95 keV line, the coincidence spectrum obtained is as shown in Figure IV-14. The gamma rays that are found to be in coincidence with the gate are those at 25.67, 58.56, 73.2, 84.20, and a group of lines at about 44 keV. The line at 73.2 keV had not been observed in singles spectra before. The group of lines at about 44 keV is of interest here, as it seems that the group consists of four lines having energies 42.79, 44.2, 45.8, and 47.2 keV Of these four, only two (42.79 and 44.2 keV) had been observed either in singles or in coincidence with the 84.20 keV line in the present work. The

Figure IV-15

Coincidence spectrum with the

102.32 keV gamma ray
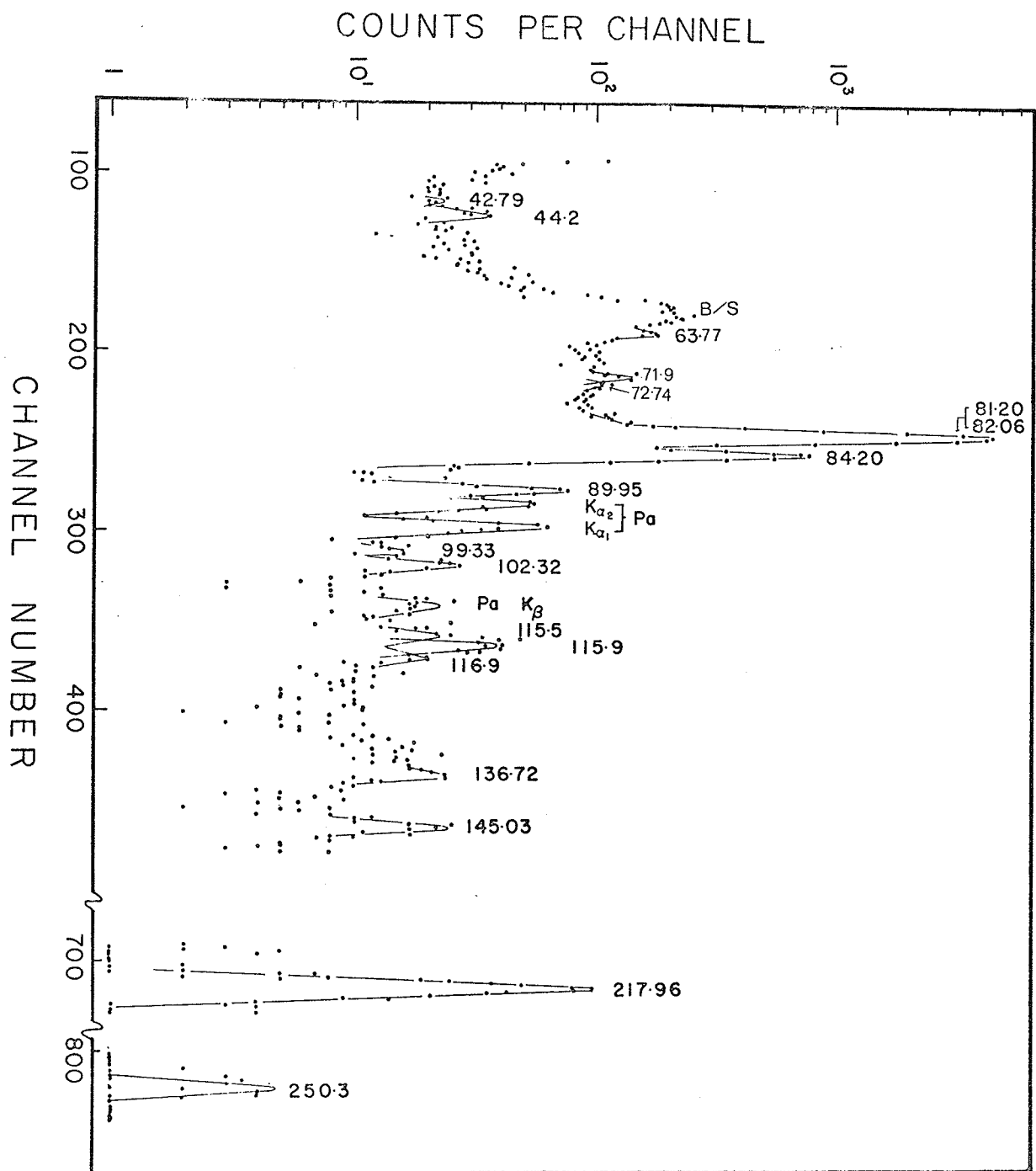
Table IV-3

^{231}Th coincidence table

Coincident Gamma ray	Gate				
	58.56	81.20 82.16	84.20	89.95	102.32
25.67		X		X	
42.79	X	X			
44.17			X	X	X
45.8				X	
47.2				X	
58.56		X		X	
63.77		X	X		X
71.8					X
72.74	X		X		
73.23				X	
81.20	X		X		X
82.06	X		X		X
84.20		X		X	
89.95	X		X		X
92.91		X			
99.33			X		X
102.32		X			
104.1	X				
105.6	X				
106.66		?			
116.9	X		X		X
124.94	X				
134.06	X		X		X
135.62	X		X		X
136.72	X	X	X		X
145.03	X		X		X
145.9	X		X		X
163.06	X		X		X
217.96	X		X		X
236.2			X		X
249.5					X

Figure IV-16

Decay scheme for the ^{231}Th decay

Energy level diagram

Right-side level energies (keV):
351·8
320·28
318·2 (3/2)
294·5
247·27 (7/2)
218·27 (7/2)
183·49 (5/2)
174·10 (5/2)
111·62 (9/2)
102·32 (3/2)
101·38 (7/2)
84·20 (5/2)
77·8 (5/2)
58·56 (7/2)
9·6 (1/2)
0 (3/2)

Transition energies from 351·8 level:
267·6 250·3 249·5 104·1

Transition energies from 320·28 level:
320·1 310·6 242·6 236·2 217·96 136·72 317·6 308·7 240·6

472 (dashed, from 294·5)

63·7 (7/2, 247·27)

188·72 169·5 163·06 145·9 145·03 135·6 73·23

134·06 116·9 115·9 106·7 44·17

183·49 124·94 105·6 99·33 82·07 81·20 174·10 165·16 115·5 89·95 72·74 71·8

102·32 92·91 18·6 42·79 17·7

84·20 25·67

58·56

Band labels (left side):
5/2 [642]
5/2 [523]
3/2 [651]
1/2 [530]

²³¹Pa

231
Pa

remaining two are less clearly understood, and have been placed in the level scheme though with lesser certainty.

102.32 keV Gate:

The gamma rays in coincidence with the 102.32 keV gamma ray is shown in Figure IV-15. The coincident gamma rays are those at 44.2, 63.77, 71.8, 72.74, 81.20, 82.06, 89.95, 99.33, 116.9, 134.06, 135.62, 136.72, 145.03, 145.9, 163.06, 217.96, 236.2 and 249.5 keV. The structure visible in the region from 50 to 60 keV is the back scattered peak of the 81.20 keV gamma ray.

Further attempts to gate on other gamma rays proved unsuccessful due mainly to the fact that their intensities were too low to yield a meaningful counting rate. The result of the coincidence work is summarized in Table IV-3.

IV.5 DISCUSSION

The result of the above studies has assisted in the construction of the decay scheme of ^{231}Th, as shown in Figure IV-16. The gamma ray energies and their intensities as well as the coincident data confirmed the decay scheme as suggested by Brown and Asaro[16]

Of all the gamma rays observed, all but two, viz

154

those at 45.8 and 114.8 keV, have been placed in the level scheme. A level at 294.5 keV is suggested to accomodate the 47.2 keV gamma ray which is observed in coincidence with the 89.95 keV gamma ray. Some support for the existence of this level comes from the fact that there is a known alpha decay of ^{237}Np to a level[16] at about 300 keV in ^{231}Th. Seven new gamma rays (six of which are observed only in coincidence experiments) are reported here, and their energies are 44.2, 45.8, 47.2, 63.77, 71.8, 73.23, 104.1 and 115.9 keV.

The ground state spin of ^{231}Pa nucleus has been measured[12] to be 3/2, and is a member of the 1/2-(530) band.[13] The I=1/2, 3/2, 5/2 and 7/2 members lie at 9.6, 0.0, 58.56 and 77.8 respectively. It is interesting to note that the I=1/2 state actually has a higher energy than the I=3/2 state. Mottelson and Nilsson[14] had shown that when the decoupling parameter a (see PREFACE at the beginning of this Thesis) is negative, and |a| is sufficiently large, it is possible for the 3/2 member to drop below the I=1/2 member.

There is also an intrinsic rotational state at about 183 keV, and has been assigned[15] as the 5/2+(642) state. This assignment is primarily based on the similarity between the spin states of ^{231}Pa and ^{233}Pa.

Brown[17] has suggested that there is a further

rotational band around 84.20 keV, and this band is given the assignment of 3/2+(651). Again, an inversion of level order is observed, and is caused by coriolis coupling between this and the 5/2+(642) band. The Nilsson assignment of 5/2-(523) is assigned to the 174.10 keV level which is populated by the beta decay of ^{231}Th.

CHAPTER V

THE DECAY OF ^{235}U

V.1 INTRODUCTION

The decay of ^{235}U is an interesting one not only because it is the first member of the actinium series, but also because of the relatively scarce spectroscopic information available[1-3] compared to the huge amount of reaction and fission data. Prior to 1971, little information on its decay scheme[4] or gamma radiation was known. Since this work was concluded, a report of Cline's work has appeared in the literature[5] This was apparently the first attempt to examine the decay of ^{235}U using high resolution semi-conductor gamma ray detectors, and the opportunity has been taken to compare the present work with his, the only comparable set of data. Nine new gamma rays were formally reported by Cline for the first time beyond those observed in the early sixties. Although Gaeta[6] reported his results on the studies of the same isotope in 1966, using NaI(Tl) scintillators, his results are not very trustworthy in the sense that the agreement with the others is very poor. It is one of the purposes of the present work to clarify these discrepancies.

Figure V-1

Decay scheme for ^{235}U decay

from Ref. 4

α ^{235}U

(9/2-) _____ 448

7/2- _____ 387

201 180 153
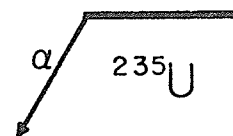
(13/2-) _____ 337

(11/2-) _____ 279

(9/2-) _____ 234

(7/2-) _____ 204

19

(5/2-) _____ 185

204 163 110 185 143

(9/2+) _____ 97

(7/2+) _____ 42

(5/2+) _____ 0

^{231}Th

It is known[7] that all uranium minerals contain approximately 0.72% of ^{235}U. It is an alpha emitter with a half life of 7.13×10^8 years. Its low activity of 4.5 disintegration per minute per micro-gram causes considerable difficulty in the investigation of its alpha spectrum, although Pilger et-al[8], Skilling[9], Baranov et al[10] and Gaeta[6] have succeeded in obtaining alpha spectra of ^{235}U using uranium samples highly enriched in ^{235}U.

The gamma rays associated with the alpha decay had been studied by a number of groups, including Pilger[3], Malich[2], Stevens[15] and Cline[5]. Until 1971, only nine gamma rays had been placed in the level scheme[4] which itself had ten levels(See Figure V-1).
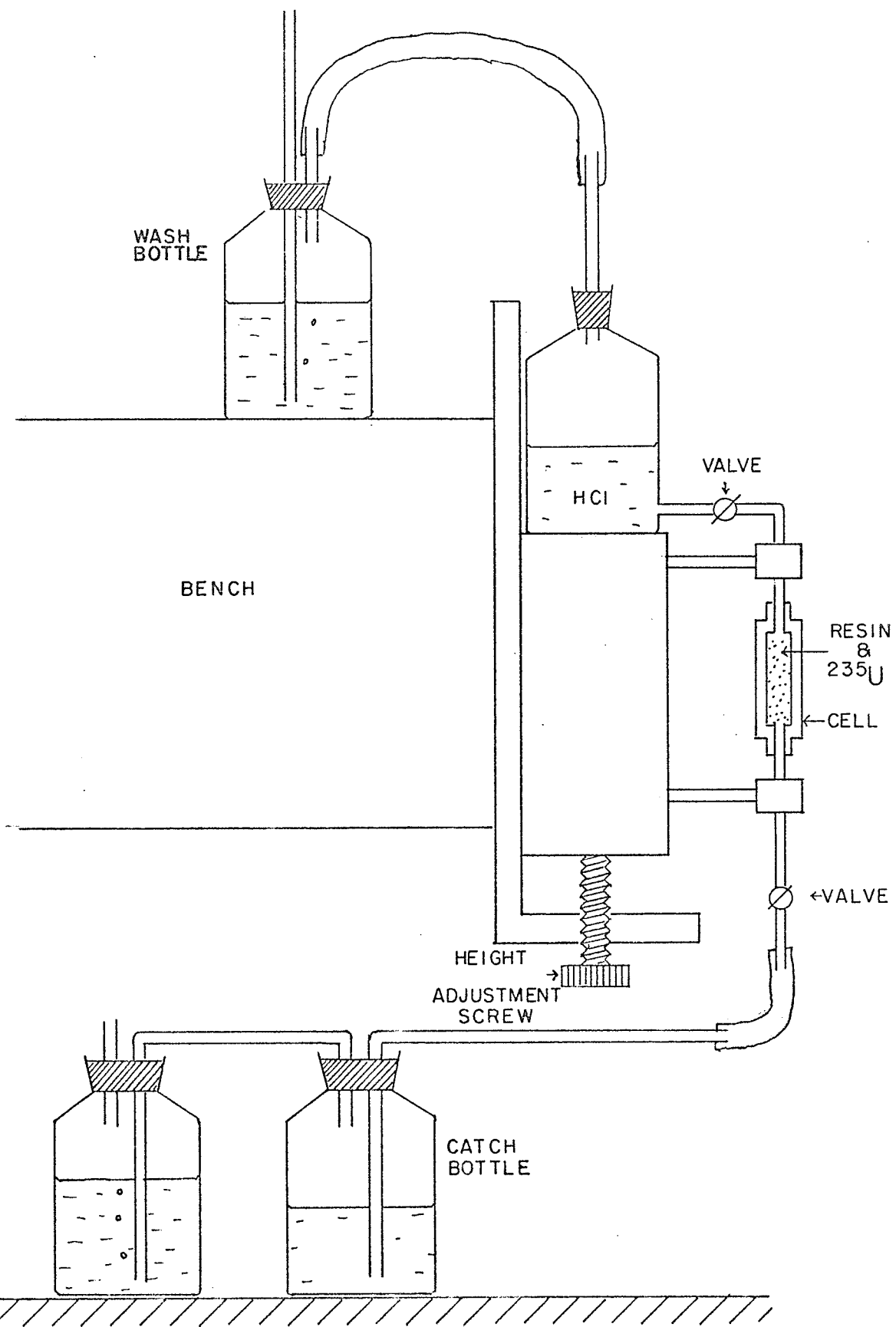
V.2 SOURCE PREPARATION

In the present work, 2.5 grams of 93% enriched ^{235}U were obtained from the Whiteshell Research Establishment, Atomic Energy of Canada, Pinawa, Manitoba. Conventional methods of source preparation were not possible because:

(i) the semi-conductor detectors used have poor detection efficiency--only 5-7% of that of a 3"x3" NaI(Tl) scintillation detector, and hence a large quantity of ^{235}U is needed in the source.

(ii) Uranium chloride (see following paragraph) tends

Figure V-2

Source holder for ^{235}U

WASH BOTTLE

HCl

VALVE

BENCH

RESIN & 235U

CELL

HEIGHT ADJUSTMENT SCREW

←VALVE

CATCH BOTTLE

to form large crystals and thus it is not possible to obtain suitable sources by placing a drop of the solution on a thin backing and evaporating to dryness. (iii) ^{235}U decays to ^{231}Th which itself has a half life of 25.52 hours (see Chapter IV). This means that the daughter activity will be in secular equilibrium with the parent in a matter of days.

It is obvious that the source to be used in the present studies should have some means of continuously removing the daughter products. A special source holder was constructed as shown in Figure V-2. A cell whose external dimensions were 4 cm by 5 cm by 0.6 cm was constructed from lucite. Each wall of the cell was made of lucite of the same thickness (0.2 cm) as the space between them. The space was packed with Amberlite AG-1x8 50-100 mesh resin previously soxhlet extracted in an all glass extraction apparatus for eight hours with 12M HCl. Uranium was loaded onto the resin column in chloride form using 12M HCl. At this acidity, the uranium ions should stay on the resin column. A reservoir provided a steady flow of 12M HCl at such a rate that the entire volume of acid inside the cell would be replaced every half hour. This way, any ^{231}Th that was produced as a result of the alpha decay of ^{235}U would be continuously washed out. The eluant was

Figure V-3

Gamma ray spectrum of ^{235}U

(10 - 150 keV)
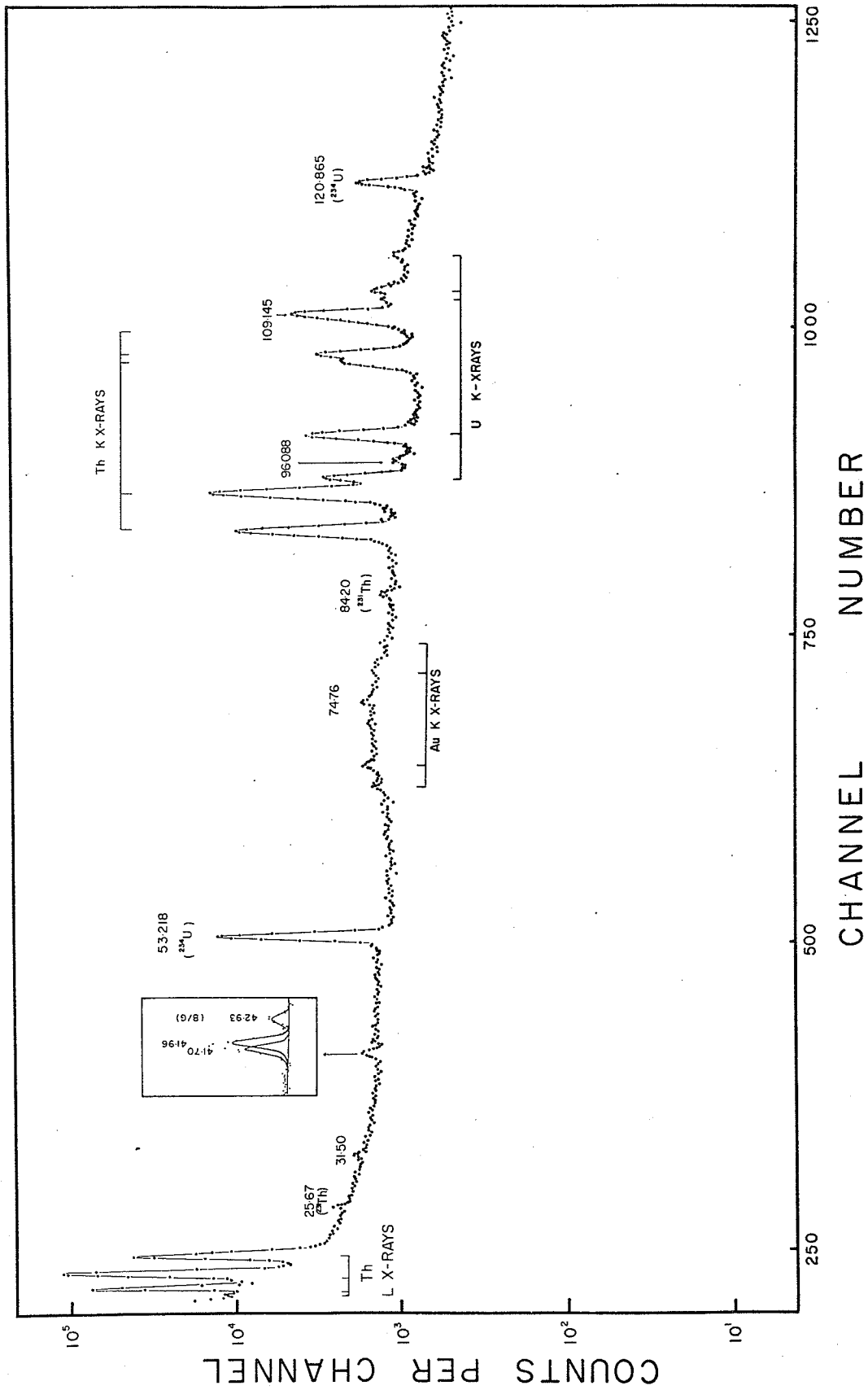
collected in a bottle. To avoid damage to the surrounding equipment from HCl vapour escaping from the system into the atmosphere, the reservoir and the catch bottle were provided with wash bottles to act as vapour traps.

V.3 GAMMA RAY SPECTRA

Figure V-3 shows the gamma ray spectrum up to 150 keV following the alpha decay of ^{235}U into ^{231}Th, taken with a Ge(Li) X-ray detector whose resolution at 5.9 keV was 290 eV. The spectrum is sufficiently simple to permit very accurate determination of the gamma ray energies, as described in Chapter I. The two weak peaks at 25.7 and 84.2 keV can be attributed to the incomplete removal of ^{231}Th from the column and its presence is revealed by these two lines which are the strongest transitions in the entire spectrum of ^{231}Th (See Chapter IV). The lines at 52.228 and 120.865 keV come from the decay of ^{234}U. The source is known to contain ^{234}U, and it is not possible to remove it by chemical means. The uranium X-rays are produced by fluorescence due to the large amount of uranium present on the column. In this low energy portion of the spectrum, the lines at 31.5, 41.70, and 41.96 keV are here reported for the first time. The insert shows the closely situated lines at $\simeq 42$ keV.

Figure V-4
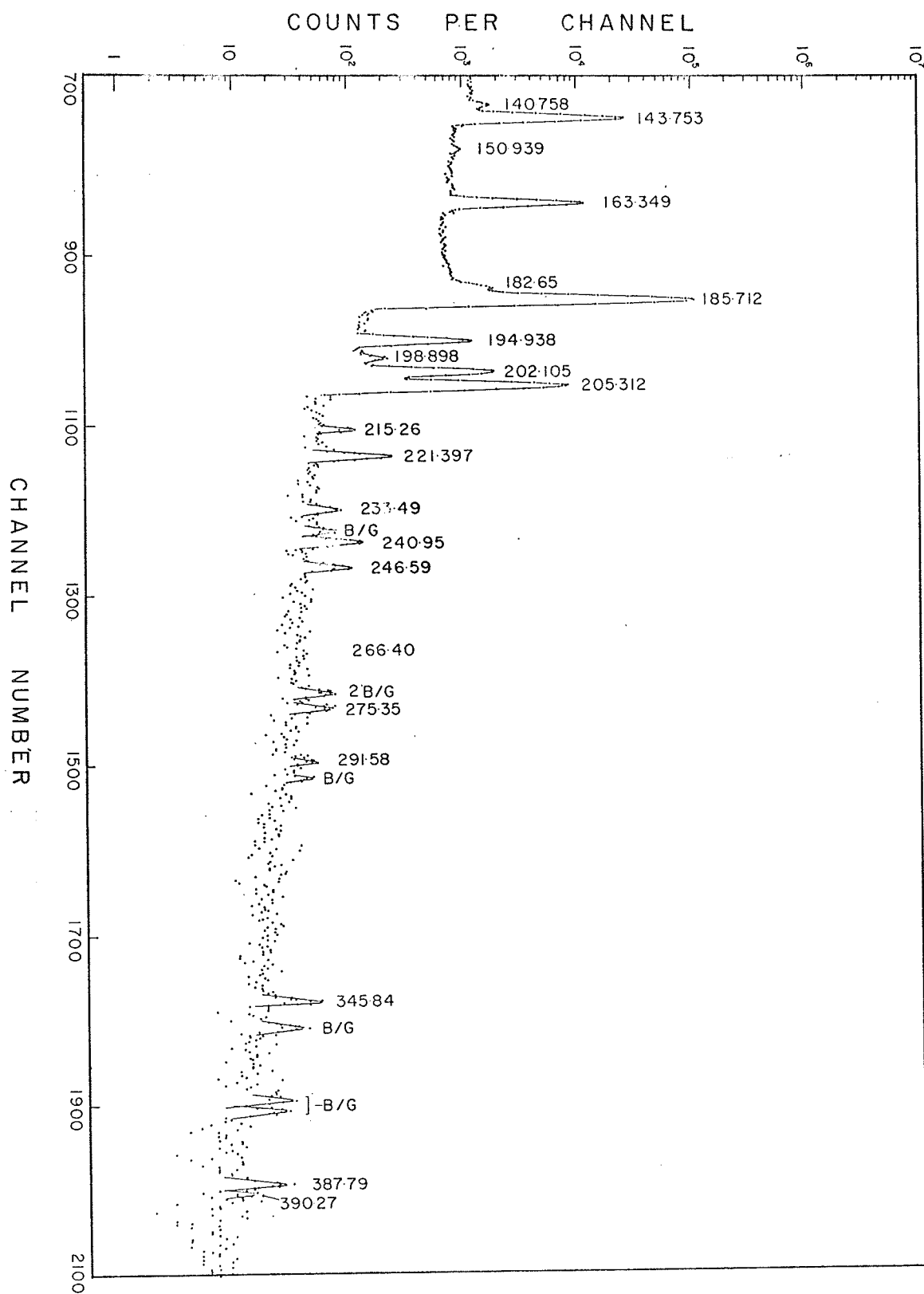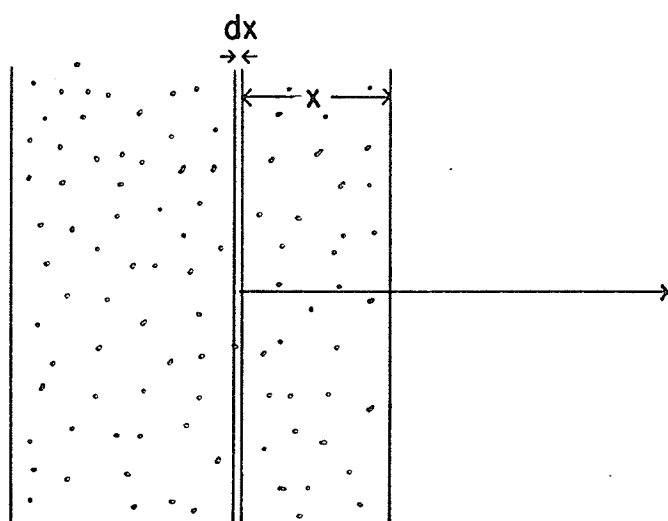
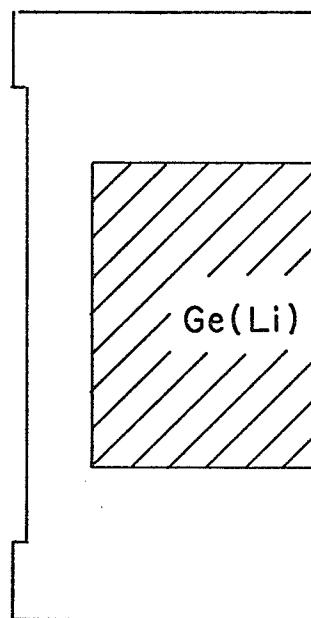Gamma ray spectrum of ^{235}U

(140 - 400 keV)

Figure V-5

Self absorption by source material

dx

x

^{235}U ON

RESIN COLUMN

Ge(Li)

DETECTOR

The high energy region of the gamma ray spectrum has also been examined using the 50 cc Ge(Li) detector whose resolution is 2.0 keV at 1.33 MeV. A typical spectrum is shown in Figure V-4. This spectrum reveals the gamma rays whose energies lie between 140.0 to 400.0 keV. Gamma rays of higher energies were searched for but not observed, hence it is concluded that there are no gamma transitions in ^{235}U decay beyond 391 keV. Of all the gamma rays observed in this region, those at 215.26, 275.35, 291.58, 345.84, 387.79 and 390.27-keV are here reported for the first time. The more intense lines had been calibrated in energy to within 10 eV, and CUTIPIE was used for the data analysis throughout (See Chapter II).

Due to the presence of the lucite cell and the large amount of uranium present on the column, gamma rays emitted will suffer some attenuation so that corrections for self absorption have to be made in the following manner. Ignoring the thickness of the lucite wall for the time being, a thin slab of distributed source of thickness dx (See Figure V-5) will yield a counting rate dR' of a gamma ray (with energy E) given by

$$dR' = p\epsilon Adx$$

if there is no self absorption. Here,

p   is the probability of emission of such a gamma ray

e   is   the   detection   efficiency   at   energy E at that
particular geometry,

A   is the area of the cell.

It should be noted that all the   quantities,   except   A
and dx, are energy dependent.

But the gamma ray emitted has to go through a thickness
x of the resin material (and uranium and acid) before
reaching the detector.   Thus the detection rate   dR   is
related to dR' by the simple relation:

$$dR = \{ \exp(-\mu x) \} dR'$$

$$= peA\{ \exp(-\mu x) \} dx$$

where μ is the gross mass absorption coefficient of the
resin material, uranium, acid, and in short, everything
that   is inside the cell.   The total counting rate R is
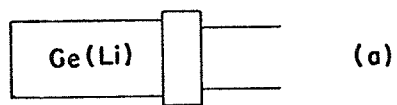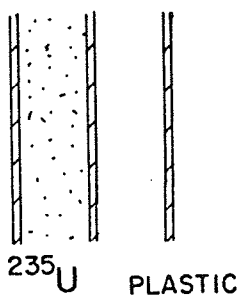then given by

$$R = \int_0^a peA\{ \exp(-\mu x) \} dx$$

At a given energy, e and p are   constant   so   that   the
integral reduces to:

$$R = peA \int_0^a \{\exp(-\mu x)\} dx$$

$$= peA \{ 1.0 - \exp(-\mu a) \}/\mu$$

$$= peAa\{ 1.0 - \exp(-\mu a) \}/\mu a$$
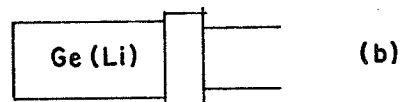
$$= R_0\{ 1.0 - \exp(-\mu a) \}/\mu a$$

Note that $R_0 = peAa$ is the detection rate at the same
geometry and energy if there were no   self   absorption,

Figure V-6

Determination of the intensities

of the gamma rays

from ^{235}U decay

235U   PLASTIC   Ge(Li)   (a)

×
SOURCE   Ge(Li)   (b)

×   Ge(LI)   (c)
SOURCE

235U

×   Ge(Li)   (d)
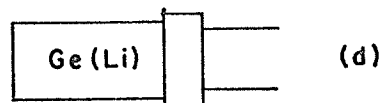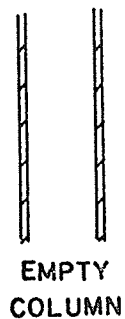SOURCE

EMPTY
COLUMN
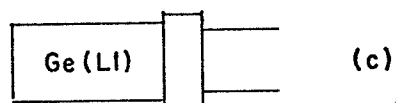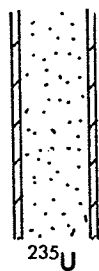
and is the quantity needed to determine the true relative intensities of the gamma rays. R is the detection rate obtained experimentally as a result of self absorption. Here a is the thickness of the resin column, and is the same as the thickness of the lucite wall.

In the present work, since the attenuation due to the lucite wall cannot be ignored, R was determined in the following manner. First, a singles gamma spectrum was taken through an extra sheet of lucite of thickness a, as shown in Figure V-6a. The detection rate R is now

$$R = R_0 \{ 1.0 - \exp(-\mu a) \}\{\exp(-2\eta a)\}/\mu a \qquad V - 1$$

where η is the mass absorption coefficient of the lucite. Next, an isotope rich in gamma rays (in this case, ^{182}Ta) was put in front of the detector, as shown in Figure V-6b. The areas of the photopeaks $N_0(E)$ of ^{182}Ta were noted. The cell containing the resin, uranium and acid was then interposed between the source and the detector (Figure V-6c) and the attenuated area of the same gamma rays N(E) were noted. Thus

$$N(E) = N_0(E) \exp(-\mu a - 2\eta a)$$

or

$$\mu a + 2\eta a = \log (N_0/N) \qquad V-2$$

In this step, the gamma rays from the ^{235}U decay were,

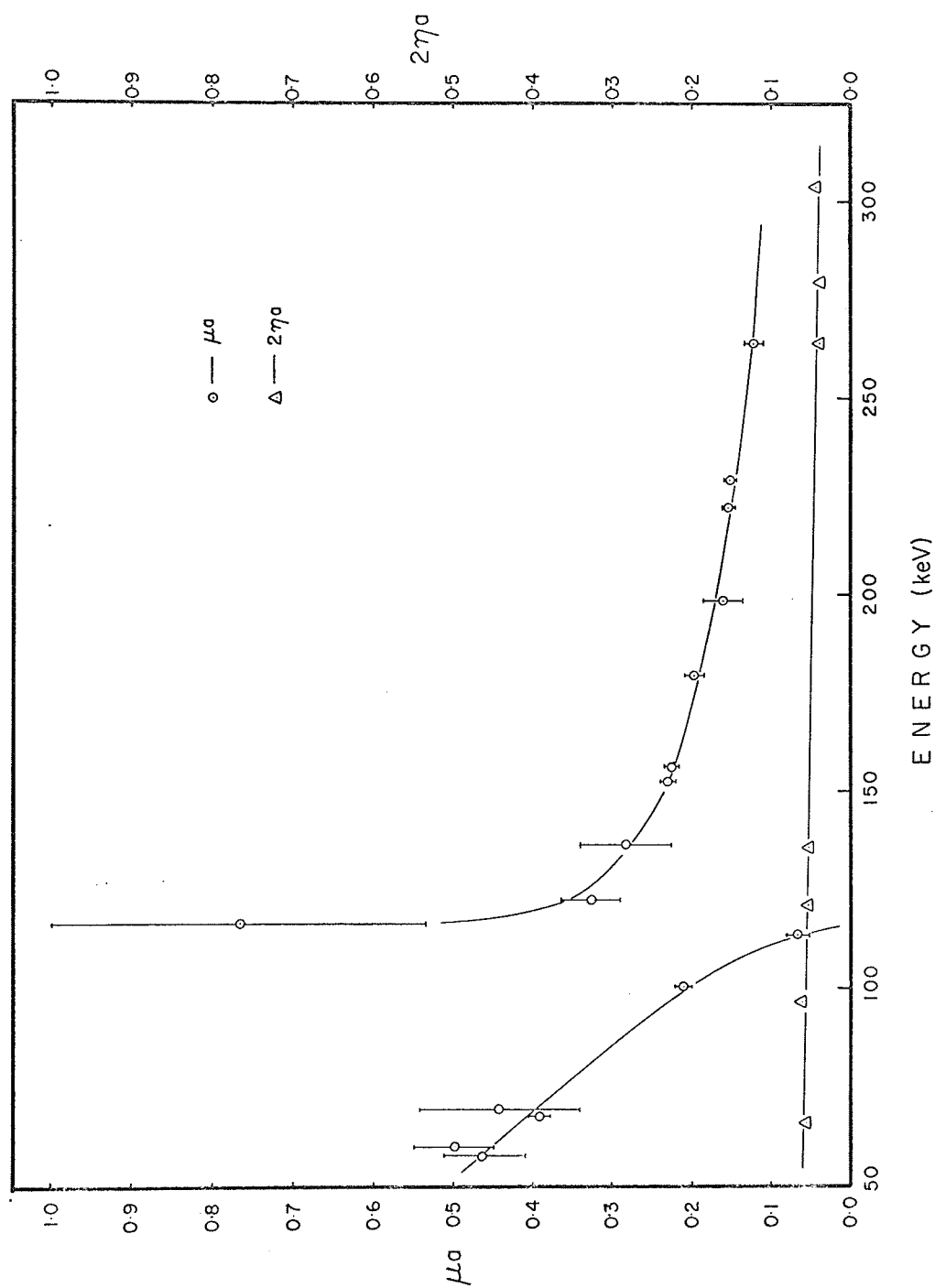Figure V-7

Plot of μa and $2\eta a$ versus E

Table   V-1

^{235}U   gamma ray table

(C) Observed in coincidence only

Present Work		Reported Value	
E_γ	I_γ	E_γ	$I_\gamma \pm 5\%$
31.50 ± 0.20	0.03 ± 0.01		
41.70 ± 0.15	0.05 ± 0.02		
41.96 ± 0.15	0.07 ± 0.03		
51.20 ± 0.10	(c)		
74.76 ± 0.20	0.09 ± 0.01	74.923± 0.023	0.002
96.09 ± 0.02	0.16 ± 0.02	109.120± 0.006	2.0
109.145± 0.010	3.1 ± 0.3	115.2 ± 0.3	0.24
140.758± 0.020	0.46 ± 0.05	140.75 ± 0.10	0.32
143.753± 0.008	19.6 ± 2.0	143.776± 0.10	10.0
150.939± 0.020	0.14 ± 0.02	150.960± 0.033	0.20
163.349± 0.009	8.74 ± 0.90	163.363± 0.010	8.5
182.65 ± 0.15	0.74 ± 0.25	182.72 ± 0.20	0.75
185.712± 0.010	100.0	185.718± 0.011	100.0
194.938± 0.010	1.06 ± 0.16	194.941± 0.009	1.2
198.698± 0.015	0.08 ± 0.01	198.91 ± 0.15	0.950
202.105± 0.012	1.88 ± 0.20	202.133±0.014	1.65
205.312± 0.010	8.55 ± 0.70	205.311± 0.012	5.20
215.26 ± 0.20	0.05 ± 0.01		
221.397± 0.025	0.21 ± 0.05	221.375± 0.040	0.22
233.49 ± 0.03	0.06 ± 0.02	233.53 ± 0.04	0.074
246.95 ± 0.04	0.11 ± 0.03	246.93 ± 0.04	0.13
246.59 ± 0.10	0.80 ± 0.03	246.83 ± 0.04	0.11
266.40 ± 0.10	0.011±0.003	266.44 ± 0.06	0.51
275.35 ± 0.15	0.09 ± 0.01		
291.58 ± 0.15	0.07 ± 0.01		
345.65 ± 0.15	0.07 ± 0.01		
387.79 ± 0.15	0.07 ± 0.01		
390.27 ± 0.26	0.07 ± 0.002		

of course, present but were not used. Finally, the cell
was replaced by an identical empty cell, (Figure V-6c),
and a third set of areas $N'(E)$ were obtained, whence

$$N'(E) = N_o(E) \exp(-2\eta a)$$

or

$$2\eta a = \log(N_o/N') \qquad\qquad V-3$$

From Equation V-2,3

$$\mu a = \log(N_o/N) - \log(N_o/N')$$

$$= \log(N'/N) \qquad\qquad V-4$$

Thus R_o in Equation V-1 may be obtained, knowing μa and
$2\eta a$. Again, it should be noted that R, R_o are functions
of energy. When the intensity calibration was made,
care was exercised to saturate the column with ^{235}U to
ensure that the distribution of active material was as
uniform as possible. Figure V-7 shows a plot of μa
versus energy E. In the same graph $2\eta a$ was also
plotted. Both were obtained experimentally. The
relative intensities of the gamma rays (relative to
I_γ (185.712) = 100.0) due to the decay of ^{235}U (after
correcting for self absorption), together with their
energies, are listed in Table V-1. Also listed in the
same Table are the results recently reported by Cline[5]
where comparable data exist. The agreement between the
present work and that by Cline is excellent. Of course
no comparision is possible for the lines not observed

172

Figure V-8

Coincidence spectrum with the

185.712 keV gamma ray
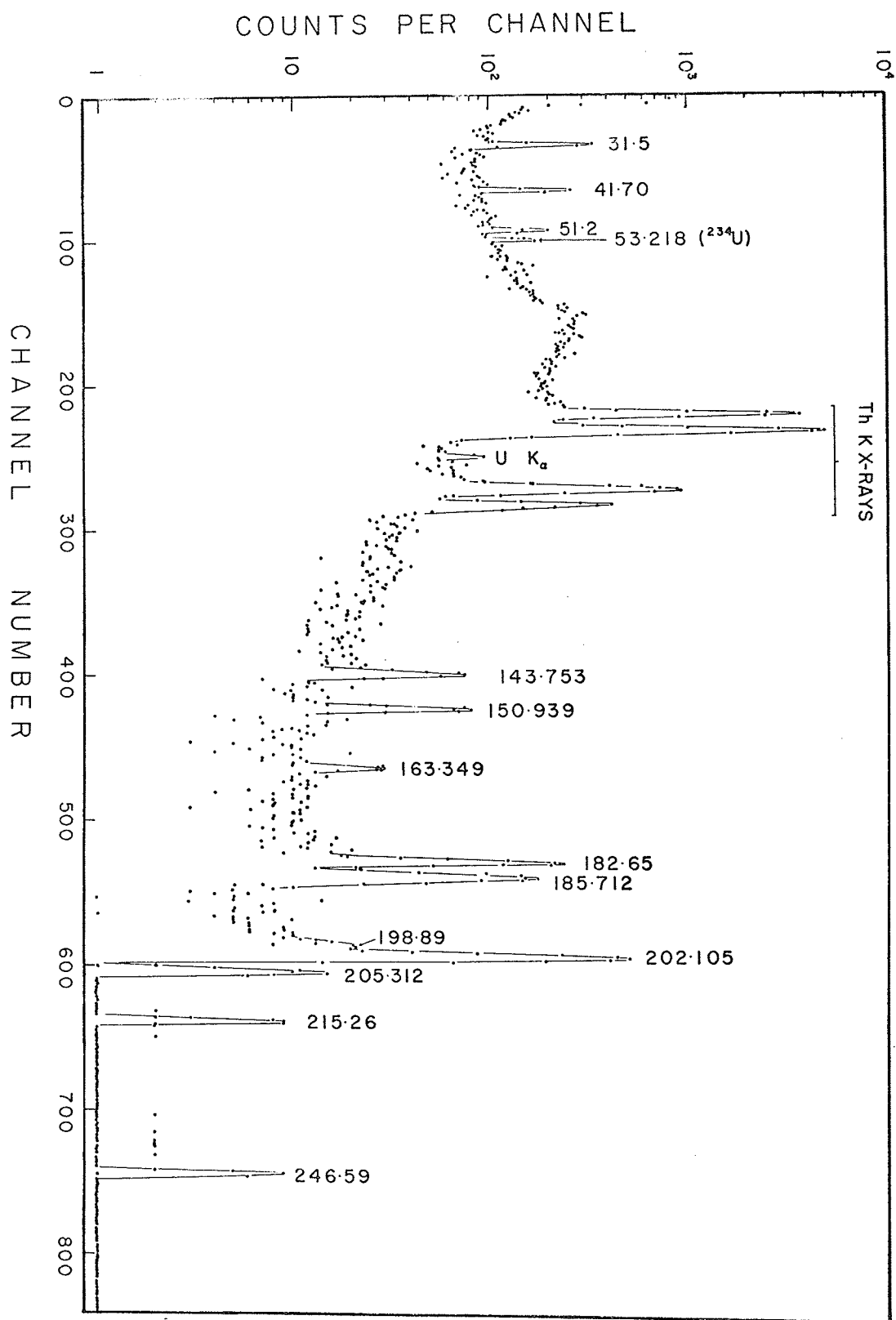
by him, namely those at 31.5, 41.70, 41.96, 215.76, 275.35, 291.58 345.84, 387.79 and 390.27 keV. Also it is interesting to note that there is some disagreement as to the energy and relative intensity of the line at 74.76 keV. This discrepancy is not understood, particularly in view of the otherwise excellent accord with the two sets of data.

V.4 GAMMA-GAMMA COINCIDENCE

Gamma-gamma coincidence work was carried out using the 50 cc detector as the gating detector on channel 1 and the Ortec Ge(Li) X-ray detector on channel 2. This combination worked quite well when strong lines were selected as gates. When less intense gamma rays were used as gates, the counting rate was so low that it was necessary to replace the X-ray detector by the Ortec 35 cc detector.

185.712 keV Gate:

Figure V-8 shows the coincidence spectrum when the gate was set on the 185.712 keV gamma ray. The lines at 31.5, 41.70 and 51.2 keV are unquestionably enhanced. The line at 51.2 keV had not been observed in singles spectra in the present work, nor had it been reported previously. Refering to the level scheme shown in Figure V-11, the fact that the line at 31.50 keV is

Figure V-9

Coincidence spectrum with the

163.349 keV gamma ray

COUNTS PER CHANNEL

CHANNEL NUMBER

Th L X-RAY

31·5

41·70 & 41·96

51·2
53·218 (^{234}U)

Th K X-RAY

143·753

150·939

182·65
185·712

202·105
205·312
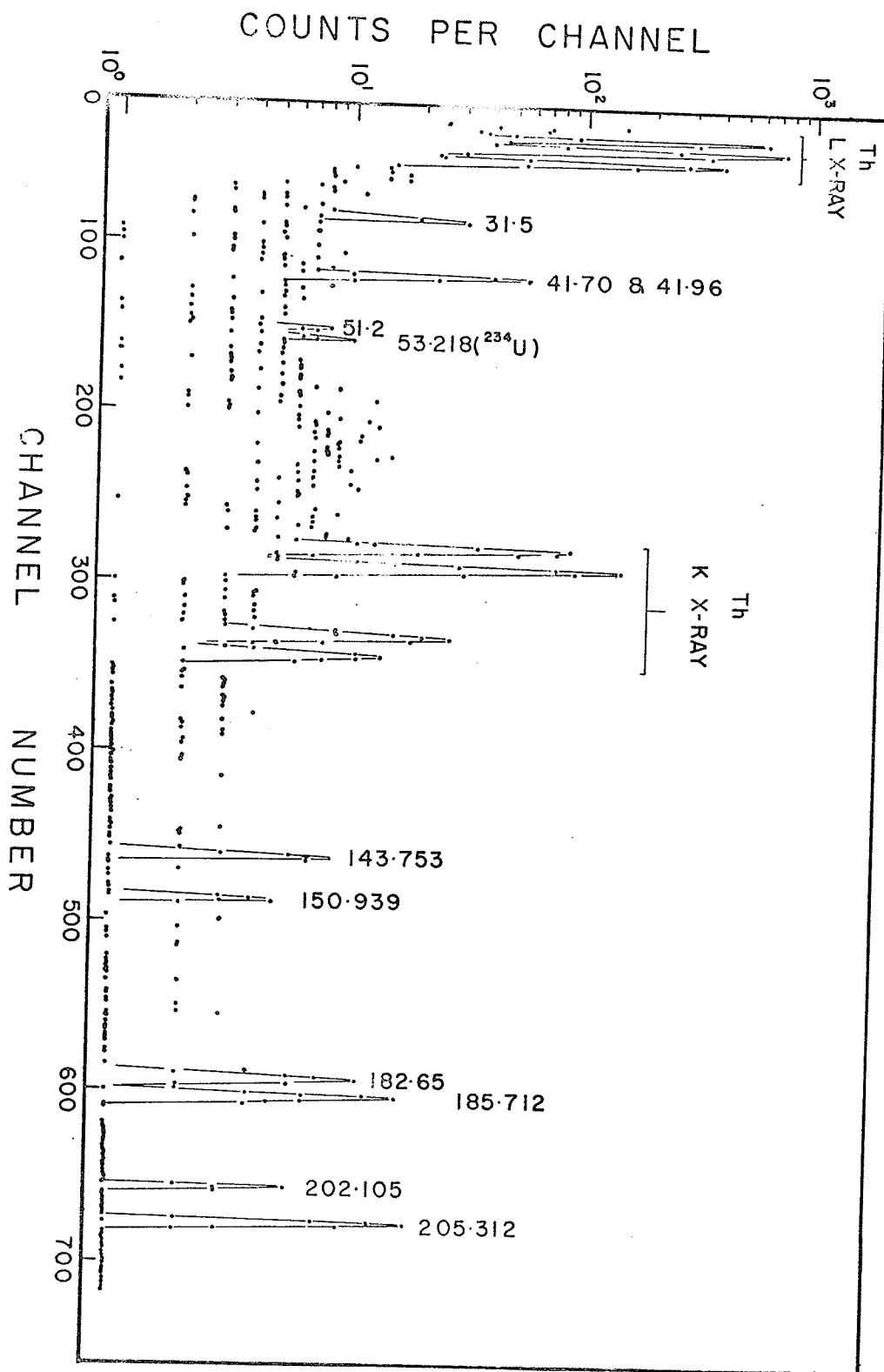
in coincidence with the 185.712 keV gate implies that there has to be a transition from the 205.306 to the 185.712 keV level, the energy difference between these two levels being 19.59 keV. A gamma ray at this energy is not observed, but this does not exclude the possibility of such a transition, since a transition at this energy could be very strongly converted. Also strongly enhanced are gamma rays at 150.939, 182.65, 198.89, 202.105, 215.26 and 246.59 keV. Although only three were previously placed in the level scheme, all the enhanced lines have been successfully placed in the present work in the level scheme.

163.349 keV Gate:

When the 163.349 keV line was selected as gate, the coincidence spectrum was as shown in Figure V-9. The enhanced lines include gamma rays at 31.5, 41.96, 51.2, 182.65 and 202.105 keV. The presence of the 41.70, 51.2, 150.939 and 202.105 keV lines are due to compton coincidences. It must be remembered that the 163.349 keV gamma ray is sitting on the low energy tail of the 185.712 keV line (See Figure V-3,4). Thus, the gating pulses are likely to contain contributions from the low energy tail of the 185.712 keV gamma ray, thereby accounting for the presence of the lines mentioned above. In fact, the entire set of enhanced

lines in coincidence with the 185.712 keV gamma ray is expected but in the present case, only the stronger ones are observed. The weaker ones were not intense enough to be observable. It should be noted, again refering to Figure V-11, that the lines at 31.50, 150.939 and 182.65 keV are also in cascade with the 163.349 keV gate. Thus it is concluded that the lines at 51.20,150.939 and 182.65 keV are enhanced due partly to genuine coincidence with the gate and partly to compton coincidence with the 185.712 keV line as discussed above.

It is interesting to note that the line at 41.96 keV does not have the same intensity (relative to I_γ (185.712) = 100.0) as that obtained with the 185.712 keV gate. In fact, it is more strongly enhanced in this case. The only logical explanation is that this line is actually double, with one component (41.70 keV) in cascade with the 185.721 keV line, and the other (41.96 keV) in cascade with the 163.349 keV line. This doublet has been observed in the singles spectrum (See Figure V-3).

(202.105 + 205.312) keV Gate:

The next gate selected was set on the 202.105, 205.312 keV doublet. These could not be separated for these gamma rays were rather weak so that the X-ray

Figure V-10

Coincidence spectrum with the

(202.105 + 205.312) keV lines
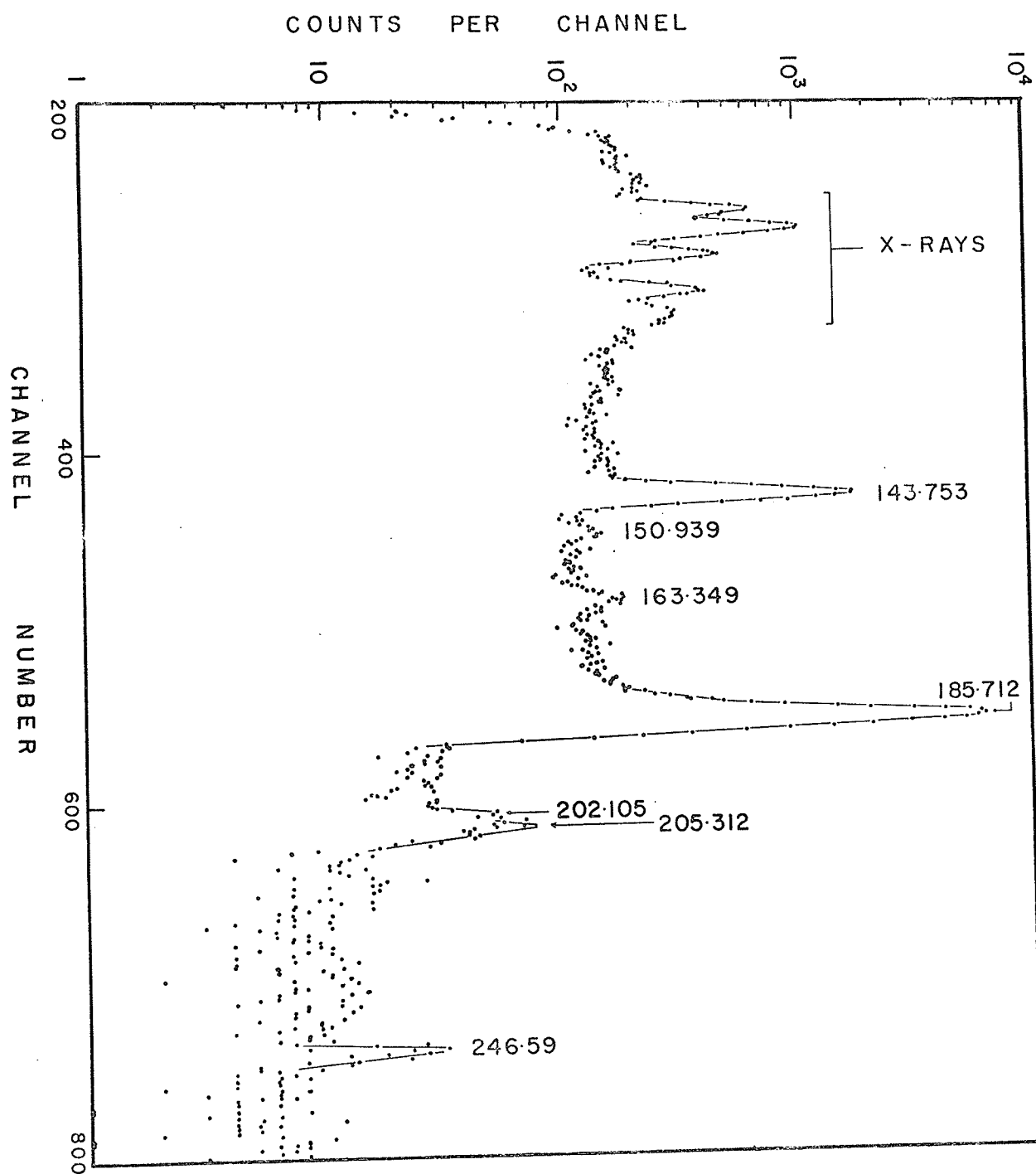
Table V-2

^{235}U coincidence table

Coincident Gamma ray	Gate		
	163.349	185.712	202.105 205.312
31.5	X	X	
41.70		X	
41.96	X		
51.2		X	
143.753			X
150.939	X	X	?
182.65	X	X	
185.712			X
198.89		X	
202.105		X	
215.26		X	X
246.59		X	X

Figure   V-11

Decay scheme for ^{235}U decay
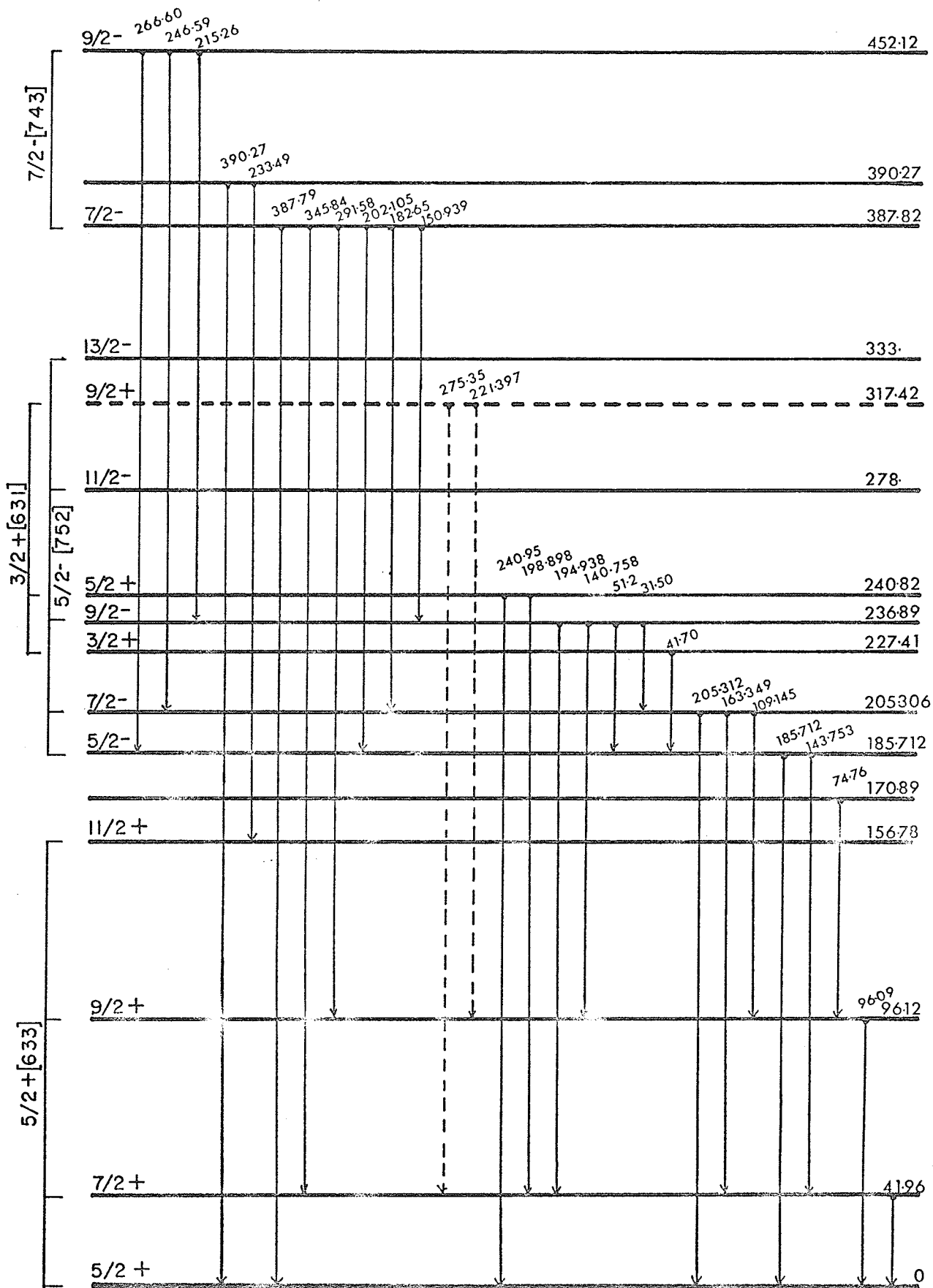
^{231}Th

detector had to be replaced by the 35 cc detector
which has a poorer resolution. Also the two gamma rays
are sufficiently close together in energy so that it is
not possible to obtain a clean gate. The coincidence
spectrum collected is shown in Figure V-10. The
enhanced lines are those at 143.753, 185.712, 215.26,
246.59 and probably 150.939 keV.

A summary of the coincidence data is shown in
Table V-2.

V.5 DISCUSSION

The result of the above investigation is best
summarized in the decay scheme as shown in Figure V-11.
All the levels except those at 390.27, 317.42 and
240.82 keV are fairly well established from the
previous alpha studies. The levels at 390.27, 317.42
and 240.82 keV are added to accommodate the gamma rays
whose energies are 390.27, 233.49, 275.35, 221.97,
240.95 and 198.897 keV. The existence of these levels
(except possibly the 317.42 keV level) is possible due
to their closeness to the other levels strongly fed by
alpha decay, which would lead to their alpha groups
being missed. In fact, the levels at 390.27 and
240.82 keV are so close to the 387.817 and 236.89 keV
levels that the previous investigations of the alpha
spectra might not have revealed them due to the

unavoidably poor resolution of the spectrometers. Further, more than one gamma ray de-exciting each of these levels gives some support to their postulated existence.

It must be conceded at this point that the proposed level at 317.43 keV, being reasonably remote from the alpha groups, is less certain than the other two levels (those at 240.82 and 390.27 keV). The complex alpha spectrum shown by Hyde[7] due to Pilger[8] does not exclude the possibility of the accomodation of such a weakly fed level, however.

All the 28 gamma rays observed in the present work have been successfully placed in the decay scheme. The energies of the levels have been re-adjusted based on the energies of the gamma rays. As mentioned above, the gamma spectra are sufficiently simple (in the sense that the gamma rays are sufficiently isolated from each other) to permit very accurate energy determination.

It has long been known that ^{231}Th exhibits rotational structure. The ground state of ^{235}U is well established[1-3] to have a Nilsson assignment of 7/2-(743), and its favoured alpha transition decays to the 387.82 keV level in ^{231}Th. This level is therefore, given the same assignment (see Figure V-11), and de-excites to the 185.712 keV level by a predominently

M1 transition[14]. Hence this band has to have odd parity, and a spin of 5/2 or 7/2. The only Nilsson level near the 7/2-(743) state satisfying these conditions is the 5/2-(752) level, and is thus assigned to this band. A very striking feature of this band is that it seems to be compressed at about 190 keV. This is due to the strong interaction between the 7/2-(743) band and the 5/2-(752) band brought about by the coriolis forces. Such an interaction had been calculated by Stephens[15], and by Karman[16] for a different nucleus. The 185.712 keV level de-excites to the ground state of ^{231}Th by E1 transition[17], and thus the ground state is unambiguously assigned as 5/2+(633). This is the same as the ground state of ^{233}U which is not un-expected, since they both have the same neutron number (141). There is a further band built on the 3/2+(631) level as suggested by the reaction data[18-20]. Braid et-al[21] has suggested that the levels at 227.41 and 240.82 keV be assigned to this band, based on the results of their (d,p) and (d,t) reaction data. The level at 317.42 keV would then correspond to the 9/2 member of this band. It is interesting to note that with E_o = 221.07 keV, A = 1.429 keV, and B = 0.100 keV (see PREFACE), the 7/2 member of this band is expected to lie at 268 keV. A level at this energy is not observed in the present work, nor has it been observed previously.

EPILOG

The gamma rays emitted as a result of the decay
of ^{235}U, ^{231}Th and ^{231}Pa have been carefully examined in
the present work.

The level schemes of ^{227}Ac and ^{231}Pa have been
reported recently by Pinho and Brown (See Ref 17, Chapter III
and Ref 16, Chapter IV). The present work substantiates
their report and extends the known data on these isotopes.
The observation of several new gamma rays in gamma-gamma
coincidence work has made it possible, in the present work,
to construct definitive and complete decay schemes of these
isotopes.

The decay of ^{235}U is interesting in that not
much was previously known about its gamma radiations.
Cline (See Ref 5, Chapter V) is apparently the first person
to examine this isotope with high resolution semi-conductor
detectors. Similar detectors are used in the present work,
and a definitive decay scheme is obtained. It would be
beneficial to examine the alpha particles emitted as a
result of ^{235}U decay, but unfortunately, the source avail-
able is not suitable for this purpose.

In passing, it should be mentioned that the
present work concludes the investigation of the Actinium
series --- a project which has been pursued in this labor-
atory for the past decade.

REFERENCE TO THE PREFACE

(1) O. R. Frisch, (Ed) The Nuclear Handbook, George Newnes Ltd., London, (1958).

(2) E. K. Hyde, I. Perlman and G. T. Seaborg, Nucl. Properties of Heavy Elements, Vol. II, Prestice Hall Inc. N. J. (1964).

(3) E. Fermi, Nucl. Phys. University of Chicago Press, Revised Edition, (1967).

(4) R. R. Roy and B. P. Nigam, Nucl.Phys. John Wiley and Sons, N.Y. (1967).

(5) M. A. Preston, Physics of the Nucleus, Addison Wesley Inc., Mass., (1962).

REFERENCE TO CHAPTER I

(1) Ge(Li) Handbook, 3rd edition, Princeton Gamma Tech, (1970).

(2) G. T. Ewan, AECL Report#1960, (1964).

(3) G. T. Ewan and A. J. Tavendale, AECL Report#2079, (1964).

(4) R. L. Heath, W. W. Black and J. E. Cline, National Reactor Testing Station, Idaho Falls, Idaho, (1968).

(5) R. W. Jewell, W. John, R. Massey and B. G. Saunders Nucl. Instr. and Meth., 62 (1968) 68.

(6) J. J. Reidy and M. L. Weindbzk (to be published).

(7) E. R. Cohen and J. W. Dumond, Rev. Mod. Phys., 37 (1965) 537.

(8) J. B. Marion, Nuclear Data A4 (1968) 301.

(9) R. L. Graham, G. T. Ewan and J. S. Geiger, Nucl. Instr. and Meth., 9 (1960) 245.

(10) G. C. Greenwood, R. G. Helmer and R. J. Gehrke, Nucl. Instr. and Meth., 77 (1970) 141.

(11) J. A. Bearden, X-Ray Wavelengths NYO-10586 (1964).

(12) P. Yueng, Private Communication (1972).

(13) J. E. Cline, Gamma Rays Enmited by Fissible Nuclides and Associated Isotopes, (1971), quoted in Nuclear Data Sheets Reference list for A=233.

(14) T. Paradellis and S. Hontzeas, Nucl. Instr. and Meth., 73 (1969) 210.

(15) G. T. Ewan, R. L. Graham and I. K. Mackenzie, AECL Report#2565, (1966).

(16) M. J. Canty, Ph.D. Thesis, University of Manitoba, (1969).

(17) R. L. Graham, I. K. Mackenzie and G. T. Ewan, AECL Report#2505, (1965).

(18) F. R. Metzger, Phys. Rev. __127__ (1962) 220.

(19) K. Siegbahn, Beta and Gamma Ray Spectroscopy, North Hollander Inc., N.Y., (1955).

(20) T. von Egidy, O. W. R. Schult, W. Kallinger, D. Breitig, R. P. Sharma, R. Koch and H. A. Baader, Z. Naturforsch, To Be Published, (1971), quoted in Nuclear Data Reference List for A=75.

REFERENCE TO CHAPTER II

(1) C. Abraham, Scientific Report#1, University of Manitoba, (1970).

(2) IBM System/360 Operating System: Utilities, GC28-6586-12, (1971).

(3) G. D. Brown, System/360 Job Control Language, Wiley, (1970).

(4) D. C. Robinson, AERE R6144 (1967).

(5) F. C. P. Huang, C. H. Osman and T. R. Ophel, Nucl. Instr. and Meth., 68 (1969) 141.

(6) V. Barnes, GASPAN, Windscale Works, (1969).

(7) J. T. Routti and S. G. Prussin, Nucl. Instr. and Meth., 72 (1969) 125.

(8) W. B. Cook, JAGSPOT, Private Communication (1970).

(9) L. Varnell and J. Trischuk, Nucl. Instr. and Meth., 76 (1969) 109.

(10) T. A. E. Pratt, Nucl. Instr. and Meth., 99 (1972) 205.

(11) M. Cliampi, L. Daddi and V. D'Angelo, Nucl. Instr. and Meth., 66 (1968) 102.

(12) P. W. Green, Nucl. Instr. and Meth., 76 (1969) 349.

(13) W. W. Black, Nucl. Instr. and Meth., 71 (1969) 317.

(14) H. P. Yule, Nucl. Instr. and Meth., 54 (1967) 61.

(15) H. Tominaga, M. Dojyo and M. Tanaka, Nucl. Instr. and Meth., 68 (1972) 69.

(16) M. A. Mariscotti, Nucl. Instr. and Meth., 50 (1967) 309.

(17) R. H. Moore and R. K. Zeigler, Los Alamos Lab. Report#LA-2367 (1957).

(18) D. G. Douglas, U. of Manitoba, Private communication (1970)

(19) S. K. Sen, U. of Manitoba. Private communication (1970)

(20) R. Hofstadter, H. R. Fechter and J. A. McIntyre, Phys. Rev. 92 (1953) 978.

(21) J. Kern, Nucl. Instr. and Meth., 79 (1970) 233.

(22) G. C. Nelson and B. G. Saunders, UCRL Report#71800 (1969).

(23) J. H. Scofield, Phys. Rev., 179 (1969) 9.

(24) J. A. Bearden, X-Ray Wavelengths, NYO-10586, (1964).

(25) R. C. Greenwood, R. G. Helmer and R. J. Gehrke, Nucl. Instr. and Meth., 27 (1970) 147.

(26) E. Brown, U.C.L.A. Private communication (1970)

(27) N. Davudoglu, U. of Manitoba. Private communication (1970)

REFERENCE TO CHAPTER III

(1) H. W. Kirby, J. Inorg. Nucl. Chem. <u>18</u> (1961) 8.

(2) S. Rosenblum, E. Cotton and G. Bouissieres, Compt. Rend. <u>229</u> (1949) 825.

(3) J. P. Hummel, F. Assaro and I. Perlman, Phys. Rev. <u>98A</u> (1955) 261.

(4) S. A. Baranov, Sov. Phys. JEPT. <u>14</u> (1962) 1053.

(5) A. G. de Pinho, Ph.D. Thesis, University of Paris, (1963).

(6) L. Meitner, Z. Phys. <u>50</u> (1928) 15.

(7) E. Haggstrom, Phys. Rev. <u>62</u> (1942) 144.

(8) G. Scharff-Goldhaber and M. Mckeown, Phys. Rev. <u>82</u> (1951) 123.

(9) R. L. Moore, Ph.D. Thesis, Ohio State University (1953).

(10) P. Falk-Variant, Compt. Rend. <u>235</u> (1952) 796.

(11) F. Assaro, F. S. Stephens, J. M. Hollander and I. Perlman, Phys. Rev. <u>117</u> (1960) 492.

(12) D. Strominger, University of California Lab. Report, UCRL-3374 (1956).

(13) R. C. Lange and G. R. Hagee, Nucl. Phys. <u>A124</u> (1969) 412.

(14) A. G. Barnett, A. R. Campbell and G. R. Hagee, J. Inorg. Chem. <u>31</u> (1969) 1553.

(15) G. R. Hagee, R. C. Lange, A. G. Barrnett, A. R. Campbell, C. R. Cothern, D. F. Griffing and H. J. Hennecke, Nucl. Phys. <u>A115</u> (1968) 157.

(16) C. F. Leang, J. de Phys. <u>31</u> (1970) 269.

(17) A. G. de Pinho, E. F. de Silveira and N. L. da Costa, Phys. Rev. <u>2</u> (1970) 572.

(18) F. S. Stephens, F. Assaro and J. M. Hollander, Private Communication, Quoted in Ref. (19).

(19) E. K. Hyde, I. Perlman and G. T. Seaborg, Nucl. Prop. of Heavy Element, Vol. II, Printice Hall Inc. N. J. (1964).

(20) J. H. Scofield, Phys. Rev. 179 (1969) 9.

(21) P. Falk-Variant and M. Riou, J. Phys. Radium 14(1953) 65.

(22) C. J. Allan, Ph.D. Thesis, University of Manitoba, (1970).

(23) D. W. Green, J. of Sci. Instr. 38 (1961) 333.

(24) C. M. Lederer, J. M. Hollander and I. Perlman, Table of Isotopes, John Wiley Inc. N. Y. 6th edition, (1968).

(25) H. W. Kirby, The Radiochem. of Protactrum, U.S. AEC, Document# NAS-NS-3016 (1959).

(26) W. F. Davidson, Ph.D. Thesis, University of Manitoba, (1967).

(27) W. F. Davidson and R. D. Connor, Nucl. Phys. A116 (1968) 342.

(28) W. H. A. Hesselink, A. H. Wapstra and J. G. Kromme, Nucl. Phys. A191 (1972) 283.

REFERENCE TO CHAPTER IV

(1) M. J. Campbell, Can. J. Phys. <u>36</u> (1958) 989.

(2) E. K. Hyde, I. Perlman and G. T. Seaborg, Nucl. Properties of heavy Elements, Vol. II, Prentice Hall Inc., N. J. (1964).

(3) O. Gratias and A. Debieyne, Proc. Roy. Soc. (Landon), <u>135A</u> (1932) 299.

(4) G. B. Knite and R. L. Macklin, Phys. Rev. <u>75</u> (1949) 34.

(5) E. Nakamura, Radiochim. Acta, <u>1</u> (1963) 66.

(6) A. H. Jaffey, L. Lerner and S. Warshaw, Phys. Rev. <u>82</u> (1951) 498.

(7) D. Buksak and A. Chow, Radiochem. Radio. anal. Letters. <u>8</u> (1971) 7.

(8) R. W. Flint, U. of Manitoba. Private communication (1972)

(9) J. A. Bearden, X-Ray Wavelengths, NYO-10586, (1964).

(10) R. C. Greenwood, R. G. Helmer and R. J. Gehrke, Nucl. Instr. and Meth., <u>77</u> (1970) 141.

(11) E. Brown, U.C.L.A. Private communication (1970)

(12) J. E. Mack, Rev. Mod. Phys., <u>22</u> (1950) 64.

(13) R. Marrus, W. A. Nierenberg and J. Winocur, Nucl. Phys. <u>30</u> (1961) 90.

(14) B. R. Mottelson and G. S. Nelsson, Hat. Skr. Dan. Vid. Sdsk., <u>1</u> (1959) 8.

(15) F. S. Stephens, F. Assaro and I. Perlman, Phys. Rev. <u>113</u> (1959) 212.

(16) E. Brown and F. Assaro, UCRL-19530 (1970), The Alpha Decay of ^{237}Np and The Decay of ^{231}Th.

(17) W. Hockstra, Phys. Rev. Lett. <u>22</u> (1969) 859.

(18) C. M. Lederer, J. M. Hollander and I. Perlman, Table
       of Isotopes, John Wiley and Sons, N.Y., 6th Edition,
       (1968).

REFERENCE TO CHAPTER V

(1) S. A. E. Johansson, Arkiv. Fysik, 10 (1956) 97.

(2) C. W. Malich, Bull. Am. Phys. Sco. 1, No.1, K12 (1956) 43.

(3) R. C. Pilger, F. S. Stephens and F. Assaro, Quoted in Ref. (7).

(4) C. M. Lederer, J. M. Hollander and I. Perlman, Table of Isotopes, John Wiley and Sons, N. Y., 6th edition, (1968).

(5) J. E. Cline, IN1448 Rev. (1971), Quoted in Nucl. Data Sheets for A=235.

(6) R. Gaeta and M. A. Vigon, Nucl. Phys. 76 (1966) 353.

(7) E. K. Hyde, I. Perlman and G. T. Seaborg, Nucl. Properties of Heavy Elements, Vol. II, Prentice Hall, N.J. (1964).

(8) R. C. Pilger Jr., Ph.D. Thesis, UCRL-3877, (1957).

(9) D. J. Skilling, Chalk River Project Progress Report CR-PRD-27, (1961).

(10) S. A. Baranov, A. G. Zelenkov and V. M. Kulakov, Izvest. Akad. Nauk., 24 (1960) 1035.

(11) K. L. Vandersluis and J. R. McNally Jr., J. Opt. Soc. Am. 45 (1955) 65.

(12) C. A. Hutchison Jr., P. M. Llewellyn, E. Wong and P. Dorain, Phys. Rev. 102 (1956) 292.

(13) J. O. Newton, Nucl. Phys. 3 (1957) 345; Physica 22 (1956) 1129.

(14) F. S. Stephens, UCLA Report; UCRL-2970, (1955).

(15) F. S. Stephens, Ph.D. Thesis, University of California, (unpublished) (1955), Quoted in Ref. (7).

(16) A. K. Kerman, Kgl. Dauske Vidaiskab, Selskab, Mat. Fys. Medd. 30 No. 15 (1956).

(17) F. S. Stephens, F. Assaro and I. Perlman, Phys. Rev. 113 No. 1 (1959) 212.

(18) J. R. Erskin, Private Communication (1970), Quoted in Nucl. Data Sheet for A=231.

(19) T. W. Elze, T. V. Egidy and J. R. Huizenga, Nucl. Phys. A128 (1969) 564.

(20) J. S. Boyno, T. W. Elze and J. R. Huizenga, Nucl. Phys. A157 (1970) 263.

(21) T. H. Braid, R. R. Chasman, J. P. Erskin and A. M. Friedman, Phys. Rev. 1, No. 1 (1970) 275.